A&A 469, 607–631 (2007)
DOI: 10.1051/0004-6361:20066855

Astronomy & Astrophysics

The subpulse modulation properties of pulsars at 92 cm and the frequency dependence of subpulse modulation⋆,⋆⋆

P. Weltevrede[1], B. W. Stappers[2,1], and R. T. Edwards[3]

[1] Astronomical Institute "Anton Pannekoek", University of Amsterdam, Kruislaan 403, 1098 SJ Amsterdam, The Netherlands
e-mail: wltvrede@science.uva.nl
[2] Stichting ASTRON, Postbus 2, 7990 AA Dwingeloo, The Netherlands
e-mail: stappers@astron.nl
[3] CSIRO Australia Telescope National Facility, PO Box 76, Epping NSW 1710, Australia
e-mail: Russell.Edwards@csiro.au

Received 1 December 2006 / Accepted 23 March 2007

ABSTRACT

Context. A large sample of pulsars has been observed to study their subpulse modulation at an observing wavelength (when achievable) of both 21 and 92 cm using the Westerbork Synthesis Radio Telescope. In this paper we present the 92-cm data and a comparison is made with the already published 21-cm results.
Aims. The main goals are to determine what fraction of the pulsars have drifting subpulses, whether those pulsars share some physical properties and to find out if subpulse modulation properties are frequency dependent.
Methods. We analysed 191 pulsars at 92 cm searching for subpulse modulation using fluctuation spectra. The sample of pulsars is as unbiased as possible towards any particular pulsar characteristics.
Results. For 15 pulsars drifting subpulses are discovered for the first time and 26 of the new drifters found in the 21-cm data are confirmed. We discovered nulling for 8 sources and 8 pulsars are found to intermittently emit single pulses that have pulse energies similar to giant pulses. Another pulsar was shown to exhibit a subpulse phase step. It is estimated that at least half of the total population of pulsars have drifting subpulses when observations with a high enough signal-to-noise ratio would be available. It could well be that the drifting subpulse mechanism is an intrinsic property of the emission mechanism itself, although for some pulsars it is difficult or impossible to detect. Drifting subpulses are in general found at both frequencies, although the chance of detecting drifting subpulses is possibly slightly higher at 92 cm. It appears that the youngest pulsars have the most disordered subpulses and the subpulses become more and more organized into drifting subpulses as the pulsar ages. The modulation indices measured at the two frequencies are clearly correlated, although at 92 cm they are on average possibly higher. At 92 cm the modulation index appears to be correlated with the characteristic age of the pulsar and the complexity parameters as predicted by three different emission models. The correlations with the modulation indices are argued to be consistent with the picture in which the radio emission can be divided in a drifting subpulse signal plus a quasi-steady signal which becomes, on average, stronger at high observing frequencies. The measured values of P_3 at the two frequencies are highly correlated, but there is no evidence for a correlation with other pulsar parameters.

Key words. stars: pulsars: general – radiation mechanisms: non-thermal

1. Introduction

Although the pulse profiles of radio pulsars are in general very stable, the shape of their single pulses are often highly variable from pulse to pulse. For some pulsars the single pulses are modulated in a highly organized and fascinating way: they exhibit the phenomenon of drifting subpulses (Sutton et al. 1970; Drake & Craft 1968). An example is shown in the left panel of Fig. 1. In this so-called "pulse-stack" fifty successive pulses are displayed on top of one another and a beautiful pattern of diagonal "drift bands" emerges.

We have embarked on an extensive observational program to survey a large sample of pulsars to study their single pulse modulation using the Westerbork Synthesis Radio Telescope (WSRT) in the Netherlands. The main goals of this program are to determine what fraction of the pulsars have drifting subpulses, whether those pulsars share some physical properties and if subpulse modulation is frequency dependent. The sample of pulsars studied is selected based only on the predicted S/N in a reasonable observing time, which makes the resulting statistics as unbiased as possible towards well-studied pulsars, pulse profile morphology or any particular pulsar characteristics. If possible, we observed the pulsars at two wavelengths around 21 and 92 cm. It should be noted that the actual central wavelength can be slightly different from observation to observation.

The results of the pulsars observed at a wavelength of 21 cm are published in Weltevrede et al. (2006a) (hereafter referred to as Paper I). Drifting subpulses were detected in 68 of 187 analyzed pulsars, 42 of which were shown to have drifting subpulses for the first time. In this paper the results of the 92-cm observations are presented and a comparison with the results

⋆ Appendix A is only available in electronic form at http://www.aanda.org.
⋆⋆ Table 2 is also available in electronic form at the CDS via anonymous ftp to cdsarc.u-strasbg.fr (130.79.128.5) or via http://cdsweb.u-strasbg.fr/cgi-bin/qcat?J/A+A/469/607

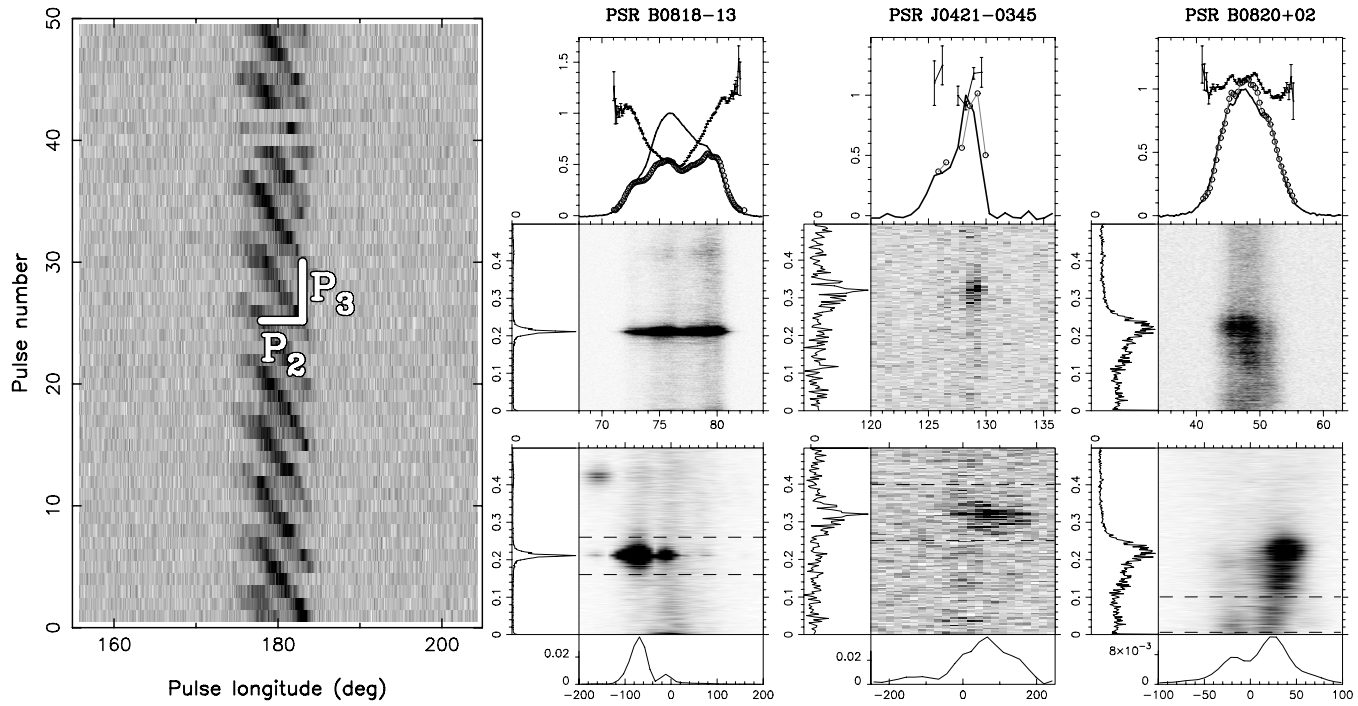

Fig. 1. The *left panel* shows a pulse-stack of fifty successive pulses of PSR B0818–13. Two successive drift bands are vertically separated by P_3 and horizontally by P_2. The products of our analysis are shown for three pulsars. The *top panel* shows the integrated pulse profile (solid line), the longitude-resolved modulation index (solid line with error bars) and the longitude-resolved standard deviation (open circles). Below this panel the LRFS is shown with – on its horizontal axis – the pulse longitude in degrees, which is also the scale for the abscissa of the plot above. Below the LRFS the 2DFS is plotted and the power in the 2DFS is vertically integrated between the dashed lines, producing the *bottom plots*. Both the LRFS and 2DFS are horizontally integrated, producing the side-panels of the spectra.

reported in Paper I is made. In the next section the method used to analyse the data is explained concisely, but for details we refer to Paper I. In Sect. 3 the individual detections are described (which are summarized in Table 2) and some remarks about the comparison of sources at the two frequencies are made in Sect. 4. The statistics of the drifting phenomenon is described in Sect. 5 and are discussed in Sect. 6. After the summary and conclusions one can find the plots for all the pulsars observed at 92 cm (Appendix A). For some of the pulsars the Two-Dimensional Fluctuation Spectrum (2DFS; Edwards & Stappers 2002) is shown for two different pulse longitude ranges. The plots of these pulsars come after the plots of the pulsars with only one 2DFS plot. The plots of the two 21-cm and 92-cm observations can be found side by side in the Ph.D. Thesis of the main author[1].

2. Observations and data analysis

2.1. The source-list

All the observations were done using the WSRT in the Netherlands and therefore the first selection for the source-list is that the pulsars must have a declination above −30° (J2000). For Paper I a source-list was compiled of all pulsars visible with the WSRT for which a pulse profile could be obtained with an integrated signal-to-noise (S/N) ratio of 130 in an observation of less then half an hour in duration. Because at 21 cm we discovered drifting subpulses for many pulsars in observations with a lower S/N a different criterion was chosen for the 92-cm observations. For this paper all visible pulsars for which we could obtain a pulse profile with a S/N ratio of 50 in less than half an hour were included in the source-list.

The 92-cm frontend at the WSRT was used in combination with the PuMa I pulsar backend (Voûte et al. 2002), which have the following parameters: the gain of the telescope $G = 1.2$ K/Jy, the number of polarizations of the antenna $n_{\rm p} = 2$, $T_{\rm sys} = 125$ K, $T_{\rm sky} \approx 100$ K (which is approximately the average of the entire sky), the bandwidth of the backend $\Delta\nu = 10$ MHz and the digitization efficiency factor $\eta_Q = 1$. It should be mentioned that $T_{\rm sky}$ is a strong function of position on the sky, particularly in galactic latitude. Because the age of the pulsar is also correlated with the galactic latitude, we are biased against young pulsars. The same bias also applies for pulsar surveys and is worse at low frequencies.

The expected observation duration required to get an integrated S/N ratio of at least 50 can be calculated for these parameters (see Paper I for more details):

$$t_{\rm obs} \geq \left(\frac{2.1\ {\rm Jy}}{S_{400}}\right)^2 \frac{w}{P_0 - w}. \quad (1)$$

Here S_{400} is the flux of the pulsar at the observation wavelength of 92 cm, P_0 the barycentric pulse period and w the FWHM of the pulse profile. Only catalogued[2] pulsars (Manchester et al. 2005) with the necessary parameters S_{400} and w were included in the source-list.

All the pulsars in the source-list, except the millisecond pulsars, were observed. For ten sources (PSRs B0154+61, J1246+22, B1754−24, B1800−21, B1804−27, B1813−26, B1834−10, B1900+06, B1907+03 and B1924+14) the S/N was either too low, there was extreme radio-frequency-interference

[1] The thesis of P. Weltevrede is online available via the following URL: http://dare.uva.nl/en/record/217315

[2] http://www.atnf.csiro.au/research/pulsar/psrcat/

(RFI) or the observation failed. Apart from these sources the results of the remaining 191 pulsars are presented in this paper.

Similar to Paper I, the brightest pulsars were observed for long enough to obtain at least one thousand pulses and archival data was used when available. Although for a number of pulsars the data greatly exceed the minimum required S/N and number of pulses, this does not bias our statistics too much toward well-studied pulsars as all pulsars in our source-list were observed long enough to have a good chance to detect drifting subpulses.

2.2. Observations and data processing

The procedure of processing the observations in this paper is identical to that described in Paper I, so we will only summarize it here. All results in this paper are based on observations done in the last six years at the WSRT. The filterbank data were (offline and incoherently) de-dispersed and the resulting time series were transformed in a two-dimensional pulse number versus pulse longitude array (pulse-stack) using the pulse period provided by the TEMPO software package[3].

An example of a pulse-stack is shown in the left panel of Fig. 1. In this plot the pulse number is plotted vertically and the time within the pulses (i.e. the pulse longitude) horizontally. The vertical separation (in pulse periods) between the drift bands is denoted by P_3 and the horizontal separation (in pulse longitude) by P_2. To be able to detect the drifting subpulse phenomenon in as many pulsars as possible, all the pulse-stacks were analyzed in a systematic procedure using fluctuation spectra.

Two types of spectra are derived from the pulse-stack: the Longitude Resolved Fluctuation Spectrum (LRFS; Backer 1970) and the Two-Dimensional Fluctuation Spectrum (2DFS; Edwards & Stappers 2002).

In Fig. 1 the LRFSs of three pulsars are shown (middle panels). The units of the vertical axis are in cycles per period (cpp), which corresponds to P_0/P_3 in the case of drifting subpulses, and the horizontal axis is the pulse longitude in degrees. The power in the LRFS is horizontally integrated, producing the side panel.

The top plots of Fig. 1, which are aligned with the LRFSs plotted below, show the pulse profiles (solid line, normalized to the integrated peak intensity), longitude resolved standard deviation (open dots) and the longitude resolved modulation index (solid line with error bars). Both the longitude resolved standard deviation and modulation index are derived from the LRFS, which allows correction for both (periodic) RFI and interstellar scintillation (see Paper I for details). The modulation index is a measure of the factor by which the intensity varies from pulse to pulse and could therefore be an indication for subpulse modulation.

By analyzing the LRFS it can be determined if the subpulse modulation is disordered or (quasi-)periodic, but the 2DFS is required to find out if the subpulses are systematically drifting in pulse longitude. In Fig. 1 the 2DFS is plotted below the LRFS. The unit of its vertical axis is identical to that of the LRFS and also the unit of the horizontal axis is cycles per period, which corresponds to P_0/P_2 in the case of drifting. In this paper and Paper I we use the convention that P_3 is always positive and the sign of P_2 indicates the drift direction. A positive value means that the subpulses appear later in successive pulses (which is called positive drifting).

The horizontally integrated power in the 2DFS is shown in the side panel and the vertically (between the dashed lines) integrated power is shown in the panel below the 2DFS. These panels are only produced to make it easier to see by eye what the structure of the feature in the 2DFS is. In the 2DFS of PSR B0818−13 the drift feature is centered at $P_3 \simeq 0.21$ cpp = $4.8P_0$ and $P_2 \simeq -70$ cpp = $-0.014P_0$, which agrees well with the values one can measure directly from the pulse-stack in Fig. 1. Notice that besides the primary drift feature also its second harmonic is clearly detected in the 2DFS (in the top left corner).

[3] http://pulsar.princeton.edu/tempo/

2.3. Analysis of the drift-features

If there appears to be a drift feature in the 2DFS that is clearly not produced by RFI its significance and the values P_2 and P_3 are determined by calculating the centroid of a rectangular region in the 2DFS containing the feature.

Any (significant) asymmetry in the 2DFS about the vertical axis indicates that there exists a preferred drift direction of the subpulses. For some pulsars the bottom panel of the 2DFS peaks at zero, but the peak has asymmetric wings which indicates that the subpulses have a preferred drift direction (see for example PSR B0823+26 in Fig. A.3). Drifters (pulsars with drifting subpulses) are defined in this work as pulsars which have at least one feature in their 2DFS which has a centroid with a significant finite P_2. Any structure in the vertical direction in the 2DFS and LRFS indicates a (quasi-periodic) intensity modulation from pulse to pulse. An increase of power toward the horizontal axis is called a low-frequency excess. As discussed in Paper I the P_2 values are just a rough measure of the presence of drift, its direction and the magnitude of the slope in an overall mean sense only.

Following Paper I the drifters are classified into three classes. PSR B0818–13 is a *coherent drifter* (class "Coh" in Table 2), because it has a vertically narrow drift feature and PSR J0421−0345 is a *diffuse drifter*, because it has a feature that is vertically broader than 0.05 cpp (Fig. 1). A diffuse drifter is indicated by "Dif" when its drift feature is clearly not reaching the alias borders ($P_0/P_3 = 0$ and $P_0/P_3 = 0.5$), as is the case for J0421−0345. This is not the case for PSR B0820+02, which has a feature that is clearly extended toward $P_0/P_3 = 0$ and it is therefore indicated by "Dif*" in Table 2. Notice also the minimum in the power along the vertical axis, which is an indication for drift reversals (see Paper I for details and simulations of this effect). If there is no significant finite value of P_2 found, but there is a preferred P_3 value, the modulation is classified as longitude stationary (class "Lon" in Table 2). These pulsars are not included in the statistics because it is not clear if and how this modulation is related to drifting subpulses.

3. Individual detections

3.1. Coherent drifters (class "Coh")

3.1.1. Known drifters (class "Coh")

B0148−06: both components of the pulse profile of this pulsar show drifting subpulses with the same P_3 value and drift direction (see Fig. A.17). The drift bands are clearly visible in the pulse-stack. This is consistent with results reported by Biggs et al. (1985), who discovered the drifting subpulses at 645 MHz. Interestingly, the drifting is most prominent in the trailing component, while in the 21-cm data the most prominent drifting was found in the leading component. This could be related to the change in the relative peak intensities of the pulse profile.

B0320+39: this pulsar is known to show very regular drifting subpulses (Izvekova et al. 1982), which is confirmed by the very narrow drift feature in our observation (Fig. A.1). Notice that the first harmonic is visible as well $P_0/P_3 \simeq 0.24$ cpp. Izvekova et al. (1993) have shown that drifting at both 102 and 406 MHz occurs in two distinct pulse longitude intervals and that the energy contribution in the drifting subpulses is less at higher frequencies, a trend which continued in the 21-cm data. The drift feature in the 2DFS shows a clear horizontal structure caused by a subpulse phase step in the drift bands. At both 328 MHz and 1380 MHz the drift bands of PSR B0320+39 are known to show a phase step (Edwards et al. 2003; and Edwards & Stappers 2003b, respectively). This is the same observation as used by Edwards & Stappers (2003b).

B0809+74: the subpulse drift is detected with a very high S/N in the 2DFS (Fig. A.3) and at least two higher harmonics are detected as well. There is no evidence for a horizontal structure in the feature in the 2DFS such as detected in the 21-cm data. This is expected, because the phase step in the drifting subpulses is only present at high frequencies (Wolszczan et al. 1981, at 1.7 Ghz; Prószyński & Wolszczan 1986, at 1420 MHz; and Edwards & Stappers 2003b, at 1380 MHz). The drift rate is affected by nulls (Taylor & Huguenin 1971) and detailed analysis of this phenomenon allowed van Leeuwen et al. (2003) to conclude that the drift is not aliased for this pulsar. Notice that the drift-feature is vertically split, which corresponds with the main drift-mode and an (about 7%) slower drift-mode. This is consistent with the decrease in driftrate observed by van Leeuwen et al. (2002). In Fig. 12 of Lyne & Ashworth (1983) a similar split of the feature can be seen.

B0818−13: this pulsar has a clear drift feature that contains almost all the power in the 2DFS, as well as a very clear second harmonic (Fig. A.3). The first fifty pulses of the observation are plotted in the left panel of Fig. 1. The drift feature has a horizontal structure similar to that observed at 21 cm. The modulation phase profile is much more complex at this frequency and seems to consist of at least four distinct pulse longitude ranges where the drift bands are linear. A decrease of the drift rate in the middle of the pulse profile has been reported at 645 MHz by Biggs et al. (1987). The longitude resolved modulation index shows a minimum at the position of the start of the subpulse phase swing (consistent with Biggs et al. 1987), something that is also observed for the phase steps of PSR B0320+39. This phase swing seems to be related to the complex polarization behavior of the single pulses as observed by Edwards (2004). Lyne & Ashworth (1983) found that the nulling in this pulsar interacts with the drifting subpulses such that the drift-rate increases after a null. Janssen & van Leeuwen (2004) confirmed this effect and argued that the drifting subpulses of this pulsar are aliased. The feature in the side panel of the LRFS peaks at $P_3 = 0.211$ cpp. Interestingly, this feature is not symmetric but there appears to be an additional overlapping component that peaks at $P_3 = 0.219$ cpp. This would correspond with a drift-mode that is 4% faster, however this feature is just too weak to be significant. Nevertheless this feature would be consistent with the drift-null interaction reported by Janssen & van Leeuwen (2004) and Lyne & Ashworth (1983).

B1540−06: this pulsar has a clear drift feature that contains almost all the power in the 2DFS (Fig. A.4). The positive drift direction is consistent with that reported by Ashworth (1982) at 400 MHz and the drifting detected in the 21-cm data. Interestingly, there is no indication that the trailing part of the pulse profile has an opposite drift direction, as found in the 21-cm data.

B1633+24: the 2DFS of this pulsar shows a clear drift feature close to the $P_3 = 2P_0$ alias border (Fig. A.5), consistent with the reported drifting of Hankins & Wolszczan (1987) at 430 MHz. This pulsar is not included in the statistics because it is just too weak to be part of the source-list. This pulsar was not observed at 21 cm.

J1650−1654: this pulsar shows a weak but clear drift feature in its 2DFS (Fig. A.6), confirming the drifting discovered in the 21-cm data. In the 21-cm data the feature seems to show horizontal structure, which could indicate that the drift bands are curved or show a phase step. At 92 cm the S/N is too low to say anything more about this. As observed at 21 cm, there is also a low-frequency excess.

B1702−19: the pulse profile of this pulsar has an interpulse (Biggs et al. 1988) and we discovered in the 21-cm data that both the main- and the interpulse show a drift feature and with the same P_3 value. At 92 cm there is no significant modulation found in the interpulse (likely because the interpulse is weaker at this frequency), but the drift feature in the main pulse is confirmed (Fig. A.6). The main- interpulse interaction of PSR B1702−19 is discussed by Weltevrede et al. (2007).

B1717−29: a very narrow drift feature is seen in both the LRFS and the 2DFS of this pulsar (Fig. A.6), confirming the drifting discovered at 21 cm and demonstrating that coherent drifting can be found in low S/N observations. Most of the power is in the drifting subpulses.

B1819−22: the 2DFS of this pulsar very clearly shows a drift feature (Fig. A.8), confirming the drifting discovered at 21 cm. At that frequency the feature was broadened by drift-mode changes, which is not the case in this observation. The P_3 in the 92-cm data is consistent with the slow drift-mode found at 21 cm. Notice also that there is a low-frequency excess, which is much stronger than at 21 cm. This low-frequency excess is probably related to "nulls", which appear at low frequencies instead of the fast drift-mode observed in the 21 cm data. Simultaneous multi-frequency observations will be required to prove this interpretation and if it turns out to be true, this pulsar would resemble PSR B0031−07 (Smits et al. 2005, 2007). The drifting subpulses can be seen by eye in the pulse-stack and this pulsar also appears to show real nulls (which are most clear at 21 cm), something which has not been reported for this pulsar before.

J1901−0906: the trailing component of this pulsar shows a clear and narrow drift feature in its 2DFS, which is not detected in the leading component (Fig. A.20). However the 2DFS of the leading component shows a drift feature with a larger P_3. This is consistent with the drifting discovered in the 21-cm data, so it is now shown in two independent measurements that both components have drifting subpulses with a different P_3.

B1918+19: this pulsar is shown to be a drifter with at least four drift modes at 430 MHz (Hankins & Wolszczan 1987). In our observation we see, besides the strongest feature (the "*B*" mode), also a $P_3 = 5.9 \pm 0.2P_0$ feature ($P_2 = 30^{\circ}{}^{+25}_{-7}$), which is the "*A*" mode. There is also a low-frequency excess at $P_3 = 70 \pm 30P_0$ (Fig. A.12), which is possibly related to the mode-switching. The drifting subpulses can be seen by eye in the pulse-stack. Drifting subpulses were not seen in the 21-cm observation, which could possibly be because of a too low S/N.

B2043−04: this pulsar has a very clear and sharp drifting subpulse feature in its 2DFS (Fig. A.14), which confirms the drifting discovered in the 21-cm data. Closer inspection shows that the drift feature appears to be extended toward the alias border. These apparent variations in the drift-rate could be related to the small P_3 values in combination with intensity fluctuations of the subpulses. Almost all the power is in the drift subpulses.

B2303+30: this pulsar is known to drift close to the alias border (e.g. Sieber & Oster 1975, at 430 MHz). This is also seen in our observation as a clear double-peaked feature in the 2DFS exactly at the alias border (Fig. A.16). This suggests that the apparent drift direction changes during the observation because the alias changes constantly. At both frequencies the same drift direction dominates. The change of drift direction can clearly be seen by eye in the pulse-stack and also in the pulse-stacks shown in Redman et al. (2005). These authors show that, besides this $P_3 \approx 2P_0$ "*B*" drift mode, there is occasionally also a $P_3 \approx 3P_0$ "*Q*" drift mode if the S/N conditions are good. The feature in the 2DFS seems to be extended all the way up to $P_0/P_3 \simeq 0.3$, but there is no evidence that this is associated with a (quantized) drift-mode. There is also a strong low-frequency excess, probably caused by nulling. This is all consistent with the 21-cm data.
B2310+42: the two components of this pulsar are clearly drifting at the alias border (Fig. A.22). The drift feature in both components are clearly double peaked, so the alias mode is probably changing during the observation. The dominant drift direction (at both frequencies) is consistent with the positive drifting found by Ashworth (1982) at 400 MHz. The low-frequency excess of the leading component is clearly drifting with two signs as well ($P_2 = 240° \pm 50$,$P_3 = 15.7 \pm 0.6P_0$ and $P_2 = -50° \pm 30$, $P_3 = 60 \pm 7P_0$), consistent with our 21-cm results. At low frequencies the low-frequency excess of the trailing component shows a preferred drift direction ($P_2 = -130° \pm 20$, $P_3 = 19 \pm 2P_0$) and this feature in the 2DFS appears to be more detached and higher above the horizontal axis compared with the 21-cm observation.
B2315+21: drifting with a negative drift direction has been reported for this pulsar at 430 MHz by Backus (1981), which is confirmed in our spectra (Fig. A.23). No drifting subpulses were found in the 21-cm data. Interestingly, the drift feature in the 92-cm data is only found in the leading half of the profile. This suggests that the non-detection of drifting subpulses in the 21-cm data could be because of a profile evolution, although the S/N of the 21-cm data is somewhat lower.

3.1.2. New drifters (class "Coh")

B0105+65: the pulsar shows a clear drift feature in the 2DFS at the $P_3 = 2P_0$ alias border that contains most of the power (see Fig. A.1). In the LRFS of the 21-cm data there appears to be a $P_3 = 2P_0$ modulation as well (although much weaker) and it did not show up in the 2DFS as a feature with a preferred drift direction. Although the S/N was slightly lower at 21 cm, this seems at most only part of the explanation. The number of recorded pulses was very similar at both frequencies and there seems to be not much frequency evolution in the pulse-profile. The drift-feature in the 2DFS of the 92-cm data appears to be split into a component left and right of the vertical axis, suggesting that the subpulses are drifting in both directions during the observation or that the drift-bands are highly non-linear. The P_2 value in the table is for the centroid of the whole feature, but it peaks at $P_2 = -7.7° \pm 0.3$.
J0459−0210: the 2DFS of pulsar has a very strong drift feature containing virtually all the power in the 2DFS (Fig. A.2). The feature has a clear horizontal structure, which is probably because there is a subpulse phase difference between the two components of the profile. This pulsar was not observed at 21 cm. Notice that the pulse profile is similar to that of PSR B0320+39 at 103 MHz (Kuz'min & Losovskii 1999), where the two out-of-phase drift components apparently are more separated than at higher frequencies.
B1730−22: there is a clear detection of a drift-feature in the spectra of this pulsar (Fig. A.7). In the 21-cm data there is probably modulation at a similar P_3 value, but it was very weak. Possibly the drifting subpulses were not discovered at 21 cm because of the remarkable profile evolution or because the 21-cm observation was too short.
J2302+6028: this pulsar shows a strong drift feature in its 2DFS (Fig. A.16). This pulsar was not observed at 21 cm.

3.2. Diffuse drifters (classes "Dif" and "Dif*")

3.2.1. Known drifters (classes "Dif" and "Dif*")

B0031−07: this pulsar shows a broad drifting feature in its 2DFS (Fig. A.1). Three drift modes have been found for this pulsar by Huguenin et al. (1970) at 145 and 400 MHz. In our observation most power in the 2DFS is due to "*B*"-mode drift ($P_3 = 6P_0$) at 0.15 cpp. The slope of the drift bands change from band to band (e.g. Vivekanand & Joshi 1997), causing the feature to extend vertically in the 2DFS. The "*A*"-mode drift ($P_3 = 12P_0$) is visible as a downward extension of the main drift feature to 0.08 cpp. At 0.25 cpp the "*C*"-mode drift ($P_2 = -19^{\circ+2}_{-1}$ and $P_3 = 4.1 \pm 0.1P_0$) is visible as well. The feature at 0.3 cpp is the second harmonic of the main drift feature. In the 21-cm data the "*A*"-mode dominated over the "*B*"-mode, which dominates this 92-cm observation, and the "*C*"-mode was not detected. This is consistent with the multi-frequency study of Smits et al. (2005, 2007).
B0136+57*: the drift feature discovered in the 21-cm data is confirmed (Fig. A.1) and it is, as observed at 21 cm, strongest in the leading part of the pulse profile. It appears that the feature extends toward the horizontal axis and there is a hint of a low-frequency excess.
B0149−16: the 2DFS of both components of this pulsar show a drift feature with the same preferred drift direction (Fig. A.17). This pulsar was discovered to have drifting subpulses in the 21-cm data. Probably because of a higher S/N in the observation at 92 cm, the drifting is detected in both components and the features are broader than could be found in the 21-cm data. Therefore this pulsar is classified a diffuse drifter, and not as a coherent drifter.
B0301+19*: both components shows a broad drift feature in their 2DFS (Fig. A.17). This pulsar is observed to have linear drift bands in both components of the pulse-stack (Schönhardt & Sieber 1973, at 430 MHz), which is confirmed by this observation. The feature in the trailing component is reported to be broader than in the leading component (Backer et al. 1975, also at 430 MHz), probably because drifting subpulses appear more erratic in the trailing component. This is also the case is our observation, as especially the feature in the trailing component is broad and may even be extended toward the alias border. The measured value for P_3 is significantly larger for the trailing component. Interestingly, no drifting is detected in the leading component at 21 cm. The LRFSs at both frequencies are similar, which suggest that the same two components are observed at the two frequencies.
B0329+54*: the power in the LRFS of this pulsar peaks toward $P_0/P_3 = 0$, as is reported by Taylor & Huguenin (1971) for low frequencies (Fig. A.17). The plotted 2DFSs are of the leading and trailing part of the central peak. The trailing part of the central peak shows a broad drift feature in its 2DFS and the subpulses have a preferred positive drift direction, something that is also reported by Taylor et al. (1975) at 400 MHz. The leading

peak and leading part central peak also show a preferred positive drift direction ($P_2 = 250^\circ \pm 150$ and $200^\circ \pm 150$ and $P_3 = 6 \pm 2$ and 4 ± 2 respectively). The right peak does not show significant drifting. This is very similar to the 21-cm results, except the preferred drift direction of the left part of the central peak which was found to be negative at high frequencies. Possibly this means that the left part of the central peak just does not have a stable preferred drift direction (at both frequencies). The value of P_3 in the leading part of the central peak appears to be, as observed at 21 cm, on average smaller than in the trailing part of the central peak. This is possibly because the drift feature, if it really is a drift feature, is much weaker and therefore the spectrum is much flatter. Notice the very high modulation index between the leading and central component of the profile.

B0450+55*: the drift feature of the main component that was discovered in the 21-cm data is confirmed (Fig. A.2). The S/N of the data is unfortunately not enough to detect any subpulse modulation in the leading component, which is almost merged with the main component at 92 cm. This component was found to have an opposite preferred drift direction and a different P_3 value.

B0525+21*: subpulse modulation without apparent drift as well as some correlation between the subpulses of the two components of the pulse profile has been detected for this pulsar by Backer (1973) at 318 MHz, and Taylor et al. (1975) at 400 MHz. We find that the leading component shows a broad drift-feature with a preferred negative drift direction (Fig. A.18), which confirms the drifting discovered in the 21-cm data. The feature is possibly extended toward the $P_3 = 2P_0$ alias border. In this observation there is no evidence for a drift feature with opposite drift direction in the trailing component, as found in the 21-cm data.

B0628−28*: sporadic drifting subpulses with a positive drift direction have been reported for this pulsar by Ashworth (1982) at 400 MHz, but the P_2 and P_3 values could not be measured. The positive drift direction has been confirmed in Paper I as a clear excess of power in the right half of the 2DFS. At this frequency (Fig. A.18) the drifting is also detected and it originates from the trailing half of the pulse profile (see the bottom panel of Fig. A.18). Interestingly, the leading half of the pulse profile shows a quasi-periodic feature with a significantly longer period. A similar behavior is revealed in the 21-cm data after re-analysing the data, however there it is less clear. There is no indication that P_3 is different at the two frequencies. The drift feature in the 2DFS of the trailing half of the profile is not separated from either alias border, like observed at 21 cm.

B0751+32*: the 2DFS of the leading component of the pulse profile of this pulsar shows a very broad drift feature with a negative P_2 value (Fig. A.18). This can be seen in the bottom plot of the first 2DFS, which shows an excess of power in the left half. This confirms the drifting found in the 21-cm data and as reported by Backus (1981) at 430 MHz. Interestingly, the trailing component shows a faster periodicity (without measured preferred drift direction), which was not significant in the 21-cm data (possibly because a lower S/N). Both components also show a strong long period fluctuation ($P_3 = 60 \pm 20P_0$ and $P_3 = 70 \pm 20P_0$ respectively) as was also reported for the 21-cm data. These features are not significantly offset from the vertical axis.

B0820+02*: the positive drifting, as has been reported by Backus (1981) at 430 MHz, is clearly detected in the 2DFS (Fig. A.3). The drift feature is spread out over the whole P_3 range, especially towards the $P_0/P_3 = 0$ axis where it is clearly double peaked (the region between the dashed lines). This means that the drift direction could be changing during the observation. The tabulated P_2 and P_3 values are for the main feature between $P_0/P_3 = 0.1$ and 0.3 cpp. In the 21-cm data (which was much shorter) no drifting was found, probably because of a too low S/N.

B0823+26*: only the pulse longitude range of the main pulse is shown in Fig. A.3 and the 2DFS of the leading component of the main pulse shows a clear broad drift feature. Backer (1973) found that at 606 MHz this pulsar shows drifting in bursts, but the drift direction is different for different bursts. In our observation there seems to exist a clear preferred subpulse drift direction, confirming the preferred drift direction found in the 21-cm data.

B0834+06*: the 2DFS of both components show a drift feature at the $P_3 = 2P_0$ alias border (Fig. A.19). This confirms the drifting detected by Sutton et al. (1970) at a similar frequency. Both components showed a positive drift with $P_3 \simeq 2P_0$ at 21 cm. However at this frequency the leading component shows a negative drift, which is consistent with the direction found by Sutton et al. (1970). Possibly the relatively short observation in combination with a changing alias mode is responsible for the different preferred drift directions found at the two frequencies. The trailing component does possibly show a positive drift, although this is not very significant. Besides this feature there is a very broad drift feature with a positive preferred drift direction in the leading component ($P_3 = 3.5 \pm 0.6P_0$ and $P_2 = 45^\circ \pm 6$). The circulation time of this pulsar ($\hat{P}_3$) has been measured by Asgekar & Deshpande (2005).

B0919+06*: the power in the 2DFS (Fig. A.4) is significantly offset from the vertical axis over the whole P_3 range, confirming the preferred negative drift direction discovered in the 21-cm data. Interestingly, the drift feature is much less clear at this frequency and there is also no sign of the low-frequency excess. Notice that the main component seems to be split into two components. This can also seen clearly in the LRFS, which shows subpulse modulation in two distinct pulse longitude ranges. No drifting has been reported for this pulsar by Backus (1981) at 430 MHz.

B0950+08*: drifting has been reported for this pulsar (e.g. Backer 1973; and Wolszczan 1980) with a variable $P_3 \simeq 6.5P_0$. This is confirmed in the 2DFS of our observation (Fig. A.4) wherein subpulse modulation is seen over the whole P_3 range with a (weak) preferred negative drift direction. In the 21-cm data there was no significant drifting detected, which could be because the lower number of pulses or because it is only detectable at low frequencies. The observing frequency of Backer (1973) was 430 MHz, but it is not mentioned in Wolszczan (1980).

B1039−19: both components of this pulsar show a clear, broad drift feature in its 2DFS with the same preferred positve drift direrection (Fig. A.19). This confirms the drifting discovered in the 21-cm data.

B1112+50*: a broad feature offset from the vertical axis is detected in the 92-cm data (Fig. A.4). This pulsar is known to show nulling and pulse profile mode switching and in one of these modes (positive) drifting subpulses are reported (e.g. Wright et al. 1986, at 1412 MHz). According to Wright et al. (1986) the leading component is weak when there are no drifting subpulses in the trailing component. Reconsidering the 21-cm data it seems that the there was no drift-feature detected at 21 cm because in that observation the leading component was strong, showing that the emission was dominated by the mode without drifting subpulses.

B1133+16*: the 2DFS of both components of this pulsar (Fig. A.19) show a very broad drift feature with a preferred positive drift direction. The trailing component shows also a long period drift feature ($P_2 = 120^\circ \pm 50$ and $P_3 = 30 \pm 8P_0$), consistent with the 21-cm data. At 92 cm also the leading component shows a long period fluctuation ($P_3 = 33 \pm 5P_0$). This positive drifting is consistent with the drifting found by Nowakowski (1996) at 430 and 1418 MHz, and by Backer (1973) & Taylor et al. (1975) at low frequencies. There is some indication that the long period feature is related to nulls which appear to be quasi-periodical.

B1237+25*: the 2DFS of the outer components of the pulse profile are clearly drifting with opposite drift direction (they are plotted in Fig. A.19). The 2DFS of the second component (which is not plotted) also shows a preferred drift direction ($P_2 = 6^\circ \pm 3$, $P_3 = 2.77 \pm 0.03$). The 92-cm and 21-cm results are similar, except that the third component shows a clear low-frequency excess and that the fourth component does not show a preferred drift direction at low frequencies. Notice also that the modulation index profiles are very different at the two frequencies. This is all consistent with Prószyński & Wolszczan (1986) at 408 and 1420 MHz, and Srostlik & Rankin (2005) at 327 MHz.

B1508+55*: Taylor & Huguenin (1971) report that the subpulse modulation of this pulsar is unorganized and without a preferred drift direction or a particular P_3 value at 147 MHz. However the 21-cm data revealed a broad drift feature, which is offset from the vertical axis over the whole P_3 range. The drifting subpulses are confirmed in the 2DFS of the 92-cm data (Fig. A.19), where the drift feature appears much stronger. Moreover, we find that the P_3 values for the leading and trailing components are significantly different from each other. The central component shows a low frequency excess without a preferred drift direction, which was also reported by Taylor & Huguenin (1971). All these details were not found at 21 cm, possibly because of a lower S/N and a shorter observation duration or because of the profile evolution with frequency.

B1530+27*: the 2DFS of this pulsar shows a preferred negative drift direction (Fig. A.4), which is confirmed in another observation. A negative drift direction was also found by Backus 1981 at 430 MHz. Notice that the feature is extended over the whole P_3 range and that the vertically integrated power in between the dashed lines appears to be double peaked. This could mean that the drift direction is constantly changing or that the drift-bands are highly non-linear. This pulsar was not observed at 21 cm.

B1604−00*: the very broad feature has a preferred positive drift direction (Fig. A.5), which confirms the discovery in the 21-cm data. There is a strong low-frequency excess as well at both frequencies. It is difficult to characterize the single pulses. It sometimes looks like there is only one component on at the time while there is also a short term flickering. The component switching can be more abrupt or more like a drift-band. The component switching would be consistent with the double peaked low-frequency excess that appears in the 2DFS.

B1612+07*: the power in the 2DFS is offset from the vertical axis over the whole P_3 range (Fig. A.5), which is consistent with the negative subpulse drift that has been reported by Backus (1981) at 430 MHz for this pulsar. At 92 cm this pulsar has a strong low frequency excess. Although the S/N was lower at 21 cm, this cannot explain why the low-frequency excess was not observed at 21 cm.

B1642−03*: drifting is observed to occur in bursts in this pulsar with both drift directions (Taylor & Huguenin 1971, at 400 MHz) and also Taylor et al. 1975 report that there is no preferred drift direction at 400 MHz. The 2DFS of our observation (Fig. A.5) reveals a clear broad drift feature with a clear preferred negative drift direction, so this pulsar is classified as a drifter. Because the observation contains almost 15 000 pulses and the drift feature is clearly offset from the vertical axis the detected preferred negative drift direction seems highly significant. Interestingly, compared with Paper I the opposite drift direction seems to dominate and also the P_3 values seems to be significantly different. At both frequencies the alias border seems to be crossed on both sides, because the feature is extended over the whole P_3 range and seems double peaked. Notice also that the LRFS are very different at the two frequencies. While at 21 cm the quasi-periodic feature in the LRFS is centered in the middle of the main component, at 92 cm it is centered at the leading edge of the profile. Because the observations at the two frequencies were not simultaneously recorded, it is impossible to prove that these differences are because of a frequency dependence in the drifting phenomenon rather than a time-dependence.

B1738−08*: the drifting subpulses discovered in both components in the 21-cm data is confirmed (Fig. A.20). There is, consistent with the 21-cm data, also a low frequency excess in both components, possibly because of nulling (not reported in the literature). The drifting subpulses and the nulls can be seen by eye in the pulse-stack. The observations are too short to make the difference in P_3 significant.

B1753+52*: the trailing part of the pulse profile shows a broad drift feature in its 2DFS (second 2DFS in Fig. A.20), consistent with the drift feature discovered at 21 cm. There is no evidence for drifting subpulses in the rest of the profile (first 2DFS). The drifting can be seen by eye in the pulse-stack at both frequencies.

B1857−26: the components at both edges of the pulse profile are drifting with the same drift direction, which can be seen in Fig. A.20 as an excess of power in the 2DFS at positive P_2 values. The drift bands are sometimes visible to the eye in the pulse-stack. The center part of the pulse profile does not show drifting in its 2DFS and is therefore not plotted. This confirms the drifting discovered in the 21-cm data. Notice the dramatic profile evolution with frequency. Nevertheless the LRFSs at both frequencies are similar, making it possible to identify which component corresponds to which at the other frequency.

B1900+01*: drifting was clearly detected over the whole P_3 range in the 21-cm data, which is (although weaker) confirmed in this observation (Fig. A.11).

B1917+00*: this pulsar shows a broad drifting component in its 2DFS, which is visible in the bottom plot as an excess of power at positive P_2 (Fig. A.12). This observation confirms the drifting subpulses discovered in the 21-cm data. The drift feature is smeared out over the whole P_3 range. According to Rankin (1986) a much longer $P_3 \simeq 50P_0$ value without a measured P_2 was reported in a preprint by Nowakowski & Hankins, but to the best of our knowledge the paper was never published. Notice also the high modulation index because of occasional strong pulses.

B1919+21: both components of this pulsar have a strong drift feature in their 2DFS (Fig. A.21) and the feature of the leading component probably shows horizontal structure, similar to that observed in the 21-cm data. The reason for this horizontal structure in the drift feature is, similar to PSR B0320+39, that there is a subpulse phase step in the drift bands. This observation confirms the reported phase step by Prószyński & Wolszczan (1986) seen at 1420 MHz. There is also a strong low-frequency excess detected in both components and the leading component shows a $P_3 = 2P_0$ flickering. This observation is too short to derive fluctuation spectra with high resolution. By comparing the

LRFSs at the two frequencies it seems that the three more separated components in the average pulse profile at 21 cm merge at lower frequencies.

B1923+04*: this pulsar shows in its 2DFS a very broad drift feature at the $P_3 = 2P_0$ alias border (Fig. A.12). It is clearly double peaked, which could indicate that the drift direction changes constantly during the observation. This pulsar was not part of the 21-cm survey. The positive drift is consistent with the findings of Backus (1981) at 430 MHz.

B1929+10*: the LRFS (Fig. A.13) shows a very clear feature with $P_3 = 11.4 \pm 0.6P_0$, comparable to what was found by Nowakowski et al. (1982) at 0.43, 1.7 and 2.7 GHz. Oster et al. (1977b) suggested, using 430 MHz data, that this pulsar has drifting subpulses. Backer (1973) reported two features in the LRFS of this pulsar at 606 MHz and the short period feature appeared to have a negative drift and the long period fluctuations appeared to be longitude stationary. Also in our data the long period fluctuations do not have a preferred drift direction, while the shorter period fluctuations (between the dashed lines) show a preferred negative drift. Also in the 21-cm data a negative drift direction was detected for the short period feature, but the long period feature shows a positive drift. The latter could be because the 92-cm observation was much longer or because this feature only shows a preferred drift at high frequencies. There is no evidence for a $P_3 \simeq 2P_0$ modulation at this frequency.

B1933+16*: this pulsar shows subpulse modulation over the whole P_3 range (Fig. A.13). Backer (1973) found that there is no preferred subpulse drift direction at 430 MHz, however regular drifting with $P_3 \simeq 2.2P_0$ has been reported by Oster et al. (1977b) at 430 MHz. We found a preferred positive drift direction in a broad feature near the $P_3 = 2P_0$ alias border in the 21-cm data, but in the 92-cm data there is a clear preferred negative drift direction with a much larger P_3.

B1944+17*: this pulsar shows a clear drift feature in its 2DFS (Fig. A.13) and the drifting can clearly be seen by eye in the pulse-stack. The feature is broadened because this pulsar shows drift-mode changes (Deich et al. 1986, at both 430 and 1420 MHz). The $P_3 = 13P_0$ "*A*"-mode drift is visible in the 2DFS at 0.075 cpp and the $P_3 = 6.4P_0$ "*B*"-mode drift (0.16 cpp) does not appear in the spectrum as a peak, although the centroid of the power in the 2DFS is offset from the vertical axis up to at least 0.2 cpp. There is also evidence for a broad feature in a different alias mode at $P_3 \simeq 20P_0$, although it appears to be weaker than in the 21-cm data. It could be that the zero drift "*C*"-mode (Deich et al. 1986) is a drift mode for which the drift direction is changing continuously. The modulation index is higher in the 92-cm data, possibly because there were longer nulls in that data-set.

B1953+50*: this pulsar showed a very clear broad drift feature in its 2DFS at 21 cm. At this frequency there is also a preferred positive drift direction (Fig. A.14), confirming the discovery at 21 cm, but the drifting subpulses are much less pronounced. The measured values for P_3 are slightly different in the two observations, but the observations are too short to state that this is really significant. The feature is reaching the $P_0/P_3 = 0$ alias border and it is double peaked, suggesting that the drift direction changes during the observation. This is probably also the case at 21 cm, although it is less clear.

B2016+28*: the 2DFSs show a very broad drifting feature (Fig. A.21), which is caused by drift mode changes (e.g. Oster et al. 1977a, at both 430 and 1720 MHz). Interestingly, at this frequency (382 MHz), there is no sign of the strong $P_3 \simeq 20P_0$ drift mode as seen in the leading component in the 21-cm data. Also Oster et al. 1977a concluded that the drift-rate distribution is frequency dependent. Also interestingly, the P_3 values are significantly different in the two components. The drift bands can be seen by eye in the pulse-stack. The differences between the two frequencies is really a frequency dependence of the drift phenomenon, because the observations at the two frequencies were recorded simultaneously. The pulse profile has also evolved significantly with frequency.

B2020+28*: the two components of the pulse profile show a broad feature close to the alias border. A strong even-odd modulation was also reported by Backer et al. (1975) at 430 MHz and by Nowakowski et al. (1982) at 1.4 GHz and the trailing component was shown to have a preferred drift direction. The leading component was shown to have a opposite preferred drift direction in the 21-cm data, which is confirmed in the 92-cm data (Fig. A.21). There is no evidence that the feature extends over the alias border, although the feature is not clearly separated from the alias border.

B2021+51*: the two components have a broad drift feature with a preferred drift direction (Fig. A.21), consistent with e.g. Oster et al. (1977b) at 1720 MHz and the 21-cm data. The drift-rate changes by a large factor during the observation, which was also observed by Oster et al. (1977b). They also suggested that perhaps the apparent drift direction changes sporadically. There is no clear evidence from the fluctuation spectra of the observation that the alias mode is changing. The 92-cm observation was much shorter than the 21-cm observation, but nevertheless the drift feature appears to be much weaker at 92 cm. Also the P_3 value seems to be significantly different at the two frequencies. Because the observations at the two frequencies were not simultaneously recorded it is not possible to prove that these differences are really because a frequency dependence of the drifting phenomenon rather than a time-dependence. Notice that the pulse profile and the modulation index profiles are also very different at the two frequencies.

B2044+15*: especially the 2DFS of the trailing component of the pulse profile convincingly shows a broad drifting feature (Fig. A.22), which was also the case at 21 cm. These observations confirm the drifting subpulses found by Backus (1981) at 430 MHz. It is not clear if the feature is connected to the $P_0/P_3 = 0$ alias border, because the S/N of both observations was low.

B2045−16*: subpulses with a negative drift have been reported for the outer components and the the fluctuation feature is observed to be broad with P_3 values between 2 and $3P_0$ (Oster & Sieber 1977, at 1720 MHz; Nowakowski et al. 1982, at 1.4 and 2.7 GHz; and Taylor & Huguenin 1971, at low frequencies). In our observation all three components show negative drifting and the 2DFSs of the leading and trailing component are plotted in Fig. A.22. The middle component shows a $P_2 = -100^\circ \pm 50$ with $P_3 = 4 \pm 2P_0$ feature. At 21 cm positive drifting was observed in the trailing component and no drifting in the other components and the drift-feature was classified as coherent. As noted in Paper I, the 21-cm observation was very short and therefore it is very well possible that the results at 21 cm are caused by a sporadic event rather than a systematic behavior of the drift phenomenon. The middle component also shows a $P_3 = 32 \pm 2P_0$ feature without a preferred drift direction at 92 cm, but because the observation at 92 cm was also relatively short, it is not clear if this is significant.

B2110+27*: this pulsar shows drifting over the whole P_3 range in its 2DFS (Fig. A.15), confirming the drifting discovered at 21 cm. Also at 92 cm, especially the lower part of the 2DFS is double peaked, which could suggest that the alias mode is constantly changing during the observation. In the pulse-stack

drifting is visible directly. The drift bands are probably distorted by nulls, causing the drift feature in the 2DFS to be extended over the whole P_3 range. There is also a strong $P_3 \simeq 2P_0$ modulation. Some single drift bands with positive drifting can be seen in the pulse-stack as well as a $P_3 \simeq 2P_0$ flickering. Drift bands with an apparent opposite drift direction can be seen as well, although they also show the $P_3 \simeq 2P_0$ flickering. Nulling has not been reported in the literature before for this pulsar.

B2111+46*: it has been reported that this pulsar shows subpulse drift with a positive and negative drift direction, but without either dominating (Taylor et al. 1975, at 400 MHz). We find that there is systematic drift in the leading component (Fig. A.22), which confirms our detection in the 21-cm data. The feature is not well separated from the $P_3 = 2P_0$ alias border. Notice also the high modulation index at 92 cm, especially in the outer components.

B2148+63*: at 21 cm the 2DFS of this pulsar showed a broad, triple, well separated features at the $P_3 = 2P_0$ alias border, which is most likely caused by apparent drift direction changes. The 2DFS of the 92-cm data shows a similar feature (Fig. A.15), confirming both the preferred drift direction and the apparent drift direction changes discovered at 21 cm. The drift feature appears to be much weaker at 92 cm, which is surprising because this observation has a higher S/N and contains more pulses.

B2154+40*: the very broad drift feature discovered at 21 cm is confirmed in this observation (Fig. A.15) and at this frequency the drift feature is also mainly produced by the leading component of the pulse profile and is possibly extended toward the alias borders. The observations at the two frequencies have comparable S/N and about the same number of recorded pulses, but nevertheless the feature is strongest at 92-cm.

B2255+58*: the drift feature discovered at 21 cm is confirmed (Fig. A.16). At 21 cm the feature in the 2DFS was clearly horizontally split which might be because of a subpulse phase step. At this frequency there is no sign of a similar feature, which could be related to the profile shape evolution that causes the pulse profile to become double at higher frequencies.

B2319+60*: this pulsar shows a clear drift component in the 2DFS of the trailing component of the pulse profile and a less clear drift component in the middle and leading component. In Fig. A.23 the 2DFS of the leading and trailing component are shown. For the feature in the central component $P_2 = 130^\circ \pm 80$ and $P_3 = 8 \pm 4P_0$ is measured. It has been found that this pulsar is a drift mode changer and that the allowed drift mode transitions follow certain rules (Wright & Fowler 1981, at 1415 MHz). In the 2DFS of the trailing component there is not much evidence for a stable $P_3 = 8P_0$ "*A*" drift mode or a stable $P_3 = 4P_0$ "*B*" drift mode, which could be because the observation is too short to fully characterize the different drift-modes. Nevertheless the preferred drift direction is detected in the trailing component. The leading component seems to show mainly the $P_3 = 3P_0$ abnormal mode, which is consistent with the results of Wright & Fowler (1981) who have shown that the abnormal mode is related to a profile mode change in which the leading component dominates the total emission. There is also a low-frequency excess, which is similar to the $P_3 \simeq 130P_0$ feature found in the 21-cm data probably related to the nulls (Ritchings 1976) or mode changes. Notice the high modulation index, especially in the outer components.

B2351+61*: the power in the 2DFS of this pulsar peaks toward low frequencies and the centroid is significantly offset from the vertical axis (Fig. A.16), confirming the preferred drift direction discovered in the 21-cm data.

3.2.2. New drifters (classes "Dif" and "Dif*")

J0421−0345: the 2DFS of this pulsar (Fig. A.1) shows a strong and clear detection of a drift feature that appears to be strongest in the trailing component. This pulsar was not observed at 21 cm.

B0942−13*: the 2DFS of this pulsar (Fig. A.4) shows a weak, but clear detection of a drift feature with a very short P_2 of only 2.5 ms. There is a hint that the feature is extended toward the $P_3 = 2P_0$ alias border and changes alias mode (similar to PSR B2148+63). This pulsar was not observed at 21 cm.

B1607−13*: there is a clear detection of drifting subpulses with a negative drift direction (Fig. A.5). The drifting subpulses are visible in the pulse-stack and the drifting subpulses are also confirmed in another observation. The drift feature is vertically extended, probably because of drift mode-changes. This pulsar was not observed at 21 cm.

J1652+2651*: the 2DFS of this pulsar shows a weak drift feature (Fig. A.6). The same feature is present in both the first and second halve of the data making us confident in the significance of this feature. This pulsar was not observed at 21 cm.

B1700−18: there is clear detection of subpulses with a negative drift direction and there is also a long period fluctuation that appears to have an opposite preferred drift direction (Fig. A.6). The drifting subpulses can be seen clearly by eye in the pulse-stack. This pulsar was not observed at 21 cm.

B1718−02: the 2DFS shows a clear broad drift feature (Fig. A.7). There is no evidence that the feature is extended to the $P_0/P_3 = 0$ alias border. This pulsar was not observed at 21 cm.

B1818−04*: the 2DFS shows a very broad feature with a preferred drift direction (Fig. A.8), which was not significant in the 21-cm data. The same preferred drift direction is detected in the first, middle and last part of the observation, making us confident in the significance. Interestingly, the 2DFS does not show a sign of a double peaked distribution, as reported for the 21-cm data, which could be related to the profile evolution. There is also a longitude stationary $P_3 = 22 \pm 3$ feature, which did not appear in the 21-cm data. It has been reported that the subpulse modulation is not well organized (Taylor & Huguenin 1971; and Taylor et al. 1975, both at 400 MHz).

B1839+56*: the 2DFS of this pulsar shows a low-frequency modulation with a preferred positive drift direction (Fig. A.9). Consistent results are obtained for the first and second half separately. Also the low-frequency excess in the 21-cm data seems to show the same positive preferred drift direction, but because of the relatively low number of pulses we were not confident in the significance.

B1905+39*: the 2DFS of both the leading and trailing part of the profile shows a drift feature (Fig. A.21), although it appears to be strongest in the trailing component. These features were not discovered in the 21-cm data, not surprisingly because of the lower S/N. The low frequency excess that was found in the 21-cm data is confirmed at this frequency ($P_3 = 27 \pm 8P_0$) and possibly also shows a preferred positive drift direction.

B2053+21*: both components of this pulsar show in the LRFS a low-frequency modulation (Fig. A.22). The power in the 2DFS of the trailing component is clearly offset from the vertical axis and shows a positive drift direction. The trailing components also show a short term ($P_3 = 2.3 \pm 0.2P_0$) fluctuation, which interestingly enough does not appear in the leading component. This pulsar was not observed at 21 cm.

B2217+47*: there is a (weak) preferred negative drift direction detected in the feature in the 2DFS of this pulsar (Fig. A.15), which exists in both halfs of the observation. This was not found in the 21-cm data, possibly because the observation contained

less pulses. At 147 MHz a flat spectrum was reported by Taylor & Huguenin (1971). The 2DFS shows also two vertical bands smeared over the whole P_3 range. This modulation is, as observed at 21 cm, primarily generated in the trailing part of the pulse profile. The interpretation is that there is a quasiperiodic intensity modulation in the pulses with a period of about 2.5 ms, but there is not much correlation in the positions of the subpulses from pulse to pulse. This quasi-periodicity is clearly visible in the single-pulses.

3.3. Longitude stationary drifters (class "Lon")

B0756−15: a low-frequency modulation was found in the 21-cm data. However this observation shows that the low-frequency excess is in fact a longitude stationary feature with a relative long P_3 (Fig. A.3). The feature in the 21-cm data is probably very similar, although with a lower number of recorded pulses the distinction between a low-frequency excess was harder to make.
B1541+09: a long period feature without preferred drift direction is detected in the LRFS and 2DFS of this pulsar (Fig. A.4). This is consistent with the low-frequency excess, mode changes and the organized, but short, drifts in both directions reported by Nowakowski 1996 at 430 MHz. In the 21-cm data no periodicity in the subpulse fluctuations could be measured, possibly because of a too low S/N and/or the drastic profile evolution. The horizontal bands in the spectra are fluctuation frequencies that were excluded because of RFI.
B1732−07: a clear long period feature without preferred drift direction is detected in the LRFS and 2DFS of this pulsar (Fig. A.7). This was not found in the 21-cm data, possibly because of the lower S/N.
B1737+13: especially the leading component shows a broad modulation feature with $P_3 \simeq 10P_0$ (Fig. A.20), consistent with the the $P_3 = 11-14P_0$ longitude stationary subpulse modulation without drifting reported by Rankin et al. (1988) at 1412 MHz. No drifting has been detected for this pulsar by Backus (1981) at 430 MHz and no fluctuation features were detected at 21 cm, most likely because of the much lower S/N.
B1811+40: there is a short period fluctuation in the spectra of this pulsar (Fig. A.8). The LRFS shows that this flickering appears mainly in the leading part of the profile, which is also clearly visible in the pulse-stack. It seems that the alias border might be crossed constantly. At 21 cm the spectra are remarkably featureless compared with the 92-cm result.
B1846−06: the 2DFS of this pulsar shows a broad fluctuation feature for which no significant preferred drift direction could be detected (Fig. A.10). The spectra look similar to that observed at 21 cm.
B1859+01: there is a broad feature without preferred drift direction detected (Fig. A.10). This pulsar was not observed at 21 cm.
B1907+10: a very clear long period feature is visible in the LRFS and 2DFS (Fig. A.11). This was not found to be significant in the 21-cm data, although it is possibly there as well (but weaker).
B1910+20: the leading component of the pulse profile shows a strong and vertically narrow feature in the LRFS (Fig. A.11) and no significant preferred drift direction could be detected. This feature appears also in the leading component of the 21-cm data, although weaker.
B1914+13: the spectra show a long period feature without a preferred drift direction (Fig. A.12). This modulation can be seen by eye in the pulse-stack. At 21 cm this pulsar was also observed to show a low-frequency excess, but it was not recognized as a longitude stationary subpulse modulation because the modulation appears to be weaker at high frequencies.
B1946+35: the LRFS and 2DFS of this pulsar show a strong low-frequency feature (Fig. A.13). No significant offset from the vertical axis has been detected in the 2DFS, confirming the longitude stationary feature that was detected also at 21 cm. At 21 cm a $P_3 = 33 \pm 2P_0$ was measured, so the P_3's appear to be different at the two frequencies. However the observations were relatively short, so possibly they were too short to obtain a good estimate for the average P_3 value.
B2327−20: a low-frequency excess has been measured at 21 cm. However at this frequency the feature appears to be quasi-periodic (Fig. A.16). This could be because the 92-cm observation was longer and has a higher S/N. This feature is most likely because of the nulls (Biggs 1992), which can clearly be seen by eye in the pulse-stack. The the two vertical bands at ±100 cpp (equals to ±3.5°) in the 2DFS are most likely related to the component separation.

3.4. Unconfirmed known drifters

B0037+56: the LRFS of this pulsar shows a low-frequency excess (Fig. A.1). The clear preferred drift direction discovered in the 21-cm data is not confirmed, possibly because of a lower S/N and number of recorded pulses.
B0138+59: a broad drift feature was found close to the horizontal axis in the 21-cm data. In the 92-cm observation there is no evidence for an offset from the vertical axis, but the low-frequency excess is confirmed (Fig. A.1). The S/N should have been enough to confirm the drifting at 92 cm. It could be that the drifting subpulses are very irregular and a longer observation is required at 92 cm to confirm the drift feature.
B0523+11: a weak drift feature has been discovered in the 21-cm data, which could not be confirmed in the 92-cm data (Fig. A.2). Nevertheless, the 2DFS shows a hint that there is a drift feature at this frequency as well, so the non-detection could possibly be explained by a slightly lower S/N and number of pulses in the 92-cm data. No drifting subpulses have been found at 430 MHz by Backus (1981).
B0540+23: sporadic bursts of both positive and negative drift have been reported by Ashworth (1982) at 400 MHz and by Nowakowski (1991) at 430 MHz. No preferred drift direction is detected in the 2DFS of this pulsar (Fig. A.2), consistent with the 21-cm data. At this frequency we see short drift bands with different drift directions in the pulse-stack confirming the reported drifting in the literature. This is similar to the drifting subpulses reported in Paper I. Because this pulsar does not show a preferred drift direction in our observations, this pulsar is not classified as a drifter in our papers. This pulsar shows a clear low-frequency excess at both frequencies. Notice the high modulation index, especially at 92 cm, caused by occasional bright pulses.
B0609+37: the very clear and narrow drift feature discovered at 21 cm is not confirmed (Fig. A.2). The S/N of this observation is a about twice as low, but that does not seem to completely explain why the feature is not observed at this frequency. With more than 10 000 pulses in this observation a mode-change also does not seems to be a likely explanation. Although an observation with a higher S/N may reveal a drift feature at 92 cm, it seems that it must be less coherent than the feature found in the 21-cm data to explain the current non-detection.
B0611+22: our observation does not show any fluctuation features in the spectra of this pulsar (Fig. A.2), something that has also been reported by Backer et al. (1975) at 430 MHz and is

consistent with the results of Paper I. Drifting with a periodicity $P_3 = 50-100P_0$ has been reported by Ferguson & Boriakoff (1980) at 430 MHz, who have analyzed successive integrated pulse profiles. It is not clear if this kind of drifting is related to subpulse drifting, because in their analysis the subpulses are not directly measured.

B1822−09: drifting subpulses and a correlation in the subpulse modulation between the main- and interpulse have been observed for this pulsar (e.g. Fowler et al. 1981). The drifting subpulses as seen in the 21-cm data are not confirmed. Possibly the S/N of our observation is not good enough to detect the very broad and weak drift feature, but it could also be related to the profile evolution from a double morphology at high frequencies to a more single morphology at low frequencies. As far as we know drifting subpulses have only been reported at high frequencies (Fowler et al. 1981, at 1.620 GHz.; Fowler & Wright 1982, at 2.695 GHz; Gil et al. 1994, at 1.408 GHz–10.55 MHz).

B1844−04: the narrow drift feature that was discovered in the 21-cm data is not confirmed at 92 cm (Fig. A.10). The S/N and the number of pulses are comparable at both frequencies. Because of the relative low number of pulses it is possible that in the two observations different drift-modes were dominating. Another possibility is that it is related to the frequency dependence of the profile morphology, because at 21 cm the drift-feature seems to be originating from the trailing component and at 92 cm only one component is observed.

B1845−01: the drift feature reported in the 21-cm data and by Hankins & Wolszczan (1987) at 1414 MHz is not visible (Fig. A.10), probably because of a lower S/N and the severe interstellar scattering.

B1911−04: the LRFS of this pulsar (Fig. A.12) shows a low-frequency modulation (which is generated mainly in the trailing part of the pulse profile), consistent with the 21-cm result. However, at this frequency there is no evidence for a preferred drift direction. Possibly this is related with the profile evolution from a triple profile at 21 cm to a single profile at 92 cm.

B1952+29: this pulsar was discovered to have drifting subpulses in the 21-cm survey. There is an intensity modulation feature with the same P_3 value at 92 cm (Fig. A.13). Because the feature in the 2DFS is not significantly offset from the vertical axis the feature is classified as longitude stationary subpulse modulation at this frequency. It is not clear if the modulation is really longitude stationary at this frequency or if the drift direction is constantly changing. The most clear detection of coherent drifting subpulses was in the trailing part of the pulse profile at 21 cm. Notice also that the profile has evolved significantly with frequency. The component which showed coherent drifting subpulses at 21 cm is at least much weaker at 92 cm, but it is also possible that this component is not visible at all.

B2000+40: despite the presence of RFI, a clear drift feature was discovered in the 21-cm data with a periodicity $P_3 = 0.4$ cpp. In the 92-cm data there is not much evidence for a similar feature (Fig. A.14). Maybe the non-detection at 92 cm is related to the profile evolution with frequency in combination with the non-linearity of the drift bands as observed at 21 cm.

B2053+36: a broad clear drift feature was discovered at 21 cm, which is not confirmed in the 92-cm data (Fig. A.14). This is surprising because the S/N and the number of pulses should be enough to detect the presence of drifting subpulses. Notice that also the modulation index is much lower at 92 cm. Subpulse modulation without a preferred drift direction has been reported for this pulsar at 430 MHz by Backus (1981). The disappearance of the drift feature at 92 cm could be related to the frequency evolution of the profile.

B2324+60: this pulsar showed a broad drift feature in its 2DFS at the alias border in the 21-cm data and some drift bands could be seen in the pulse-stack. There was also a strong low-frequency feature detected. Unfortunately, the S/N of the 92-cm data is insufficient to confirm any of this (Fig. A.16).

J2346−0609: the 2DFS of the trailing component of the pulse profile has a drift feature close to the $P_3 = 2P_0$ alias border in the 21-cm data. There is probably some short period periodicity modulation present in the trailing component in the 92-cm data, although it is very weak (Fig. A.23). Drifting subpulses could possibly be confirmed at 92 cm in an observation with a higher S/N. There is a strong sharp longitude stationary low-frequency modulation in the leading component, which was also found in the 21-cm data. This pulsar is not included in the statistics because it is just too weak to be part of the source-list.

3.5. Pulsars with low-frequency modulation

B0011+47: a low-frequency excess was found in the 21-cm data, which is confirmed in the 92-cm data (Fig. A.1). Notice the high modulation index. It seems that the low-frequency excess and the high modulation index are both caused by the burst like behavior of the emission. This pulsar is not a known nuller.

B0355+54: the spectra of this pulsar (Fig. A.1) show a low-frequency excess, consistent with the results from the 21-cm data. The explanation for the low-frequency excess and the high modulation index is that the emission is burst like.

B0402+61: the power in the spectra of this pulsar is dominated by the modulation in the leading component and is concentrated toward long periodicities at 92 cm (Fig. A.17). At 21 cm the modulation of the trailing component dominated and a long period feature without preferred drift direction was found. The 2DFS of the trailing component shows a hint of a similar feature at 92 cm, but this is much weaker and not significant.

B0740−28: the LRFS of this pulsar shows low-frequency modulation (Fig. A.3), which is stronger than was found in the 21-cm data.

B1600−27: the low-frequency excess (Fig. A.5) was not observed at 21 cm, not unlikely because the S/N of this observation is higher.

B1620−09: the observation is contaminated by RFI, but nevertheless there appears a weak low-frequency excess in its LRFS. This pulsar was not observed at 21 cm.

B1649−23: this pulsar shows short period modulation as well as long period modulation in its trailing component (Fig. A.5). Similar features are possibly also seen in the 21-cm data, although it was not found to be convincingly detected.

B1706−16: this pulsar has a strong low-frequency excess (Fig. A.6), which was also found at 21 cm. The low-frequency modulation is most likely caused by nulling, which can clearly be seen in the pulse-stack. No nulling has previously been reported for this pulsar.

B1758−03: the low-frequency excess peaks at $P_3 \simeq 60P_0$, which is probably caused by the burst like behavior of the emission. This pulsar is not a known nuller and was not observed at 21 cm.

J1808−0813: there is a clear low-frequency excess (Fig. A.8), which was also found in the 21-cm data. The feature peaks at $P_3 = 150P_0$, while at 21 cm the feature peaked at $P_3 = 90P_0$. Because the observations are relatively short, this difference is not significant. The low-frequency excess is probably related to nulling, which can be seen by eye in the pulse stack at 21 cm. This pulsar is not known as a nuller.

B1826−17: the LRFS shows a (very weak) detection of a low frequency excess (Fig. A.9), consistent with the 21-cm data. The profile is scatter broadened at 92 cm.
B1842+14: subpulse modulation without a drift direction has been detected by Backus (1981) at 430 MHz, which is consistent with the spectra of our observation which do not reveal any preferred periodicity or drift direction (Fig. A.10). The side panels of the LRFS and 2DFS shows that the power is increasing towards the horizontal axis, indicating that the pulsar shows a low-frequency intensity modulation. In the 21-cm data only the modulation index could be measured.
B1848+12: this pulsar has a strong low-frequency excess (Fig. A.10), probably related to nulling. This pulsar was not observed at 21 cm and is not known to be a nuller.
B1907+00: the spectra show a low frequency excess (Fig. A.11). This was not found in the 21-cm data, possibly because of a lower S/N.
B2003−08: there is a low-frequency excess observed in the all components (Fig. A.14), which is probably also present at 21 cm.
B2106+44: the spectra of this pulsar were found to peak towards low frequencies at 21 cm, which is confirmed at this frequency (Fig. A.15). There is no evidence for a $P_3 \simeq 20P_0$ (longitude stationary) feature as found in the 21-cm data. This could be related to the lower S/N at 92 cm.

3.6. Pulsars with a flat fluctuation spectrum

B0447−12	B0450−18	B0458+46	J0520−2553
B0531+21	B0559−05	B0626+24	B0643+80
B0727−18	B0906−17	B1254−10	B1322+83
J1603–2531	J1654−2713	B1717−16	B1726−00
J1732−1930	B1745−12	B1749−28	J1758+3030
B1804−08	B1821+05	B1831−04	B1831−03
B1839+09	B1845−19	B1851−14	B1900−06
B1902−01	B1907-03	B1907+02	B1914+09
B1915+13	B1920+21	B1929+20	B1937−26
B1940−12	B1943−29	B1946−25	B2002+31
B2022+50	B2027+37	B2113+14	B2224+65
B2227+61	B2306+55	B2334+61	

B0450−18: the three components (of which the outer ones are plotted in Fig. A.18) show flat featureless spectra, consistent with Paper I.
B0531+21: both the 2DFS of the main- and interpulse of the Crab pulsar do not show any sign of drifting subpulses (Fig. A.18). A very large modulation index is measured ($m = 5$), which is caused by its giant pulses (Staelin & Reifenstein 1968). Notice that the modulation index is lower at low frequencies, most likely because the giant pulses are much more scatter-broadened at low frequencies. Notice also that the precursor (that peaks at a pulse longitude of 65°) has a much lower modulation index, which is consistent with the interpretation that its emission is the "normal" emission of the pulsar (Popov et al. 2006). This pulsar is not included in the statistics because its emission is clearly dominated by a different type of emission than that of the "normal" pulsars.
B0643+80: the spectra are featureless (Fig. A.3). This pulsar was not observed at 21 cm. A "burst" in the central component has been reported by Malofeev et al. (1998) at 102.5 MHz. In a 22 min observation (1120 pulses) they find that central component of the profile was nine times brighter than usual, but because no single pulses were recorded, it was not clear how long the burst lasted. If it was caused by a single pulse, it must have been 10^4 times brighter than the average. We do not see any evidence for strong pulses in our 92-cm observation.
B0727−18: the spectra are featureless (Fig. A.3). Notice the high modulation index, which are caused by bright single pulses which are intermittently emitted. This pulsar was not observed at 21 cm.
J1603−2531: the spectra are featureless (Fig. A.5). Notice the high modulation index, which is probably caused by a few bright single pulses that appear above the noise-level. This pulsar was not observed at 21 cm.
B1749−28: this pulsar shows flat featureless spectra (Fig. A.7), consistent with Paper I and the results of Taylor & Huguenin 1971.
B1804−08: a low-frequency excess was reported for the 21-cm data, which is not confirmed at 92 cm (Fig. A.8), possibly because of the lower S/N or the drastic profile evolution.
B1821+05: subpulse modulation without a drift direction has been reported by Backus (1981) at 430 MHz. No clear features are seen in the 2DFS (Fig. A.8), possibly because of the low S/N of our observation. At 21 cm there was no detection of a modulation index.
B1839+09: subpulse modulation without any drift direction has been detected by Backus (1981) at 430 MHz. We also observe subpulse modulation without any sign of drifting subpulses (Fig. A.9). The spectra of the 21-cm data were featureless.
B1915+13: no features are seen in the spectra of this pulsar by Backer et al. (1975) at 430 MHz, which is also the case for our observation (Fig. A.12). In the 21-cm data the modulation index was not measured, probably because of a too low S/N.
B1920+21: the 2DFS and LRFS of this pulsar shows three sharp features with 0.19, 0.24 and 0.28 cpp (Fig. A.12). This is most likely because the single pulses "flicker". The 0.24 cpp feature is in the first half of the data and the other two in the last half. The observation is too short to state that there exist a discrete number of flickering-frequencies that are switched on and off similar to a mode-change rather than that a continuous range of flickering-frequencies that can be excited. At 21 cm the spectra are featureless, probably because of a lower S/N.
B1937−26: a broad feature was detected at the $P_3 = 2P_0$ alias border at 21 cm, but the spectra are flat at 92 cm (Fig. A.13). The two observations have a comparable S/N.
B2022+50: only the 2DFS of the mainpulse of this pulsar is plotted, because no modulation is measured for the interpulse (Fig. A.14). A flat spectrum was found for the mainpulse in the 21-cm data.
B2113+14: the spectra are flat (Fig. A.15). Subpulse modulation without preferred drift-direction and nulling has been reported by Backus (1981). This pulsar was not observed at 21 cm.
B2334+61: notice the very high modulation index of this pulsar (Fig. A.16). This is because this pulsar appears to intermittently emit bright single pulses (or it is off most of the time except a few single pulses). In the 21-cm data the modulation index is lower.

3.7. Pulsars without a measured modulation index

B0410+69	B1552−23	B1648−17	B1657−13
B1709−15	B1732−02	J1744−2335	B1756−22
J1759−2922	B1821−19	B1822+00	J1823−0154
J1835−1106	J1837-0045	J1848−1414	J1852−2610
B1859+03	B1900+05	B1913+10	B1924+16
J2005−0020	B2011+38	B2148+52	J2248-0101

B1648−17: the vertical line in the LRFS at pulse longitude 218° is most likely because of spikes of RFI in the data (Fig. A.5).

Because we do not believe the measured modulation is caused by subpulse modulation, this pulsar is not included in the statistics. This pulsar was not observed at 21 cm.
B1821−19: a low-frequency excess was found in the 21-cm data, which is not confirmed at this frequency (Fig. A.8). The profile is severely scatter-broadened. It is likely that the measured modulation index is a result of statistical fluctuations of the very small available off-pulse intensity level (baseline) that is subtracted from the pulses. Because we do not believe the measured modulation is caused by subpulse modulation, this pulsar is not included in the statistics.
B1822+00: no modulation index could be measured (Fig. A.9), which is, with an upperlimit of 0.4, unusual. This pulsar was not observed at 21 cm.
B1859+03: a flat spectrum was measured for this pulsar in the 21-cm data. Although we also measure a flat spectrum in the 92-cm data (Fig. A.11), it is probably related to the severely scatter-broadened profile. Therefore this pulsar is, similar to pulsar B1821−19, not included in the statistics.
B2011+38: no modulation index could be measured for this pulsar (Fig. A.14), probably because of a too low S/N. In the 21-cm data a long period longitude stationary feature has been found.

4. Individual sources at the two frequencies

One of the aims of this paper is to discuss the frequency dependence of the drifting phenomenon. Is the drifting phenomenon broadband, that is, if the pulsar shows drifting subpulses at one frequency, does it also have drifting subpulses at the other frequency? A related question is if drifting subpulses are more regular at a certain frequency. Other questions, such as how similar the values of P_3 are at the two frequencies, will be adressed in the next section. In this section a comparison is made between the results on the individual sources at the two frequencies. This will summarise some aspects of the more detailed description in the previous section.

In total there are 130 pulsars which were observed at both 92 and 21 cm. Considering the pulsars that have the most clear and regular drifting subpulses: 22 of them are observed to have coherent drifting subpulses at at least one frequency. Of these pulsars 11 were classified at both frequencies as coherent drifters, but 11 pulsars were classified differently. In two cases the different classification is related to different dominating drift-modes in the two observations (PSRs B2319+60 and B1819−22). This could be because the observations at the two frequencies were recorded at different times, which means that one of the drift-modes could just have been missed in one of the observations. Another explanation could be that some drift-modes are only visible at certain frequencies, while at the same time no drifting subpulses are observable at other frequencies. An example of the latter is PSR B0031−07 (Smits et al. 2005, 2007).

Also PSRs B0149−16 and B2045−16 are observed to have drifting subpulses at both frequencies, but most likely because of a higher S/N the drift-feature is found to be broader at 92 cm. The drifting subpulses of PSR B1918+19 were only in the observation at one frequency, which could just be because of a lack of S/N at one frequency, although this pulsar is also known to be a drift-mode changer. In the case of PSR B0105+65 the drifting subpulses appear to only be observable at one frequency, but it must be noted that subpulse modulation with the same P_3 is observed at the other frequency. This is also the case for PSR B1730−22, which moreover has a severe profile evolution. In the case of PSR B2315+21 the drifting subpulses are only observed in a very narrow pulse longitude range, so again profile evolution could be responsible for the non-detection at the other frequency. For B1844−04 and B2000+40 it cannot be ruled out that the observations were too short to catch the drift-mode (if they would turn out to have drift-mode changes), but it could also be related to the profile evolution. The most convincing evidence that drifting subpulses can in some cases only appear at one frequency is found for PSR B0609+37, which does not have detectable drifting subpulses in a long observation with only a slightly lower S/N at 92 cm.

It seems that the majority of the pulsars with coherent drifting subpulses have similar drifting subpulses at both frequencies, at least when the S/N of the observations are similar. In most cases when drifting subpulses are only observed at one frequency the profile evolution could be responsible. For the diffuse drifters the picture is similar. In total there are 55 pulsars which are classified as a diffuse drifter at at least one frequency and the majority of them (36) are identically classified at both frequencies. Moreover, four of them were classified as coherent drifters at one frequency (as discussed above) and one pulsar is classified as a pulsar with longitude stationary subpulse modulation. The remaining 14 pulsars are only found to have drifting subpulses at one frequency. This could in many cases just be a S/N issue, although interstellar scattering or profile evolution could also be responsible in some cases.

It is clear that at least a large fraction of the pulsars with drifting subpulses at one frequency have drifting subpulses at the other frequency as well. It is difficult to say what the exact fraction of pulsars is that have drifting subpulses at both frequencies, because in many cases where drifting subpulses were found at only one frequency it could be related to the S/N and the length of the observation. Longer observations are therefore required for these pulsars to confirm with more confidence that they really show drifting subpulses at only one frequency.

The drifting subpulse phenomenon appears to be in general a broadband phenomenon in the sense that the chance is high to find drifting subpulses at both frequencies. However it is also clear that the details of the drifting subpulses can be different at both frequencies. This is clear for PSR B2016+28, the only pulsar in our sample which was observed simultaneously at both frequencies with the WSRT, but also for instance PSRs B1642−03 and B2021+51 appear to have clearly different drifting subpulse characteristics at the two frequencies.

Because the subpulse modulation patterns are in general similar at different frequencies it is possible to use the LRFS to identify which component in the pulse profile corresponds to which at the other frequency. Especially when the frequency evolution of the profile is drastic, this can be a powerful tool to track components between different frequencies. Two examples of this application of the LRFS are PSRs B1857−26 and B1919+21.

A number of pulsars are found which intermittently emit single pulses that have pulse energies of about, or even brighter than, ten times the average pulse energy. These pulses are not true giant pulses (Staelin & Reifenstein 1968), because they have widths comparable with the width of the pulse profile. Nevertheless the emission of these 8 pulsars (PSRs B0011+47, B0355+54, B0540+23, B0727−18, J1603−2531, B1917+00, B2319+60 and B2334+61) could potentially be different from that of normal pulsars and be related to that of PSR B0656+14 and the RRATs (Weltevrede et al. 2006b,c).

Another side result of our single pulse analysis is that we have discovered nulls in a number of sources which were not known to null before. These 8 sources are: PSRs B0011+47, B1706−16, B1738−08, B1758−03, J1808−0813, B1819−22, B1848+12 and B2110+27. Also one more pulsar has been

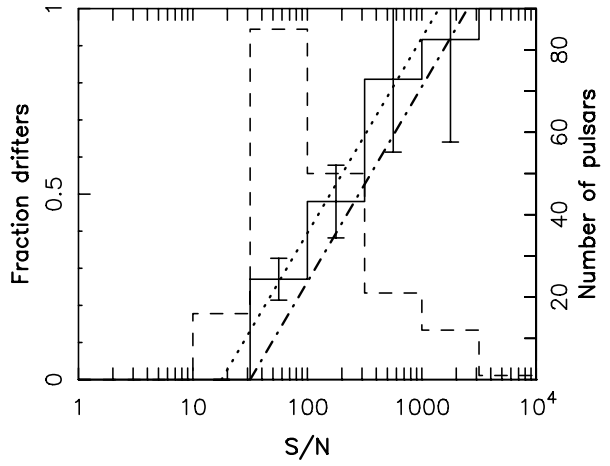

Fig. 2. The solid line shows the fraction of pulsars we observe to exhibit the drifting phenomenon versus the measured S/N ratio of the observation. The dashed histogram shows the total number of pulsars observed in each S/N ratio bin. The root-mean-square (rms) is calculated as an estimate for the error (if the bin contains more than one observation). The dotted line is a fit for the S/N dependence of the chance to detect drifting subpulses and the dash-dotted line is that of Paper I.

discovered that shows a pulse phase step: PSR J0459−0210. This means that this pulsar has highly non-linear driftbands with an almost discontinuous step in subpulse-phase. This is possibly caused by destructive interference between two drifting subpulse patterns (Edwards et al. 2003).

5. Statistics

5.1. The numbers

This survey has revealed another 15 new drifters to go with those discovered in the 21-cm survey. For 76 pulsars out of the 185 that are included in the 92-cm source-list drifting subpulses are detected, which is about one detection per three pulsars. This number is similar to that found at 21 cm, which is maybe not that surprising because 130 of these pulsars were also observed in the 21-cm survey. This means that a considerable fraction of the source-lists at both frequencies are overlapping, and as discussed in the previous section the chance of detecting drifting subpulses at both frequencies is high. As discussed in Paper I, it is not surprising that drifting is not always seen, even if drifting would be an intrinsic property of the emission mechanism.

In Fig. 2 the fraction of pulsars that show drifting subpulses is plotted versus the integrated S/N of the observation. It can be seen that the chance of detecting drifting subpulses is correlated with the S/N. The dash-dotted line is the correlation found for the 21-cm survey, which is similar to the observed relation at 92 cm (dotted line). High S/N observations could in principle be biased toward well studied or long period pulsars. However, very similar correlations are found when observations containing more than 3000 pulses or the pulsars with periods longer than 0.5 s are excluded. Therefore this correlation seems to be a real observational bias in the sense that drifting subpulses can only be significantly detected in a low S/N observation when the drifting is reasonably coherent (e.g. PSR J1650−1654).

If there is any significant difference in the fraction of drifters found at the two different frequencies, it would be that at 92 cm the chance of detecting drifting subpulses for a given S/N is somewhat higher than at 21 cm (see Fig. 2). This could in principle be because drifting subpulses are more likely to exist at low frequencies, or they may be more regular or more intense at low frequencies. From the observations there is not much evidence that there are more coherent drifters at 92 cm than at 21 cm, but we will argue that there is some additional evidence that it is easier to detect drifting subpulses at 92 cm (Sect. 6).

To reduce the effect of low S/N observations on the statistics, the observations with the lowest S/N's were excluded from further analysis. Because it turns out that the correlation between the chance to detect drifting subpulses and the S/N ratio of the observation is very similar at both frequencies, the same threshold as in Paper I is applied. Only observations with a S/N higher than 100 are included in the statistics. Of the 185 observed pulsars 84 have a high enough S/N to be included in the statistics, which is slightly lower than at 21 cm. Of these pulsars 53 (63%) show drifting subpulses and 9 (11%) show longitude stationary modulation. These fractions are slightly higher than those found at 21 cm, so our conclusion that at least half of the pulsars have drifting subpulses seems to be justified also at 92 cm.

Scatter-broadening of the pulses is very likely to reduce the probability to detect drifting subpulses when the amount of broadening is comparable or even larger than the subpulse separation P_2. The amount of scatter broadening increases rapidly with decreasing observing frequency f. For instance the scattering time is expected to be proportional with f^{-4} in the thin screen model (Scheuer 1968), so scattering was expected to potentially be a severe problem at 92 cm. However it turns out that of the sources that have enough S/N to be included in the statistics, only PSRs B1821−19 and B1859+03 are severely scatter broadened. So by excluding these two pulsars from further analysis the statistics are not much affected by the effect of scatter-broadening.

5.2. The drifting phenomenon and the $P - \dot{P}$ diagram

Many of the important physical parameters of pulsars are derived from the pulse period and its time derivative $\dot{P}$ (spin-down parameter). It is therefore useful to look for correlations in the $P - \dot{P}$ diagram. All the pulsars analysed at 92 cm are plotted in Fig. 3 and the coherent drifters, diffuse drifters and pulsars with a longitude stationary subpulse modulation have different symbols. This figure looks qualitatively similar to that in Paper I and this may not be that surprising as a considerable fraction of the source-lists at both frequencies are overlapping.

As seen at 21 cm, the different groups of pulsars occupy a large fraction of the $P - \dot{P}$ diagram and are clearly overlapping each other. This implies that there is no strict correlation between the drifting phenomenon and P, $\dot{P}$ or any combination of them. Nevertheless, there appears to be a weak trend that pulsars with drifting subpulses, especially the coherent drifters, are located closer to the death-line. This would confirm the correlation reported in Paper I.

To confirm this trend the characteristic age distributions (where $\tau = \frac{1}{2}P/\dot{P}$) are plotted in the left panel of Fig. 4. Indeed the pulsars with drifting subpulses are on average older, as has also been reported by Ashworth (1982). Moreover the pulsars with coherent drifting subpulses are even older. This correlation suggests that there is an evolutionary trend that the youngest pulsars have the most disordered subpulses and that the subpulses become more and more organized into drifting subpulses as the pulsar ages. We will come back to the interpretation of this trend in the summary and conclusions (Sect. 7).

To determine the significance of this trend the KS-test (Kolmogorov-Smirnov test) is used, which calculates how likely it is that two distributions are drawn from an identical

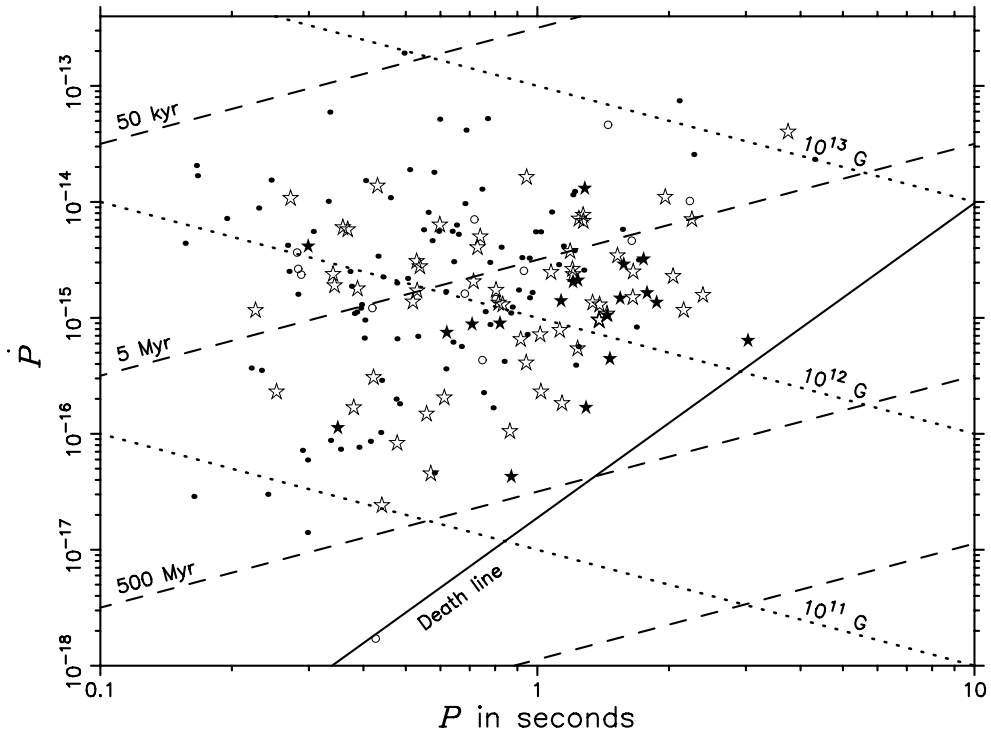

Fig. 3. The $P - \dot{P}$ diagram of the analysed pulsars at 92 cm (including the low S/N observations). The pulsars without drifting subpulses are the dots, the diffuse (Dif and Dif*) drifters are the open stars, the coherent drifters are the filled stars and the pulsars showing longitude stationary subpulse modulation are the open circles. Lines of equal surface magnetic field strength and characteristic ages are plotted, as well as a death line (Chen & Ruderman 1993).

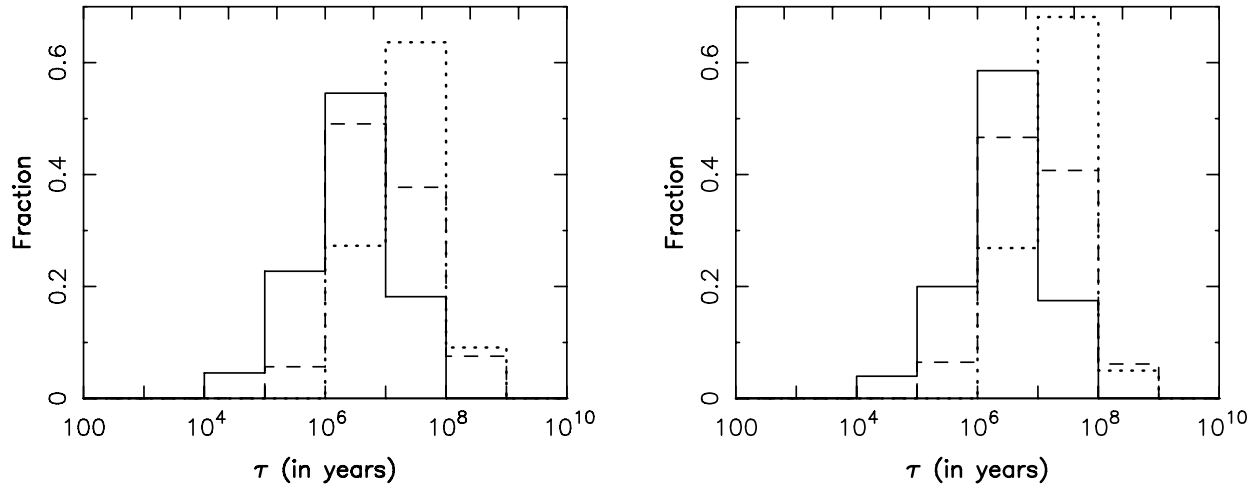

Fig. 4. The *left panel* shows the histogram of the characteristic ages of the analyzed pulsars with a $S/N \geq 100$. The solid line is the age distribution of pulsars without drifting subpulses, the dashed line shows all the drifters and the dotted line shows the coherent drifters. The *right panel* shows the "S/N versus age bias" corrected histogram.

distribution. There is only a 2% chance that the age distribution of the pulsars with and without drifting subpulses are the same. This is too high to state that this trend is significant. There is only a 0.1% chance that the age distribution of the coherent drifters and the pulsars without drifting subpulses are the same, which therefore appear to be significantly different. There is only a 0.9% chance that the age distribution of the drifters with and without coherent drifting subpulses are the same.

The same trend is found when the low S/N pulsars are included in the statistics. We checked if the trend could be explained by a difference in the S/N of the observations in different age bins. As noted in Sect. 2.1, such bias can be expected if both the age of the pulsar and $T_{\rm sky}$ are correlated with the galactic latitude. The S/N versus age bias corrected age distributions are plotted in the right panel of Fig. 4 and they are qualitatively the same as the left panel, giving us confidence in the correlation found (the procedure used is described in Paper I).

Because the drifting subpulse phenomenon appears to be broadband, it is useful to combine the sample of pulsars at both frequencies to increase the significance of the statistics. For the sources that were observed at two frequencies the observation with the highest S/N was used. According to the KS-test there is only a 0.02% chance that the age distribution of the pulsars with and without drifting subpulses are the same and this chance is

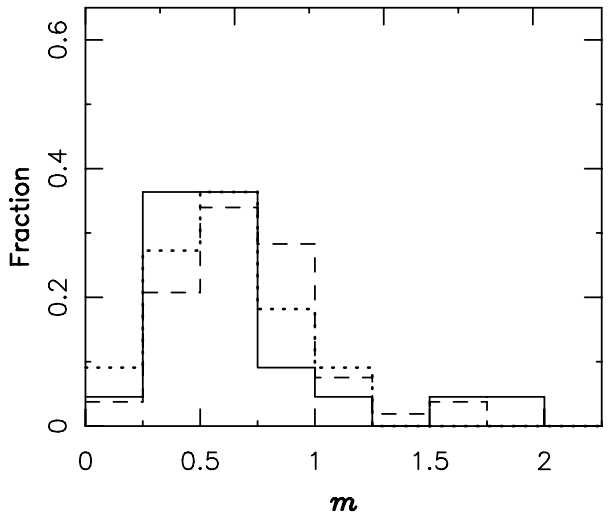

Fig. 5. The modulation index distribution of the pulsars without drifting subpulses (solid line), with drifting subpulses (dashed line) and with coherent drifting subpulses (dotted line). Only observations with a $S/N \geq 100$ are included this plot.

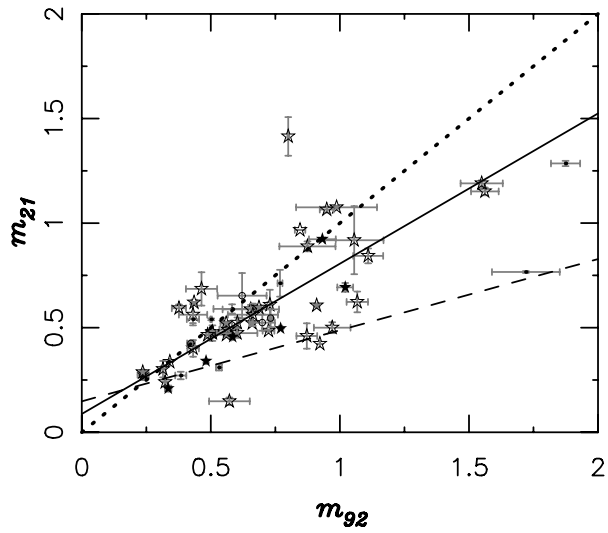

Fig. 6. The modulation index measured at 21 cm versus that measured at 92 cm. The points would lie on the dotted line when the modulation index is frequency independent. Only observations with a $S/N \geq 100$ are included this plot. The dashed and solid line are straight line fits through the data-points with and without weighting for the errorbars. The symbols are identical to those in Fig. 3.

3% for the age distribution of the coherent drifters and the other pulsars. The difference between the age distribution of the pulsars with and without drifting subpulses is significant, while the different age distribution of the coherent drifters and the other drifters is not significant. Nevertheless the data at both frequencies is consistent with each other. Because the sample of pulsars at the two frequencies are partially overlapping, the 92-cm data cannot independently confirm the trend observed at 21 cm.

Another interesting quantity that can be derived from the $P - \dot{P}$ diagram is the surface magnetic field strength ($B_s = 10^{12}\sqrt{10^{15}P\dot{P}}$ Gauss). There is a 10% chance that the magnetic field strength distribution of the pulsars with and without drifting subpulses are the same and this chance is 3% for the magnetic field strength distribution of the pulsars with coherent drifting subpulses and those without drifting subpulses. This means that, as was found in Paper I, there is no evidence that the surface magnetic field strength distribution is significantly different for the pulsars with and without drifting subpulses.

5.3. The drifting phenomenon and the modulation index

It is clear that the modulation index is a parameter that is closely related with the drifting phenomenon, because drifting subpulses imply an intensity modulation. However, it is somewhat arbitrary how *the* modulation should be defined, because the longitude-resolved modulation index is in most cases highly dependent on pulse longitude. Following Paper I (and Jenet & Gil 2003) the statistics are calculated using the minimum in the modulation index profile. The motivation is that the minimum in the modulation index profile is often found at the pulse longitude of a maximum in the intensity profile. This means that for instance the longitude-averaged modulation index will depend on the S/N of the observation, because a higher S/N allows the detection of a modulation index farther away from the peaks in the pulse profile where the modulation index tends to be higher.

The modulation index distributions are shown in Fig. 5 for the pulsars with and without drifting subpulses and those with coherently drifting subpulses. There is no indication that the distributions are significantly different, although the modulation index of the pulsars with drifting subpulses tend to be higher. Interesting, in the 21-cm data there was an indication that the pulsars with coherent drifting subpulses appeared to have a lower modulation index (however not statistically significant). We will come back to this point in Sect. 6.

It is also interesting to compare the measured modulation indices at 92 and 21 cm. In Fig. 6 the minimum modulation index of each pulsar measured at 21 cm are plotted versus the minimum modulation index measured at 92 cm. Only the pulsars that are observed at both frequencies with a $S/N \geq 100$ are included in this plot. Moreover, all the observations which had a modulation index at one frequency that was below the detection threshold at the other frequency were not included. This means that all the pulsars included in this plot had the S/N to measure an identical minimum in the modulation index profile at both frequencies.

In Fig. 6 it can be seen that the modulation indices measured at the two frequencies are not independent, but they are clearly correlated. If the modulation index was independent of observing frequency the points would be scattered symmetrically around the dotted line $m_{21} = m_{92}$. However, there are more pulsars with a higher modulation index at 92 cm than visa versa. It is also interesting that there are more pulsars which have large (>1) modulation indices at 92 cm than at 21 cm.

To confirm the trend, and to check its significance, a straight line fit was made through the data. This is done by minimizing the χ^2 using the methethod described by Press et al. (1992), which incorporates the measurement errors of both coordinates. The dashed line shows the best fit through the data-points by weighting them by their measurement errors (dashed line: $m_{21} = 0.34 \pm 0.03 \times m_{92} + 0.15 \pm 0.03$). However, including the measurement errors heavily biases the correlation to a few high S/N observations, such as PSR B0329+54 with $m_{92} = 0.9$ and $m_{21} = 0.4$. To avoid the best fit being dominated by a few high S/N observations, the fitting is also done by weighting the data-points equally. This fit confirms that the modulation index at 92 cm is on average higher than at 21 cm (solid line: $m_{21} = 0.72 \pm 0.08 \times m_{92} + 0.09 \pm 0.06$), although the scatter around the correlation is large.

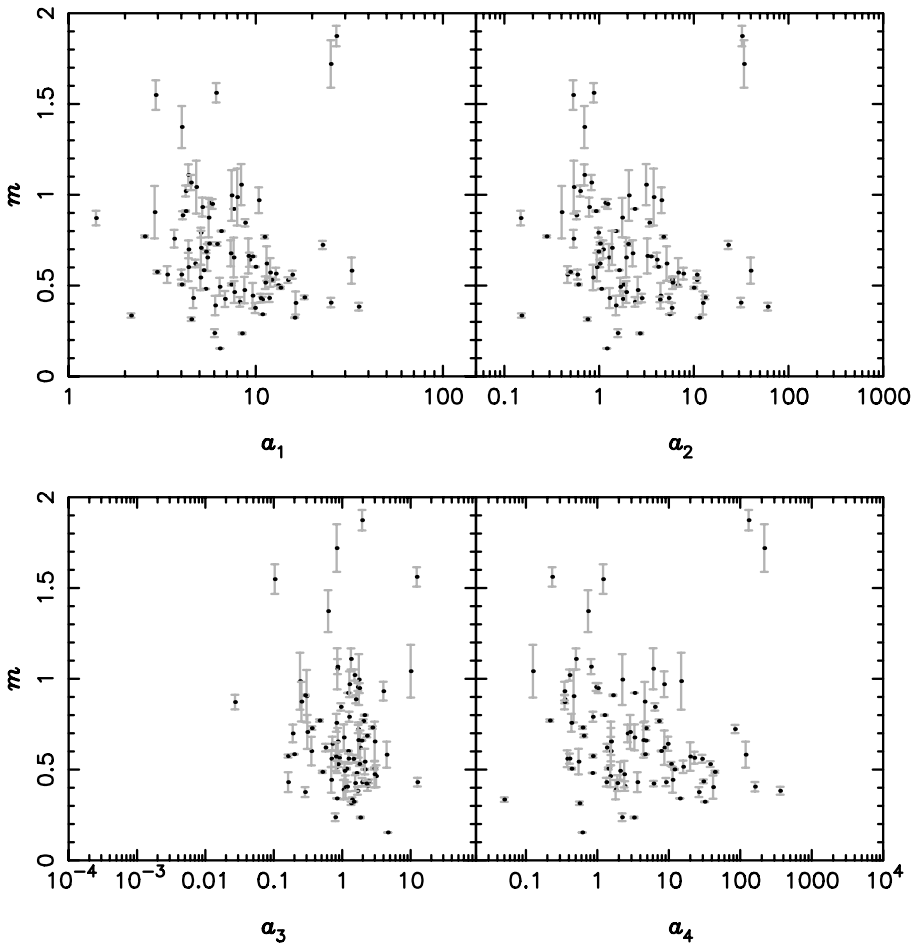

Fig. 7. The modulation index for all analyzed pulsars with a $S/N \geq 100$ versus the four complexity parameters as described in the text.

5.4. Complexity parameter

One way to try to distinguish between emission theories is to try to find correlations between the modulation index and the so-called complexity parameters. The idea is that the modulation index will be low when there are many overlapping subpulses in a single pulse, because then the intensity will also vary less from pulse to pulse. The number of subpulses per pulse depends, for instance, for the sparking gap model on the number of sparks on the polar gap, which can be quantified by a complexity parameter (Gil & Sendyk 2000). In the case of the sparking gap model the complexity parameter is the polar cap radius $r_{\rm p}$ divided by the gap height h. The complexity parameter is a model dependent function of P and $\dot{P}$ and the modulation index should have an anti-correlation with this function (Jenet & Gil 2003).

Following Jenet & Gil (2003) and Paper I the correlations between the measured modulation indices and four complexity parameters are calculated. These parameters correspond to the sparking gap model (a_1; Gil & Sendyk 2000), continuous current outflow instabilities (a_2; Arons & Scharlemann 1979; Hibschman & Arons 2001), surface magnetohydrodynamic wave instabilities (a_3; Lou 2001) and outer magnetospheric instabilities (a_4; Jenet & Gil 2003) respectively. As noted in Paper I, a_2 is also proportional to the acceleration parameter, the total current outflow from the polar cap, the square root of the spin down energy loss rate and roughly to the circulation time of the sparks expressed in pulse periods. Physically, a_3 and a_4 are proportional to the magnetic field strength at the surface and at the light cylinder respectively.

Because the modulation index appears to be frequency dependent, we did not combine the sample of pulsars at the two frequencies. In Fig. 7 the modulation index is plotted versus the four complexity parameters for the 92-cm data. In contrast to the corresponding plot in Paper I, only pulsars with a $S/N \geq 100$ are included. This means that the measurement uncertainties are relatively small on the data-points, which makes any correlation found more convincing. There is a hint of an anti-correlation for each of the four complexity parameters, although the correlation with a_3 appears to be the weakest. To determine the significance of these trends we followed the procedure of Paper I. This involves the calculation of the Spearman rank-ordered correlation coefficient ρ and its significance parameter Δ in a Monte Carlo approach. This results in a probability distribution $P(\rho)$, which is plotted in Fig. 8. In Table 1 the measured location and widths of the peaks of the probability functions are tabulated. For details of the method used we refer to Paper I[4].

Based on a sample of 12 pulsars Jenet & Gil (2003) found the highest anti-correlation for the sparking gap model (a_1) and that the surface magnetohydrodynamic wave instabilities (a_3) is unlikely. In the 21-cm data the modulation index was found to be both consistent with being anti-correlated, as well as being uncorrelated, with any of the four complexity parameters. It was therefore not expected to find any strong correlations in the 92-cm data. However, at this frequency the modulation

[4] The normalization of the probability functions in Fig. 11 of Paper I is incorrect, but the values in Table 1 and therefore all the conclusions of Paper I are unaltered.

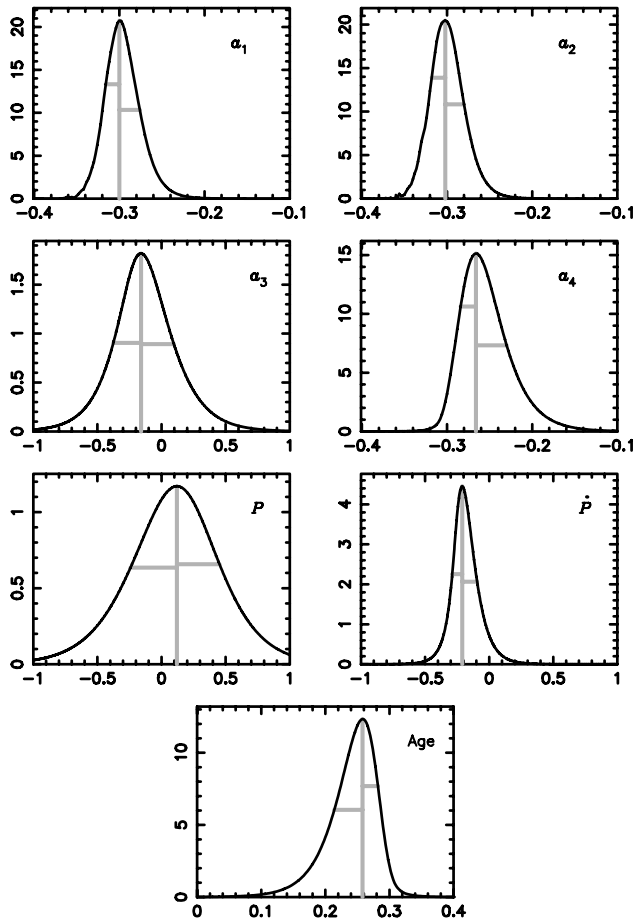

Fig. 8. The probability functions $P(\rho)$ of the correlation coefficient ρ for the four complexity parameters, the pulse period, the spin-down parameter and the characteristic age of the pulsar. The position of the maximum and the 1-σ widths are indicated by the gray lines.

Table 1. The correlation coefficients ρ and their significance as derived from Fig. 8 for all the pulsars (right column) and for only pulsars with a $S/N \geq 100$.

Parameter	Function	ρ ($S/N \geq 100$)	ρ (all)
$a_1 = r_p/h$	$5\frac{(\dot{P}/10^{-15})^{2/7}}{(P/1\mathrm{s})^{-9/14}}$	$-0.30^{+0.02}_{-0.02}$	$-0.30^{+0.02}_{-0.01}$
$a_2 \propto B_s/P^2$	$\sqrt{\dot{P}P^{-3}}$	$-0.30^{+0.02}_{-0.02}$	$-0.31^{+0.02}_{-0.02}$
$a_3 \propto B_s$	$\sqrt{P\dot{P}}$	$-0.2^{+0.3}_{-0.2}$	$0.0^{+0.5}_{-0.5}$
$a_4 \propto B_{lc}$	$\sqrt{\dot{P}/P^{-5}}$	$-0.27^{+0.04}_{-0.02}$	$-0.29^{+0.02}_{-0.01}$
P	P	$0.1^{+0.3}_{-0.4}$	$0.21^{+0.01}_{-0.03}$
$\dot{P}$	$\dot{P}$	$-0.21^{+0.12}_{-0.08}$	$-0.2^{+0.1}_{-0.1}$
Age	$\frac{1}{2}P/\dot{P}$	$0.26^{+0.02}_{-0.04}$	$0.22^{+0.03}_{-0.02}$

index appears to be much more strongly anti-correlated with all four complexity parameters. All four complexity parameters are consistent with being anti-correlated with the data and therefore none of the corresponding models can be ruled out. However, it must be noted the data provide little support for the surface magnetohydrodynamic wave instabilities, as only marginal anti-correlation is seen for a_3.

To further investigate the significance of these correlations we excluded all the pulsars with $m > 1$, as they are possibly forming a separate group. None of the correlations seems to be influenced much by excluding these points. It turns out that including all the low S/N pulsars also does not make much difference, except that the significance of the positive correlation between the modulation index and P becomes stronger.

It should be noted that the modulation index is also likely to be affected by the viewing geometry. Better results are expected when only pulsars are included that are known to emit core emission (Jenet & Gil 2003). Because not all the pulsars in our source-list have an established classification into core or conal emission we have included all pulsars with a measured modulation index in our analysis. However, the modulation index is chosen to be the minimum in the longitude-resolved modulation index (as in Jenet & Gil 2003), which should give the best estimate for the modulation index of the core component if present.

A difficulty in the interpretation of the correlations between the modulation index and the complexity parameters is that it is assumed that the (longitude-resolved) modulation arises solely because of the movement of the subbeams. However the reality is in many cases more difficult, because the subpulses also have intrinsic fluctuating intensities. This additional component in the modulation index could in principle have a very different (or none) correlation with P and $\dot{P}$ than that of the complexity parameter. It would therefore be important to disentangle these different effects on the modulation index. Also it should also be noted that the whole concept of an anti-correlation between the modulation index with the complexity parameter only is predicted when there is a significant broadening in the mapping from the polar gap to the radiation beam pattern. If this is not the case the subpulses cannot overlap, hence there is no anti-correlation expected.

It is intriguing that the correlations with the modulation index are much more constrained at 92 cm than at 21 cm. There are no obvious observational biases we can think of that could explain this. For instance, excluding the ms-pulsars from the 21-cm data (which were excluded in this 92-cm survey) does not lead to different results. If only the sources are considered which were observed with a $S/N \geq 100$ at both frequencies the results are again very similar, although the significance of the correlations go down which is probably simply related to the decreased number of data-points. Therefore there is no reason to believe these correlations are not real, although they are weak with a large scatter (Fig. 7).

5.5. Properties of drift behavior

It is generally thought that the value of P_3 is independent of the observing frequency, while the value of P_2 could vary (e.g. Edwards & Stappers 2003a). All pulsars with a measured P_3 at two frequencies are compared in Fig. 9 to test the absence of a dependency on the observing frequency of P_3. The correlation is indeed extremely tight and it is important to note that this correlation also applies for the pulsars with a diffuse drift feature. This correlation confirms the report for nine pulsars by Nowakowski et al. (1982). Moreover, many points that do not fall on the correlation can be explained. In the case of PSRs B0031−07 and B1819−22 drift-modes with different P_3 values dominate at the two frequencies. For others, such as PSRs B1738−08 and B1946+35 it seems not unlikely that longer observations will reveal that the P_3 values are consistent at the two frequencies. The different values for P_3 of B0628−28 at the two frequencies are because in the 21-cm observation the two differing values of P_3 in the leading and trailing halves of the profile were not separated. There seems to be only three cases

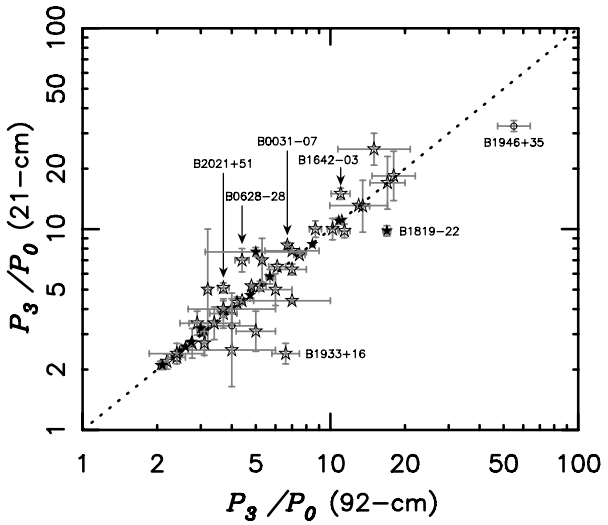

Fig. 9. The measured value of the vertical drift band separation P_3 compared at the two frequencies. Also the low-S/N observations are included. The diffuse (Dif and Dif*) drifters are the open stars, the coherent drifters are the filled stars and the pulsars with longitude stationary subpulse modulation are the open circles. The dotted line shows the expected correlation when P_3 is independent of frequency.

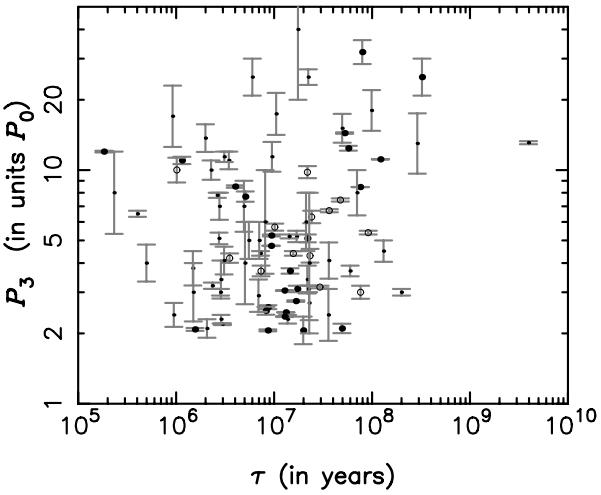

Fig. 10. The measured values of the vertical drift band separation P_3 versus the pulsar age of all the pulsars showing the drifting phenomenon. The coherent drifters are the filled circles, the Dif drifters (with drift feature clearly separated from the alias borders) are the open circles and the Dif* drifters are the small dots. This figure contains both 92 and 21-cm observations.

in which there is evidence for frequency dependence of P_3: PSRs B1642−03, B1933+16 and B2021+51. It would be interesting to have simultaneous observations at multiple frequencies to really proof if they exhibit a frequency dependent drifting subpulse pattern.

If the pulse profile is double peaked and there are drifting subpulse then the P_3 values measured for both components are in many cases very similar. This can be expected when the drifting subpulses in both components share a common physical origin. Nevertheless there are also some clear exceptions to this rule, for example PSRs B0628−28, B0751+32, B1508+55, J1901−0906 and B2016+28. Therefore this behavior cannot be explained in the framework of the sparking gap model by a cut of the line of sight through a single carousel of subbeams.

In the 21-cm data there was no obvious correlation between P_3 and the pulsar age contrary to reports in the past (Wolszczan 1980; Ashworth 1982; Rankin 1986). Because we find that P_3 is, at least in the majority of the pulsars, highly correlated between the two frequencies, the observations at the two frequencies are combined in Fig. 10. If the pulsar was observed at both frequencies, the observation with the highest S/N was used. It can be seen that there is, as was found for the 21-cm data, no evidence for any correlation between P_3 and the characteristic age. Possibly, such a correlation would be most pronounced for pulsars with dominating conal emission. Because no distinction in emission type has been made, the correlation could be less precise. However the absence of a correlation with age in this large sample of pulsars with drifting subpulses (90) suggests that if such a correlation would exist, it must be a very weak correlation. Also, the evidence for a pulsar subpopulation located close to the $P_3 = 2P_0$ Nyquist limit (Wright 2003; Rankin 1986) is weak. No correlations were reported in Paper I between P_3 and the magnetic field strength (contrary to what was reported by Wolszczan 1980; and Ashworth 1982), the pulse period (consistent with Wolszczan 1980; contrary to the tendency reported by Backer 1973). In the combined sample of 21 and 92-cm observations there is also no evidence for any of these correlations with P_3.

While P_3 appears to be highly independent of the observing frequency, the value of P_2 is expected, and found, to vary with frequency (e.g. Edwards & Stappers 2003a) and measuring a value for P_2 can be far from trivial (e.g. Edwards & Stappers 2003b). Moreover, P_2 is only a meaningful parameter if the drift bands are linear. Also, when the pulsar only occasionally shows drifting subpulses the value measured for P_2 will depend on the fraction of time the pulsar spent in the drift-mode. This is because when the pulsar does not show drifting subpulses most of the time, there will be more power in the 2DFS along the vertical axis, which will make P_2 larger. Nevertheless the measured values at the two frequencies appear to be roughly correlated (not plotted). As reported for the 21-cm data, there is no correlation between the drift direction and the pulsar spin-down (contrary to what was reported by Ritchings & Lyne 1975; Backus 1981; Ashworth 1982) and there is no difference between the number of pulsars with positive and negative drifting subpulses.

6. The quasi-steady emission component

Nowakowski et al. (1982) concluded, based on a multi-frequency study of nine pulsars, that it is a common feature of pulsars to have a quasi-steady component in their emission which becomes stronger with increasing frequency. This confirmed the idea of Cordes (1975), who found that the drifting subpulse signal of PSR B1919+21 becomes relatively weaker at higher observing frequencies. A similar effect is observed for PSR B0320+39 by Izvekova et al. (1982) at 102 and 406 MHz and Edwards & Stappers (2003b) at 328 and 1380 MHz. Other examples are PSR B0809+74 (Edwards & Stappers 2003b, at 328 and 1380 MHz) and PSR B0031−07 (Smits et al. 2007, at 243, 607, 840 and 4850 MHz). This effect can also be seen very clearly by comparing the side-panels of the spectra of PSR B0809+74 in this paper and those in Paper I.

A pure sinusoidal drifting subpulse signal would have a modulation index $m = 1/\sqrt{2}$ and subpulse patterns with different waveforms or drift band shapes will generally have larger modulation indices. However, a considerable fraction of the pulsars with drifting subpulses have a modulation index lower than 0.75

at 92 cm (see Fig. 5) and this fraction appears to be even larger in the 21-cm data (see Fig. 8 of Paper I). This confirms the idea that there is a quasi-steady component in the emission of pulsars which is relatively strong at higher frequencies. This interpretation is also consistent with Fig. 6, which shows the trend that the modulation index is, on average, lower at 21 cm.

This picture may also explain why the chance of detecting drifting subpulses is higher at low frequencies, independent of S/N (Fig. 2). This again suggests that the drifting subpulse signal is relatively stronger at lower frequencies. The drifting subpulse signal appears to be, on average, stronger for older pulsars (see Fig. 4 and the corresponding plot in Paper I). It is therefore expected that older pulsars have a higher modulation index and this is confirmed by the positive correlation between the modulation index and the characteristic age (Fig. 8).

So why was the correlation between the modulation index and the age of the pulsar not found for the 21-cm data? This can possibly be explained because the quasi-steady component of the emission is not entirely unmodulated, which means that there is a limit on how low the modulation index can become by increasing the strength of the quasi-steady component. Therefore the modulation index of especially the pulsars with a strong drifting subpulse signal (which tend to be older) will be suppressed by the strengthening of the quasi-steady component with frequencies. This means that the (positive) correlation between the modulation index and age is expected to be weaker at high frequencies, as is observed.

There are a few pulsars known which show an almost discontinuous step in subpulse-phase in the middle of the profile. The modulation index is very low at the pulse longitude of the step, which can be understood in terms of destructive interference between two drifting subpulse patterns (Edwards et al. 2003). As pointed out in Paper I, if especially the coherent drifters can have highly non-linear driftbands, then those pulsars will have an on average lower modulation index. This trend was indeed found in the 21-cm data, although it was not proved to be significant. Both PSRs B0320+39 and PSR B0809+74 show such phase-steps at high frequencies (Edwards & Stappers 2003b) and also the phase step found for PSR B2255+58 in the 21-cm data is not present at low-frequencies. If phase-steps are in general more likely to occur at high frequencies, than it is expected that the modulation indices of the coherent drifters are only found to be on average low at high frequencies. Indeed, there is not much evidence for such a correlation in the 92-cm data (Fig. 5).

It must be noted that the interpretations made in this section are based on correlations that are only weak and often not proved to be significant. Nevertheless it is encouraging that it is possible to explain the trends with concepts that are, at least from an observational point of view, not unfounded.

Observations at higher frequencies are thought to correspond to lower emission heights and this would imply that the emission beam is narrower at higher frequencies (radius-to-frequency mapping; Cordes 1978). If the components of pulse profiles are therefore more overlapping at higher frequencies, then also the subpulses could be expected to overlap more and this would imply a lower modulation index (i.e. a stronger quasi-steady component) at higher frequencies. This effect could also be related to refraction of plasma waves caused by plasma density gradients in the pulsar magnetosphere. The effect of refraction is stronger at higher frequencies (e.g. Petrova 2000; Weltevrede et al. 2003; Fussell & Luo 2004). Additionally, if refraction smears out the subpulses in time, the subpulses will overlap more. Refraction could therefore be (partially) responsible for the increasing quasi-steady component at higher frequencies.

7. Summary and conclusions

One of the main points of Paper I was that drifting subpulses are at the very least a common phenomenon for radio pulsars, if not an intrinsic property of the emission mechanism. This conclusion is further supported by the 92-cm data. For 15 pulsars drifting subpulses are discovered for the first time in the 92-cm data and 26 of the new drifters found in the 21-cm data are confirmed. Drifting subpulses are detected in total for 76 pulsars out of the 185 and it is estimated that at least half of the total population of pulsars will show drifting subpulses when observations with high enough S/N would be available. This fraction is similar to that found at 21 cm, which is not surprising because a considerable fraction of the source-lists at both frequencies are overlapping (130 pulsars) and we find that the chance of detecting drifting subpulses at both frequencies is high, indicating that the drifting phenomenon is in general broadband. The fraction of pulsars with drifting subpulses is possibly even slightly higher at 92 cm than at 21 cm and the majority of the pulsars show subpulse modulation.

It is not expected that all pulsars show drifting subpulses. This could simply be because some of the observations had a lower than expected S/N, because of unfortunate interstellar scintillation, a higher sky temperature than the average over the whole sky, severe RFI during the observation, or because the signal of the pulsar was weaker than expected from the flux quoted in the database used. But also if line of sight cuts the magnetic pole centrally, longitude stationary subpulse modulation is expected. Refractive distortion in the pulsar magnetosphere or nulling will disrupt the drift bands, making it difficult or even impossible to detect drifting subpulses. Also the P_3 values of some pulsars could be very large, or the fraction of time the pulsar spends in a drift mode could be very short. There are also pulsars (such as B0540+23) for which sporadic, regular bursts of drifting subpulses can be seen by eye in the pulse-stack, but because the apparent drift direction and rate is very different each time they are not found to have a significant preferred drift direction. In order to understand drifting subpulses better, it will be important to not only study the pulsars with highly regular drifting subpulses, but also those systems that show very variable drifting subpulses properties.

Because drifting subpulses are at the very least a common phenomenon for radio pulsars, which implies that the physical conditions required for the emission mechanism and the drifting mechanism to work are similar. This is consistent with the absence of a correlation with the surface magnetic field strength.

The measured values of P_3 at the two frequencies are highly correlated and the same is true for pulsars with drifting subpulses and double peaked intensity profiles. These correlations are expected when the drifting subpulses share a common physical origin, such as expected for instance in the framework of the sparking gap model. Therefore it will be a great challenge for theoretical models to explain the pulsars that deviate from these correlations.

A correlation between P_3 and other pulsar parameters is expected if the drift rate depends on any physical parameters of the pulsar and the strongest correlation is expected to be found when P_2 is identical for different pulsars. Such a correlation would be a very important observational restriction on pulsar emission models. However, there are no such correlations found. As explained in Paper I this could suggest that many pulsars in our sample are aliased or that P_2 is highly variable from pulsars to pulsar.

In the sparking gap model, drifting subpulses are expected for conal emission and therefore for pulsars with an on average higher modulation index. As noted in Paper I, drifting subpulses are found for pulsars classified as "core single stars" (for instance PSR B2255+58; Rankin 1993). This stresses the importance of being unbiased on pulsar type when studying the drifting phenomenon.

Our sample of pulsars is not biased on pulsar type or any particular pulsar characteristics, which allows us to do meaningful statistics on the drifting phenomenon. There is a weak trend found that pulsars with drifting subpulses are on average older, especially the coherent drifters, confirming the trend found at 21 cm. This correlation suggests that there is an evolutionary trend such that the youngest pulsars have the most disordered subpulses and that the subpulses become more and more organized into drifting subpulses when the pulsar ages. This trend does not necessarily imply a direct link between the true age of the pulsar and the drifting phenomenon. It could well be that the characteristic age is correlated to some other physical quantity, which is correlated with the drifting subpulse mechanism. This could be some electrodynamical quantity in the polar gap of the pulsar, but it could also be explained by the evolution of the angle between the magnetic axis and the rotation axis or the evolution of the pulse morphology. In the non-radial pulsations model (Clemens & Rosen 2004) this trend can also be explained, because the appearance of narrow drifting subpulses is favored in pulsars with an aligned magnetic axis. As discussed in Paper I, this trend cannot explained by nulling.

The coherent drifters appear to have low modulation indices at high frequencies. This trend can be explained if especially the coherent drifters show subpulse-phase steps, which are related to low modulation indices and appear to be more common at high frequencies.

The modulation indices measured at the two frequencies are clearly correlated, although they tend to be higher at low frequencies. The modulation index also appears to be correlated with three of the four complexity parameters and with the characteristic age of the pulsar. Such correlations were not found in the 21-cm data. This is consistent with the picture in which the radio emission can be divided into a drifting subpulse signal plus a quasi-steady component which becomes stronger at high observing frequencies.

Acknowledgements. The authors would like to express their gratitude to the staff of the WSRT for their flexibility with scheduling and assisting with the observations. The Westerbork Synthesis Radio Telescope is operated by the ASTRON (Netherlands Foundation for Research in Astronomy) with support from NWO.

References

Arons, J., & Scharlemann, E. T. 1979, ApJ, 231, 854
Asgekar, A., & Deshpande, A. A. 2005, MNRAS, 357, 1105
Ashworth, M. 1982, Ph.D. Thesis, The University of Manchester
Backer, D. C. 1970, Nature, 227, 692
Backer, D. C. 1973, ApJ, 182, 245
Backer, D. C., Rankin, J. M., & Campbell, D. B. 1975, ApJ, 197, 481
Backus, P. R. 1981, Ph.D. Thesis, The University of Massachusetts
Biggs, J. D. 1992, ApJ, 394, 574
Biggs, J. D., Hamilton, P. A., McCulloch, P. M., & Manchester, R. N. 1985, MNRAS, 214, 47P
Biggs, J. D., Lyne, A. G., Hamilton, P. A., McCulloch, P. M., & Manchester, R. N. 1988, MNRAS, 235, 255
Biggs, J. D., McCulloch, P. M., Hamilton, P. A., & Manchester, R. N. 1987, MNRAS, 228, 119
Chen, K., & Ruderman, M. 1993, ApJ, 402, 264
Clemens, J. C., & Rosen, R. 2004, ApJ, 609, 340
Cordes, J. M. 1975, ApJ, 195, 193
Cordes, J. M. 1978, ApJ, 222, 1006
Deich, W. T. S., Cordes, J. M., Hankins, T. H., & Rankin, J. M. 1986, ApJ, 300, 540
Drake, F. D., & Craft, H. D. 1968, Nature, 220, 231
Edwards, R. T. 2004, A&A, 426, 677
Edwards, R. T., & Stappers, B. W. 2002, A&A, 393, 733
Edwards, R. T., & Stappers, B. W. 2003a, A&A, 407, 273
Edwards, R. T., & Stappers, B. W. 2003b, A&A, 410, 961
Edwards, R. T., Stappers, B. W., & van Leeuwen, A. G. J. 2003, A&A, 402, 321
Ferguson, D. C., & Boriakoff, V. 1980, ApJ, 239, 310
Fowler, L. A., & Wright, G. A. E. 1982, A&A, 109, 279
Fowler, L. A., Wright, G. A. E., & Morris, D. 1981, A&A, 93, 54
Fussell, D., & Luo, Q. 2004, MNRAS, 349, 1019
Gil, J. A., Jessner, A., Kijak, J., et al. 1994, A&A, 282, 45
Gil, J. A., & Sendyk, M. 2000, ApJ, 541, 351
Hankins, T. H., & Wolszczan, A. 1987, ApJ, 318, 410
Hibschman, J. A., & Arons, J. 2001, ApJ, 560, 871
Huguenin, G. R., Taylor, J. H., & Troland, T. H. 1970, ApJ, 162, 727
Izvekova, V. A., Kuz'min, A. D., Lyne, A. G., Shitov, Y. P., & Graham Smith, F. 1993, MNRAS, 261, 865
Izvekova, V. A., Kuz'min, A. D., & Shitov, Y. P. 1982, Sov. Astron., 26, 324
Janssen, G. H., & van Leeuwen, J. 2004, A&A, 425, 255
Jenet, F. A., & Gil, J. 2003, ApJ, 596, L215
Kuz'min, A. D., & Losovskii, B. Y. 1999, Astron. Rep., 43, 288
Lou, Y. 2001, ApJ, 563, L147
Lyne, A. G., & Ashworth, M. 1983, MNRAS, 204, 519
Malofeev, V. M., Malov, O. I., & Shchegoleva, N. B. 1998, ARep, 42, 241
Manchester, R. N., Hobbs, G. B., Teoh, A., & Hobbs, M. 2005, AJ, 129, 1993
Nowakowski, L., Usowicz, J., Wolszczan, A., & Kępa, A. 1982, A&A, 116, 158
Nowakowski, L. A. 1991, ApJ, 377, 581
Nowakowski, L. A. 1996, ApJ, 457, 868
Oster, L., Hilton, D. A., & Sieber, W. 1977a, A&A, 57, 1
Oster, L., Hilton, D. A., & Sieber, W. 1977b, A&A, 57, 323
Oster, L., & Sieber, W. 1977, A&A, 58, 303
Petrova, S. A. 2000, A&A, 360, 592
Popov, M. V., Soglasnov, V. A., Kondrat'Ev, V. I., et al. 2006, ARep, 50, 55
Press, W. H., Teukolsky, S. A., Vetterling, W. T., & Flannery, B. P. 1992, Numerical recipes in C. The art of scientific computing (Cambridge: University Press), 2nd edn.
Prószyński, M., & Wolszczan, A. 1986, ApJ, 307, 540
Rankin, J. M. 1986, ApJ, 301, 901
Rankin, J. M. 1993, ApJS, 85, 145
Rankin, J. M., Wolszczan, A., & Stinebring, D. R. 1988, ApJ, 324, 1048
Redman, S. L., Wright, G. A. E., & Rankin, J. M. 2005, MNRAS, 357, 859
Ritchings, R. T. 1976, MNRAS, 176, 249
Ritchings, R. T., & Lyne, A. G. 1975, Nature, 257, 293
Scheuer, P. A. G. 1968, Nature, 218, 920
Schönhardt, R. E., & Sieber, W. 1973, ApJL, 14, 61
Sieber, W., & Oster, L. 1975, A&A, 38, 325
Smits, J. M., Mitra, D., & Kuijpers, J. 2005, A&A, 440, 683
Smits, J. M., Mitra, D., Stappers, B. W., et al. 2007, A&A, 465, 575
Srostlik, Z., & Rankin, J. M. 2005, MNRAS, 362, 1121
Staelin, D. H., & Reifenstein, E. C. 1968, Science, 162, 1481
Sutton, J. M., Staelin, D. H., Price, R. M., & Weimer, R. 1970, ApJ, 159, L89
Taylor, J. H., & Huguenin, G. R. 1971, ApJ, 167, 273
Taylor, J. H., Manchester, R. N., & Huguenin, G. R. 1975, ApJ, 195, 513
van Leeuwen, A. G. J., Kouwenhoven, M. L. A., Ramachandran, R., Rankin, J. M., & Stappers, B. W. 2002, A&A, 387, 169
van Leeuwen, A. G. J., Stappers, B. W., Ramachandran, R., & Rankin, J. M. 2003, A&A, 399, 223
Vivekanand, M., & Joshi, B. C. 1997, ApJ, 477, 431
Voûte, J. L. L., Kouwenhoven, M. L. A., van Haren, P. C., et al. 2002, A&A, 385, 733
Weltevrede, P., Stappers, B. W., van den Horn, L. J., & Edwards, R. T. 2003, A&A, 412, 473
Weltevrede, P., Edwards, R. T., & Stappers, B. W. 2006a, A&A, 445, 243
Weltevrede, P., Stappers, B. W., Rankin, J. M., & Wright, G. A. E. 2006b, ApJ, 645, L149
Weltevrede, P., Wright, G. A. E., Stappers, B. W., & Rankin, J. M. 2006c, A&A, 458, 269
Weltevrede, P., Wright, G. A. E., & Stappers, B. W. 2007, A&A, 467, 1163
Wolszczan, A. 1980, A&A, 86, 7
Wolszczan, A., Bartel, N., & Sieber, W. 1981, A&A, 100, 91
Wright, G. A. E. 2003, MNRAS, 344, 1041
Wright, G. A. E., & Fowler, L. A. 1981, A&A, 101, 356
Wright, G. A. E., Sieber, W., & Wolszczan, A. 1986, A&A, 160, 402

Table 2. The details of all the analysed pulsars. The classification of the pulsar in the second column, where "Coh" is a coherent drifter, "Dif" and "Dif*" are diffuse drifters with or without drift features which are clearly separated from the alias borders and "Lon" are pulsars showing longitude stationary subpulse modulation. The next columns are the pulse period, its dimensionless time derivative, the number of pulses in the observation, the signal to noise ratio, the minimum in the longitude resolved modulation index, the minimum detectable modulation index, the horizontal and vertical driftband separation and the figure number.

Pulsar	Class	P_0 (s)	$\dot{P}$	Pulses	S/N	m	$m_{\rm thresh}$	P_2 (deg)	P_3 (P_0)	Figure
B0011+47		1.2407	5.6×10^{-16}	2565	88	1.51 ± 0.04	0.35			A.1
B0031−07	Dif	0.9430	4.1×10^{-16}	7666	887	1.4 ± 0.1	0.12	$-21.9^{+0.2}_{-0.1}$	6.7 ± 0.1	A.1
B0037+56		1.1182	2.9×10^{-15}	1555	48	0.73 ± 0.05	0.47			A.1
B0105+65	Coh	1.2837	1.3×10^{-14}	1363	99	0.49 ± 0.04	0.33	-13^{+2}_{-4}	2.08 ± 0.03	A.1
B0136+57	Dif*	0.2725	1.1×10^{-14}	6303	201	0.72 ± 0.02	0.24	-35^{+5}_{-15}	6.1 ± 0.5	A.1
B0138+59		1.2229	3.9×10^{-16}	1904	147	0.56 ± 0.05	0.27			A.1
B0148−06	Coh	1.4647	4.4×10^{-16}	1180	77	0.9 ± 0.1	0.44	$-14.0^{+0.6}_{-0.5}$	14.4 ± 0.1	A.17
								-36^{+6}_{-2}	14.51 ± 0.04	
B0149−16	Dif	0.8327	1.3×10^{-15}	1026	190	0.39 ± 0.05	0.17	-13^{+2}_{-4}	5.7 ± 0.2	A.17
								-14^{+4}_{-10}	5.6 ± 0.4	
B0301+19	Dif*	1.3876	1.3×10^{-15}	2541	221	1.11 ± 0.06	0.18	-25^{+4}_{-3}	5.2 ± 0.3	A.17
								-25^{+6}_{-12}	4.5 ± 0.4	
B0320+39	Coh	3.0321	6.4×10^{-16}	3545	477	0.33 ± 0.01	0.11	$6.4^{+0.2}_{-0.3}$	8.46 ± 0.01	A.1
B0329+54	Dif*	0.7145	2.0×10^{-15}	16 379	8005	0.9222 ± 0.0001	0.002	300^{+150}_{-50}	4 ± 2	A.17
								60^{+8}_{-2}	6 ± 1	
B0355+54		0.1564	4.4×10^{-15}	18 897	230	1.7 ± 0.1	0.26			A.1
B0402+61		0.5946	5.6×10^{-15}	8995	181	0.62 ± 0.09	0.30			A.17
B0410+69		0.3907	7.7×10^{-17}	2965	50			0.42		A.1
J0421−0345	Dif	2.1613	1.2×10^{-15}	1090	51	0.91 ± 0.03	0.36	5^{+3}_{-1}	3.16 ± 0.04	A.1
B0447−12		0.4380	1.0×10^{-16}	4010	60	0.7 ± 0.1	0.62			A.2
B0450+55	Dif*	0.3407	2.4×10^{-15}	5161	124	0.57 ± 0.03	0.30	-170^{+15}_{-100}	8.7 ± 0.5	A.2
B0450−18		0.5489	5.8×10^{-15}	1560	273	0.53 ± 0.01	0.15			A.18
B0458+46		0.6386	5.6×10^{-15}	2750	53	0.66 ± 0.08	0.60			A.2
J0459−0210	Coh	1.1331	1.4×10^{-15}	3123	129	0.79 ± 0.03	0.24	-9^{+1}_{-3}	2.36 ± 0.01	A.2
J0520−2553		0.2416	3.0×10^{-17}	7275	38	0.69 ± 0.09	0.61			A.2
B0523+11		0.3544	7.4×10^{-17}	4948	142	0.43 ± 0.05	0.26			A.2
B0525+21	Dif*	3.7455	4.0×10^{-14}	949	333	1.56 ± 0.05	0.12	-70^{+10}_{-10}	3.7 ± 0.5	A.18
B0531+21		0.0331	4.2×10^{-13}	106 150	983	0.36 ± 0.02	0.21			A.18
B0540+23		0.2460	1.5×10^{-14}	3481	111	1.87 ± 0.06	0.31			A.2
B0559−05		0.3960	1.3×10^{-15}	2168	58	0.6 ± 0.1	0.54			A.2
B0609+37		0.2980	5.9×10^{-17}	11 926	64	0.62 ± 0.07	0.53			A.2
B0611+22		0.3350	5.9×10^{-14}	2504	112	0.58 ± 0.07	0.22			A.2
B0626+24		0.4766	2.0×10^{-15}	1791	89	0.43 ± 0.04	0.30			A.3
B0628−28	Dif*	1.2444	7.1×10^{-15}	1397	566	0.7 ± 0.1	0.09	?	10 ± 3	A.18
								70^{+80}_{-20}	4.4 ± 0.3	
B0643+80		1.2144	3.8×10^{-15}	2749	42	0.53 ± 0.05	0.49			A.3
B0727−18		0.5102	1.9×10^{-14}	2822	54	0.93 ± 0.05	0.46			A.3
B0740−28		0.1668	1.7×10^{-14}	4317	336	0.38 ± 0.02	0.15			A.3
B0751+32	Dif*	1.4423	1.1×10^{-15}	2445	84	1.2 ± 0.1	0.28	-90^{+20}_{-30}	6 ± 2	A.18
								?	2.5 ± 0.7	
B0756−15	Lon	0.6823	1.6×10^{-15}	5212	101	0.68 ± 0.07	0.39	?	20 ± 5	A.3
B0809+74	Coh	1.2922	1.7×10^{-16}	15 984	3107	0.77 ± 0.01	0.04	$-13.2^{+0.1}_{-0.7}$	11.12 ± 0.01	A.3
B0818−13	Coh	1.2381	2.1×10^{-15}	8686	1935	0.482 ± 0.001	0.04	$-5.1^{+0.1}_{-0.6}$	4.74 ± 0.01	A.3
B0820+02	Dif*	0.8649	1.0×10^{-16}	15 905	903	0.9 ± 0.1	0.11	10^{+2}_{-1}	4.5 ± 0.5	A.3
B0823+26	Dif*	0.5307	1.7×10^{-15}	1617	865	0.85 ± 0.02	0.03	70^{+10}_{-12}	5.3 ± 0.1	A.3
B0834+06	Dif*	1.2738	6.8×10^{-15}	2314	898	0.51 ± 0.01	0.08	-20^{+5}_{-35}	2.19 ± 0.02	A.19
								?	2.17 ± 0.02	
B0906−17		0.4016	6.7×10^{-16}	2132	86	0.79 ± 0.03	0.39			A.3
B0919+06	Dif*	0.4306	1.4×10^{-14}	1988	292	0.44 ± 0.01	0.15	-200^{+150}_{-200}	4 ± 2	A.4
B0942−13	Dif*	0.5703	4.5×10^{-17}	1503	237	0.57 ± 0.01	0.14	$-1.5^{+0.1}_{-6}$	3.0 ± 0.1	A.4
B0950+08	Dif*	0.2531	2.3×10^{-16}	16 395	343	1.0 ± 0.2	0.26	-500^{+100}_{-300}	6 ± 3	A.4

Table 2. continued.

Pulsar	Class	P_0 (s)	$\dot{P}$	Pulses	S/N	m	$m_{\rm thresh}$	P_2 (deg)	P_3 (P_0)	Figure
B1039−19	Dif	1.3864	9.4×10^{-16}	1258	70	0.8 ± 0.1	0.46	50^{+300}_{-20}	4.2 ± 0.2	A.19
								12^{+20}_{-1}	4.2 ± 0.2	
B1112+50	Dif*	1.6564	2.5×10^{-15}	1055	55	2.1 ± 0.1	0.52	40^{-10}_{+20}	9 ± 5	A.4
B1133+16	Dif*	1.1879	3.7×10^{-15}	3999	2170	0.800 ± 0.003	0.04	170^{+60}_{-50}	4 ± 2	A.19
								120^{+50}_{-20}	30 ± 8	
B1237+25	Dif*	1.3824	9.6×10^{-16}	5219	851	0.505 ± 0.005	0.05	-33^{+4}_{-1}	2.77 ± 0.01	A.19
								37^{+10}_{-2}	2.77 ± 0.04	
B1254−10		0.6173	3.6×10^{-16}	2811	58	0.91 ± 0.07	0.49			A.4
B1322+83		0.6700	5.7×10^{-16}	2590	50	0.58 ± 0.08	0.58			A.4
B1508+55	Dif*	0.7397	5.0×10^{-15}	10 486	1949	0.660 ± 0.002	0.05	-18^{+2}_{-12}	3.2 ± 0.1	A.19
								-35^{+2}_{-7}	2.4 ± 0.1	
B1530+27	Dif*	1.1248	7.8×10^{-16}	1543	65	1.50 ± 0.07	0.47	-40^{+10}_{-25}	4 ± 4	A.4
B1540−06	Coh	0.7091	8.8×10^{-16}	5130	588	0.24 ± 0.02	0.09	$6.0^{+3}_{-0.5}$	3.05 ± 0.01	A.4
B1541+09	Lon	0.7484	4.3×10^{-16}	2349	131	0.62 ± 0.02	0.17	?	17 ± 4	A.4
B1552−23		0.5326	6.9×10^{-16}	4962	21		1.73			A.4
B1600−27		0.7783	3.0×10^{-15}	1101	70	1.21 ± 0.05	0.39			A.5
J1603−2531		0.2831	1.6×10^{-15}	12 552	34	1.4 ± 0.1	0.99			A.5
B1604−00	Dif*	0.4218	3.1×10^{-16}	2225	361	0.73 ± 0.01	0.11	100^{+10}_{-15}	2.9 ± 0.5	A.5
B1607−13	Dif*	1.0184	2.3×10^{-16}	1710	37	1.2 ± 0.1	0.85	-20^{+5}_{-20}	8 ± 2	A.5
B1612+07	Dif*	1.2068	2.4×10^{-15}	1455	113	0.96 ± 0.02	0.21	-60^{+40}_{-60}	6 ± 4	A.5
B1620−09		1.2764	2.6×10^{-15}	1377	56	0.74 ± 0.05	0.40			A.5
B1633+24		0.4905	1.2×10^{-16}	4806	74	0.65 ± 0.06	0.48	-25^{+8}_{-40}	2.2 ± 0.1	A.5
B1642−03	Dif*	0.3877	1.8×10^{-15}	14 587	2192	0.3413 ± 0.0005	0.02	-70^{+15}_{-30}	11 ± 1	A.5
B1648−17		0.9734	3.0×10^{-15}	1804	59			0.41		A.5
B1649−23		1.7037	3.2×10^{-15}	1030	65	0.94 ± 0.04	0.41			A.5
J1650−1654	Coh	1.7496	3.2×10^{-15}	1002	33	0.9 ± 0.2	0.67	15^{+8}_{-4}	2.6 ± 0.1	A.6
J1652+2651	Dif*	0.9158	6.5×10^{-16}	3875	78	0.7 ± 0.1	0.47	-40^{+10}_{-80}	25 ± 2	A.6
J1654−2713		0.7918	1.7×10^{-16}	4480	31	0.9 ± 0.1	0.72			A.6
B1657−13		0.6410	6.2×10^{-16}	2743	13		1.91			A.6
B1700−18	Dif	0.8043	1.7×10^{-15}	1067	72	1.24 ± 0.05	0.39	-9^{+1}_{-3}	3.7 ± 0.2	A.6
B1702−19	Coh	0.2990	4.1×10^{-15}	11 885	115	0.40 ± 0.06	0.38	-90^{+40}_{-50}	10.8 ± 0.2	A.6
B1706−16		0.6531	6.3×10^{-15}	1314	228	0.77 ± 0.01	0.13			A.6
B1709−15		0.8688	1.1×10^{-15}	2024	32		0.56			A.6
B1717−16		1.5656	5.8×10^{-15}	2252	94	0.65 ± 0.03	0.34			A.6
B1717−29	Coh	0.6204	7.5×10^{-16}	1380	54	1.0 ± 0.2	0.90	$-10.9^{+0.4}_{-0.7}$	2.461 ± 0.001	A.6
B1718−02	Dif	0.4777	8.3×10^{-17}	3665	61	1.2 ± 0.1	0.67	100^{+60}_{-10}	5.4 ± 0.1	A.7
B1726−00		0.3860	1.1×10^{-15}	9191	68	0.54 ± 0.08	0.51			A.7
B1730−22	Coh	0.8717	4.3×10^{-17}	3027	93	0.52 ± 0.03	0.33	-25^{+5}_{-50}	25 ± 5	A.7
B1732−02		0.8394	4.2×10^{-16}	2093	14		1.68			A.7
B1732−07	Lon	0.4193	1.2×10^{-15}	2047	121	0.64 ± 0.04	0.18	?	13 ± 2	A.7
J1732−1930		0.4838	1.8×10^{-16}	7345	77	0.7 ± 0.1	0.48			A.7
B1737+13	Lon	0.8031	1.5×10^{-15}	2188	109	0.49 ± 0.05	0.35	?	10 ± 4	A.20
B1738−08	Dif*	2.0431	2.3×10^{-15}	1003	63	1.13 ± 0.07	0.41	80^{+80}_{-10}	4.8 ± 0.1	A.20
								15^{+2}_{-3}	4.7 ± 0.1	
J1744−2335		1.6835	8.3×10^{-16}	2101	18		1.43			A.7
B1745−12		0.3941	1.2×10^{-15}	9015	111	0.44 ± 0.07	0.42			A.7
B1749−28		0.5626	8.1×10^{-15}	5791	1087	0.501 ± 0.003	0.08			A.7
B1753+52	Dif*	2.3914	1.6×10^{-15}	1474	36	1.4 ± 0.1	0.55	14^{+8}_{-4}	7 ± 1	A.20
B1756−22		0.4610	1.1×10^{-14}	5766	48		0.52			A.7
J1758+3030		0.9473	7.2×10^{-16}	1855	45	1.0 ± 0.1	0.73			A.8
B1758−03		0.9215	3.3×10^{-15}	3855	194	1.0 ± 0.1	0.21			A.8
J1759−2922		0.5744	4.6×10^{-15}	1494	12		1.53			A.8
B1804−08		0.1637	2.9×10^{-17}	5123	78	0.57 ± 0.03	0.34			A.8
J1808−0813		0.8760	1.2×10^{-15}	4049	45	0.71 ± 0.07	0.61			A.8
B1811+40	Lon	0.9311	2.5×10^{-15}	3811	213	0.43 ± 0.04	0.20	?	2.3 ± 0.4	A.8

Table 2. continued.

Pulsar	Class	P_0 (s)	$\dot{P}$	Pulses	S/N	m	$m_{\rm thresh}$	P_2 (deg)	P_3 (P_0)	Figure
B1818−04	Dif*	0.5981	6.3×10^{-15}	4943	513	0.43 ± 0.02	0.07	-300^{+50}_{-100}	3 ± 1	A.8
B1819−22	Coh	1.8743	1.4×10^{-15}	1095	58	0.9 ± 0.2	0.47	-17^{+2}_{-6}	16.9 ± 0.6	A.8
B1821+05		0.7529	2.3×10^{-16}	1137	60	0.70 ± 0.02	0.29			A.8
B1821−19		0.1893	5.2×10^{-15}	4528	39		0.92			A.8
B1822+00		0.7789	8.8×10^{-16}	4561	70		0.40			A.9
B1822−09		0.7690	5.2×10^{-14}	3841	90	0.30 ± 0.01	0.12			A.9
J1823−0154		0.7598	1.1×10^{-15}	1129	18		0.94			A.9
B1826−17		0.3071	5.6×10^{-15}	2781	62	0.62 ± 0.08	0.49			A.9
B1831−03		0.6867	4.2×10^{-14}	1246	87	0.42 ± 0.03	0.27			A.9
B1831−04		0.2901	7.2×10^{-17}	3099	17	0.6 ± 0.1	0.62			A.9
J1835−1106		0.1659	2.1×10^{-14}	5052	22		1.33			A.9
J1837−0045		0.6170	1.7×10^{-15}	2361	14		1.48			A.9
B1839+09		0.3813	1.1×10^{-15}	2245	79	0.61 ± 0.06	0.37			A.9
B1839+56	Dif*	1.6529	1.5×10^{-15}	1052	100	0.89 ± 0.02	0.24	120^{+130}_{-20}	40 ± 40	A.9
B1842+14		0.3755	1.9×10^{-15}	2287	164	0.52 ± 0.03	0.29			A.10
B1844−04		0.5978	5.2×10^{-14}	1431	97	0.37 ± 0.05	0.18			A.10
B1845−01		0.6594	5.3×10^{-15}	1295	29		1.36			A.10
B1845−19		4.3082	2.3×10^{-14}	1029	117	1.0 ± 0.2	0.33			A.10
B1846−06	Lon	1.4513	4.6×10^{-14}	1002	78	1.11 ± 0.08	0.25	?	4 ± 1	A.10
B1848+12		1.2053	1.2×10^{-14}	2950	73	1.0 ± 0.1	0.40			A.10
J1848−1414		0.2978	1.4×10^{-17}	4897	10		3.04			A.10
B1851−14		1.1466	4.2×10^{-15}	3093	77	0.81 ± 0.04	0.39			A.10
J1852−2610		0.3363	8.8×10^{-17}	5200	45		0.65			A.10
B1857−26	Dif	0.6122	2.0×10^{-16}	3196	297	0.60 ± 0.08	0.11	160^{+100}_{-20}	7.5 ± 0.4	A.20
								200^{+90}_{-30}	6.8 ± 0.2	
B1859+01	Lon	0.2882	2.4×10^{-15}	12 337	96	0.65 ± 0.03	0.35	?	14 ± 1	A.10
B1859+03		0.6555	7.5×10^{-15}	5418	108		0.31			A.11
B1900+01	Dif*	0.7293	4.0×10^{-15}	2395	152	0.7 ± 0.1	0.18	180^{+20}_{-30}	3.4 ± 0.9	A.11
B1900+05		0.7466	1.3×10^{-14}	4751	40		0.90			A.11
B1900−06		0.4319	3.4×10^{-15}	1987	54	0.7 ± 0.1	0.54			A.11
J1901−0906	Coh	1.7819	1.6×10^{-15}	984	35	1.27 ± 0.08	0.38	-50^{+30}_{-50}	5.1 ± 0.3	A.20
								-7^{+4}_{-2}	3.1 ± 0.1	
B1902−01		0.6432	3.1×10^{-15}	2717	35	0.67 ± 0.08	0.60			A.11
B1905+39	Dif*	1.2358	5.4×10^{-16}	1176	158	0.76 ± 0.05	0.25	40^{+110}_{-7}	4.1 ± 0.8	A.21
								17^{+10}_{-4}	4.3 ± 0.1	
B1907+00		1.0169	5.5×10^{-15}	1139	90	0.60 ± 0.02	0.26			A.11
B1907+02		0.9898	5.5×10^{-15}	1170	109	0.41 ± 0.03	0.20			A.11
B1907+10	Lon	0.2836	2.6×10^{-15}	3024	219	0.53 ± 0.02	0.21	?	13 ± 2	A.11
B1907−03		0.5046	2.2×10^{-15}	1701	55	0.35 ± 0.04	0.30			A.11
B1910+20	Lon	2.2330	1.0×10^{-14}	1095	40	0.93 ± 0.04	0.81	?	2.70 ± 0.04	A.11
B1911−04		0.8259	4.1×10^{-15}	1908	955	0.236 ± 0.005	0.07			A.12
B1913+10		0.4045	1.5×10^{-14}	4333	16		1.87			A.12
B1914+09		0.2703	2.5×10^{-15}	3105	52	0.58 ± 0.09	0.46			A.12
B1914+13	Lon	0.2818	3.6×10^{-15}	12 615	54	1.0 ± 0.1	0.90	?	21 ± 5	A.12
B1915+13		0.1946	7.2×10^{-15}	3739	115	0.41 ± 0.03	0.26			A.12
B1917+00	Dif*	1.2723	7.7×10^{-15}	1144	127	0.46 ± 0.06	0.15	90^{+20}_{-20}	7 ± 2	A.12
B1918+19	Coh	0.8210	9.0×10^{-16}	1397	111	0.65 ± 0.07	0.28	20^{+15}_{-5}	3.7 ± 0.1	A.12
B1919+21	Dif	1.3373	1.3×10^{-15}	466	730	0.31 ± 0.01	0.05	$-8.5^{+0.5}_{-1.5}$	4.4 ± 0.1	A.21
								-8^{+1}_{-2}	4.4 ± 0.1	
B1920+21		1.0779	8.2×10^{-15}	1350	177	0.47 ± 0.07	0.15			A.12
B1923+04	Dif*	1.0741	2.5×10^{-15}	1077	57	1.01 ± 0.07	0.43	80^{+30}_{-30}	2.9 ± 0.5	A.12
B1924+16		0.5798	1.8×10^{-14}	4580	24		1.26			A.12
B1929+10	Dif*	0.2265	1.2×10^{-15}	13 044	1274	0.49 ± 0.01	0.05	?	11.4 ± 0.6	A.13
								-350^{+60}_{-70}	5.0 ± 0.5	
B1929+20		0.2682	4.2×10^{-15}	6535	43	0.7 ± 0.1	0.70			A.13

Table 2. continued.

Pulsar	Class	P_0 (s)	$\dot{P}$	Pulses	S/N	m	$m_{\rm thresh}$	P_2 (deg)	P_3 (P_0)	Figure
B1933+16	Dif*	0.3587	6.0×10^{-15}	4791	1041	0.323 ± 0.002	0.05	-150^{+30}_{-30}	6.6 ± 0.9	A.13
B1937−26		0.4029	9.6×10^{-16}	2082	72	1.31 ± 0.05	0.45			A.13
B1940−12		0.9724	1.7×10^{-15}	1190	81	0.87 ± 0.05	0.27			A.13
B1943−29		0.9594	1.5×10^{-15}	1206	47	0.81 ± 0.06	0.35			A.13
B1944+17	Dif*	0.4406	2.4×10^{-17}	3990	143	1.55 ± 0.08	0.28	-30^{+5}_{-10}	13.5 ± 0.9	A.13
B1946+35	Lon	0.7173	7.1×10^{-15}	2396	414	0.42 ± 0.02	0.10	?	55 ± 9	A.13
B1946−25		0.9576	3.3×10^{-15}	1834	38	0.91 ± 0.05	0.48			A.13
B1952+29	Lon	0.4267	1.7×10^{-18}	5755	127	0.87 ± 0.04	0.26	?	13 ± 4	A.13
B1953+50	Dif*	0.5189	1.4×10^{-15}	1650	153	1.1 ± 0.1	0.19	60^{+30}_{-20}	15 ± 6	A.14
B2000+40		0.9051	1.7×10^{-15}	1268	53	0.61 ± 0.07	0.49			A.14
B2002+31		2.1113	7.5×10^{-14}	1114	104	0.43 ± 0.02	0.20			A.14
B2003−08		0.5809	4.6×10^{-17}	4521	44	1.18 ± 0.09	0.87			A.14
J2005−0020		2.2797	2.6×10^{-14}	1066	18		1.21			A.14
B2011+38		0.2302	8.9×10^{-15}	7597	33		1.47			A.14
B2016+28	Dif*	0.5580	1.5×10^{-16}	25 909	1461	0.910 ± 0.004	0.11	$-8.0^{+0.2}_{-1.5}$	3.7 ± 0.2	A.21
								$-8.5^{+0.2}_{-3}$	4.3 ± 0.2	
B2020+28	Dif*	0.3434	1.9×10^{-15}	6857	415	0.57 ± 0.08	0.11	-65^{+5}_{-25}	2.4 ± 0.2	A.21
								50^{+10}_{-5}	2.4 ± 0.2	
B2021+51	Dif*	0.5292	3.1×10^{-15}	3471	331	0.97 ± 0.07	0.12	150^{+150}_{-50}	3 ± 1	A.21
								40^{-5}_{+15}	3.7 ± 0.2	
B2022+50		0.3726	2.5×10^{-15}	6590	35	0.74 ± 0.07	0.60			A.14
B2027+37		1.2168	1.2×10^{-14}	1444	54	0.75 ± 0.06	0.45			A.14
B2043−04	Coh	1.5469	1.5×10^{-15}	1521	147	1.02 ± 0.03	0.28	$4.3^{+0.5}_{-0.1}$	2.75 ± 0.02	A.14
B2044+15	Dif*	1.1383	1.8×10^{-16}	1540	70	0.56 ± 0.05	0.26	-25^{-10}_{+10}	18 ± 4	A.22
								-16^{+3}_{-4}	13 ± 1	
B2045−16	Dif*	1.9616	1.1×10^{-14}	896	1969	0.154 ± 0.001	0.02	-26^{+4}_{-2}	3.0 ± 0.1	A.22
								-40^{+2}_{-17}	2.7 ± 0.1	
B2053+21	Dif*	0.8152	1.3×10^{-15}	2497	76	0.54 ± 0.04	0.37	?	105 ± 20	A.22
								15^{+5}_{-5}	130 ± 7	
B2053+36		0.2215	3.7×10^{-16}	14 369	132	0.38 ± 0.03	0.25			A.14
B2106+44		0.4149	8.6×10^{-17}	4216	102	0.70 ± 0.05	0.38			A.15
B2110+27	Dif*	1.2029	2.6×10^{-15}	2041	273	0.95 ± 0.03	0.13	50^{+10}_{-20}	7 ± 3	A.15
B2111+46	Dif*	1.0147	7.1×10^{-16}	1136	550	1.07 ± 0.04	0.04	-200^{+10}_{-30}	3.1 ± 0.1	A.22
B2113+14		0.4402	2.9×10^{-16}	5619	69	0.63 ± 0.07	0.39			A.15
B2148+52		0.3322	1.0×10^{-14}	5265	48		0.49			A.15
B2148+63	Dif*	0.3801	1.7×10^{-16}	9336	196	0.9 ± 0.1	0.28	-40^{+30}_{-90}	2.4 ± 0.7	A.15
B2154+40	Dif*	1.5253	3.4×10^{-15}	1140	536	0.69 ± 0.01	0.07	100^{+30}_{-10}	5 ± 1	A.15
B2217+47	Dif*	0.5385	2.8×10^{-15}	4934	1214	0.603 ± 0.002	0.04	-140^{+10}_{-100}	4.1 ± 0.6	A.15
B2224+65		0.6825	9.7×10^{-15}	2553	66	0.77 ± 0.04	0.37			A.15
B2227+61		0.4431	2.3×10^{-15}	8007	76	0.64 ± 0.09	0.62			A.15
J2248−0101		0.4772	6.6×10^{-16}	2423	25		1.35			A.15
B2255+58	Dif*	0.3682	5.8×10^{-15}	6705	183	0.56 ± 0.02	0.19	200^{+150}_{-60}	10.2 ± 0.5	A.16
J2302+6028	Coh	1.2064	2.0×10^{-15}	2643	87	0.33 ± 0.05	0.30	-40^{+10}_{-40}	5.25 ± 0.05	A.16
B2303+30	Coh	1.5759	2.9×10^{-15}	1685	200	0.54 ± 0.07	0.22	$10.6^{+0.8}_{-0.2}$	2.06 ± 0.02	A.16
B2306+55		0.4751	2.0×10^{-16}	3697	113	0.71 ± 0.09	0.36			A.16
B2310+42	Coh	0.3494	1.1×10^{-16}	5260	1518	0.585 ± 0.002	0.04	13^{+4}_{-6}	2.10 ± 0.05	A.22
								13^{+1}_{-1}	2.11 ± 0.03	
B2315+21	Coh	1.4447	1.0×10^{-15}	1214	165	0.56 ± 0.03	0.22	-8^{+2}_{-6}	5.1 ± 0.2	A.23
B2319+60	Dif*	2.2565	7.0×10^{-15}	1568	104	0.93 ± 0.05	0.38	80^{+30}_{-20}	5 ± 3	A.23
								20^{+6}_{-2}	6 ± 2	
B2324+60		0.2337	3.5×10^{-16}	7486	21		1.56			A.16
B2327−20	Lon	1.6436	4.6×10^{-15}	1603	647	0.73 ± 0.01	0.06	?	20 ± 10	A.16
B2334+61		0.4953	1.9×10^{-13}	3546	37	1.7 ± 0.2	1.10			A.16
J2346−0609		1.1815	1.4×10^{-15}	2972	53	1.09 ± 0.08	0.53	?	100 ± 30	A.23
B2351+61	Dif*	0.9448	1.6×10^{-14}	1859	79	1.33 ± 0.06	0.35	50^{+20}_{-15}	17 ± 3	A.16

Online Material

Appendix A: Figures

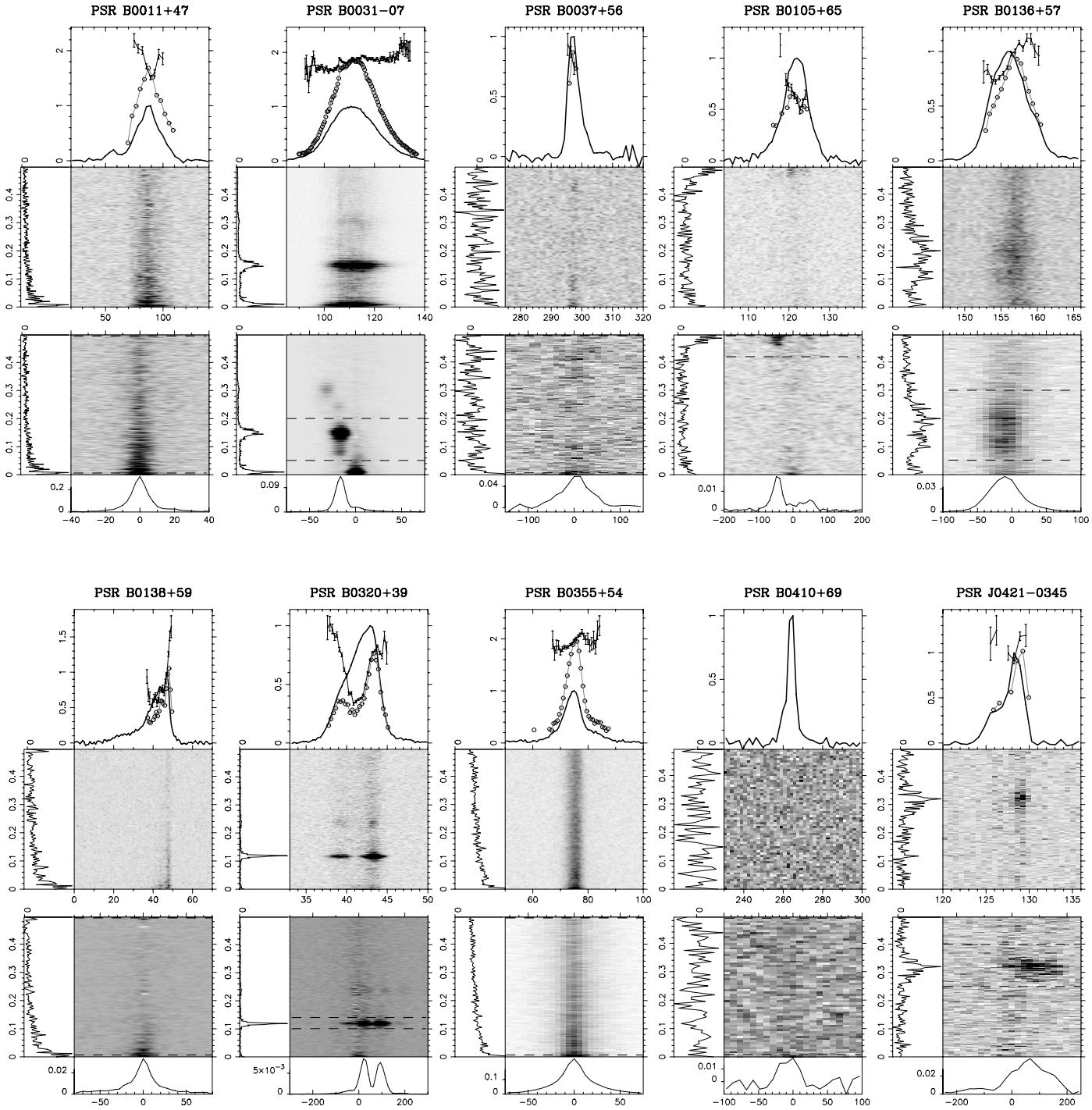

Fig. A.1. The integrated pulse profile (solid line) and the modulation index (solid points) are shown in the top plot, which is aligned with the LRFS. Below the LRFS is the 2DFS plotted. The integrated power of the spectra are shown the side- and bottom-panels of the spectra. See the main text and Fig. 1 for further details about the plots. The badly affected frequencies in the spectra are set to zero.

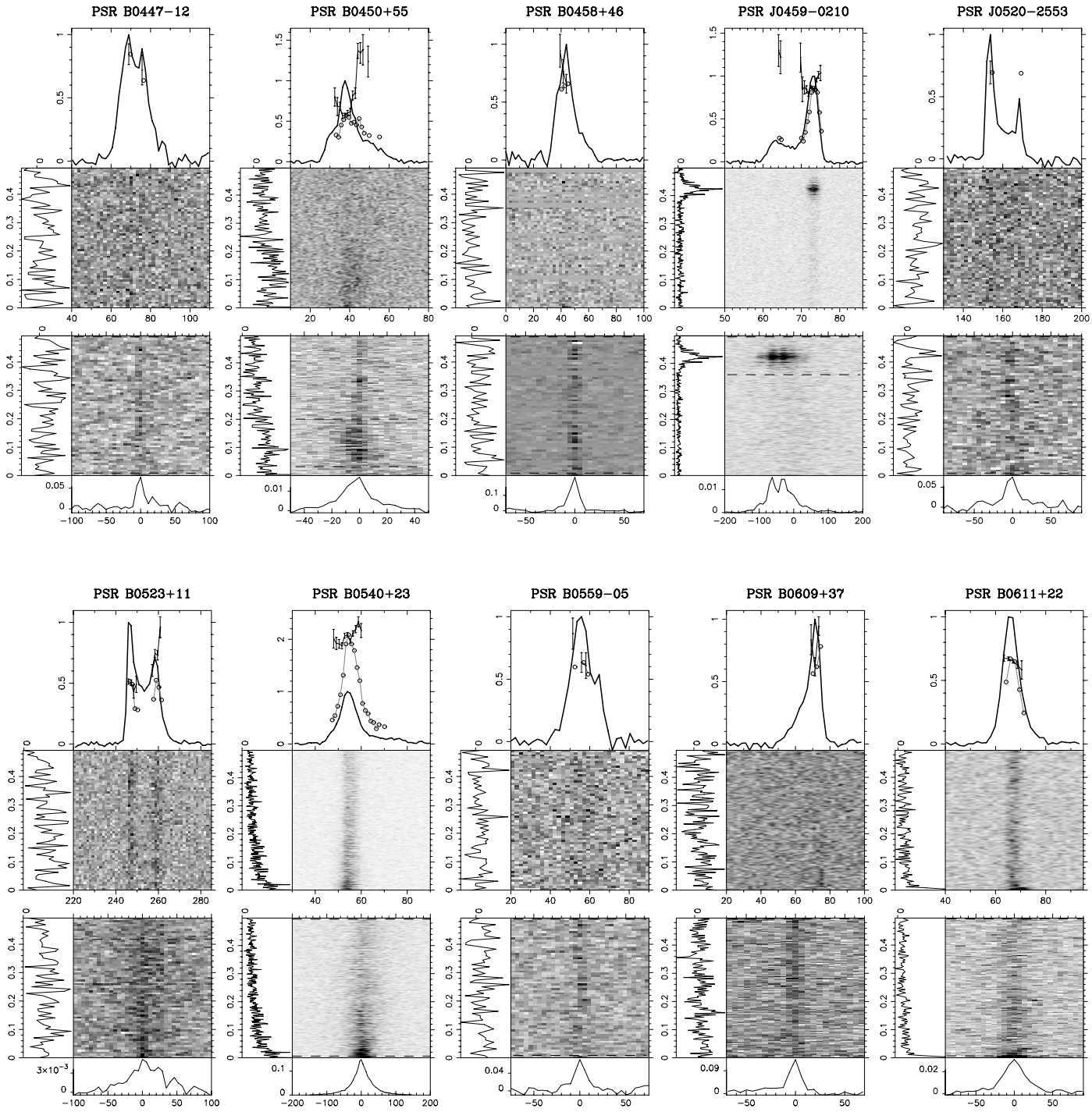

Fig. A.2. The integrated pulse profile (solid line) and the modulation index (solid points) are shown in the top plot, which is aligned with the LRFS. Below the LRFS is the 2DFS plotted. The integrated power of the spectra are shown the side- and bottom-panels of the spectra. See the main text and Fig. 1 for further details about the plots. The badly affected frequencies in the spectra are set to zero.

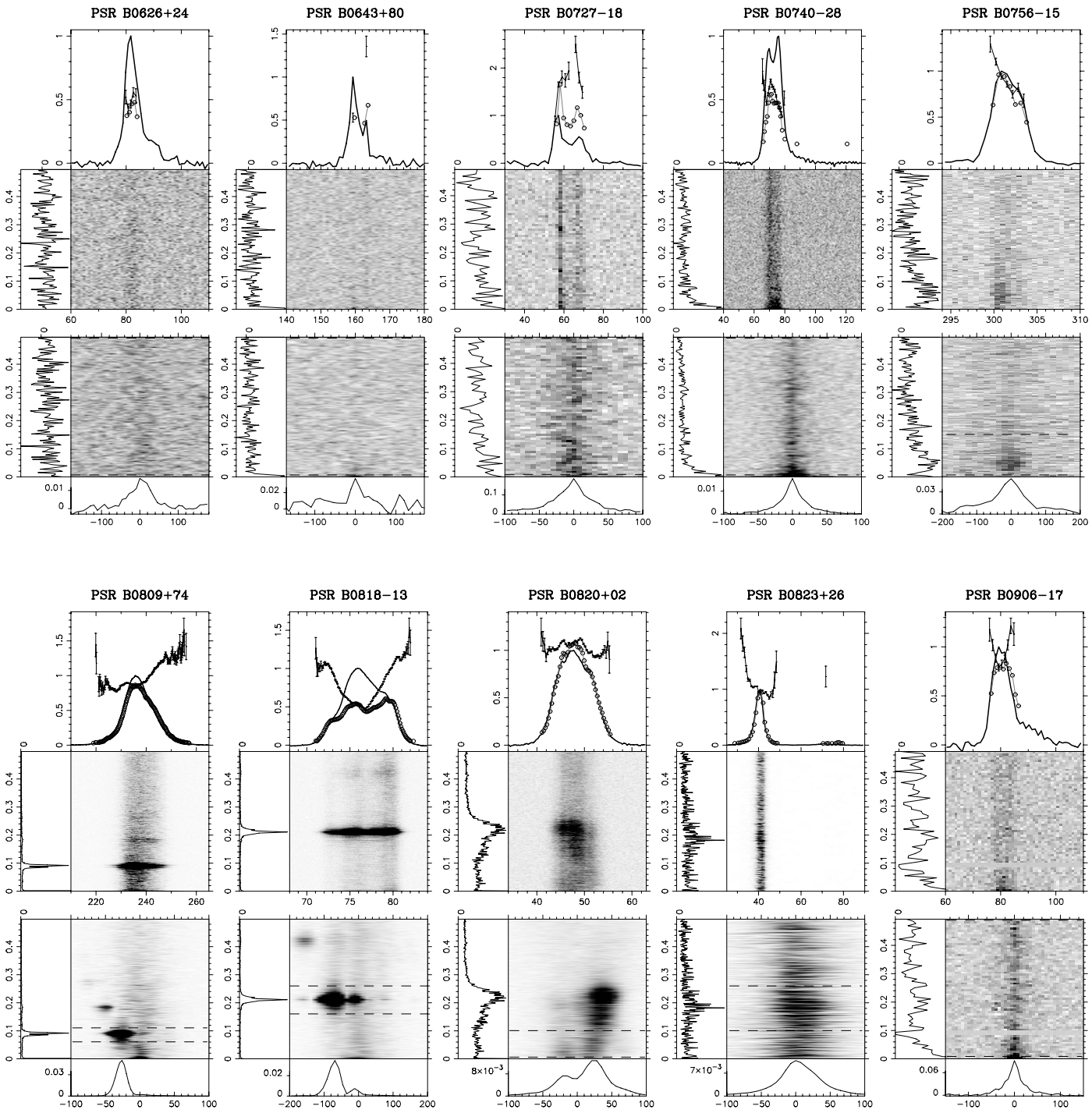

Fig. A.3. The integrated pulse profile (solid line) and the modulation index (solid points) are shown in the top plot, which is aligned with the LRFS. Below the LRFS is the 2DFS plotted. The integrated power of the spectra are shown the side- and bottom-panels of the spectra. See the main text and Fig. 1 for further details about the plots. The badly affected frequencies in the spectra are set to zero.

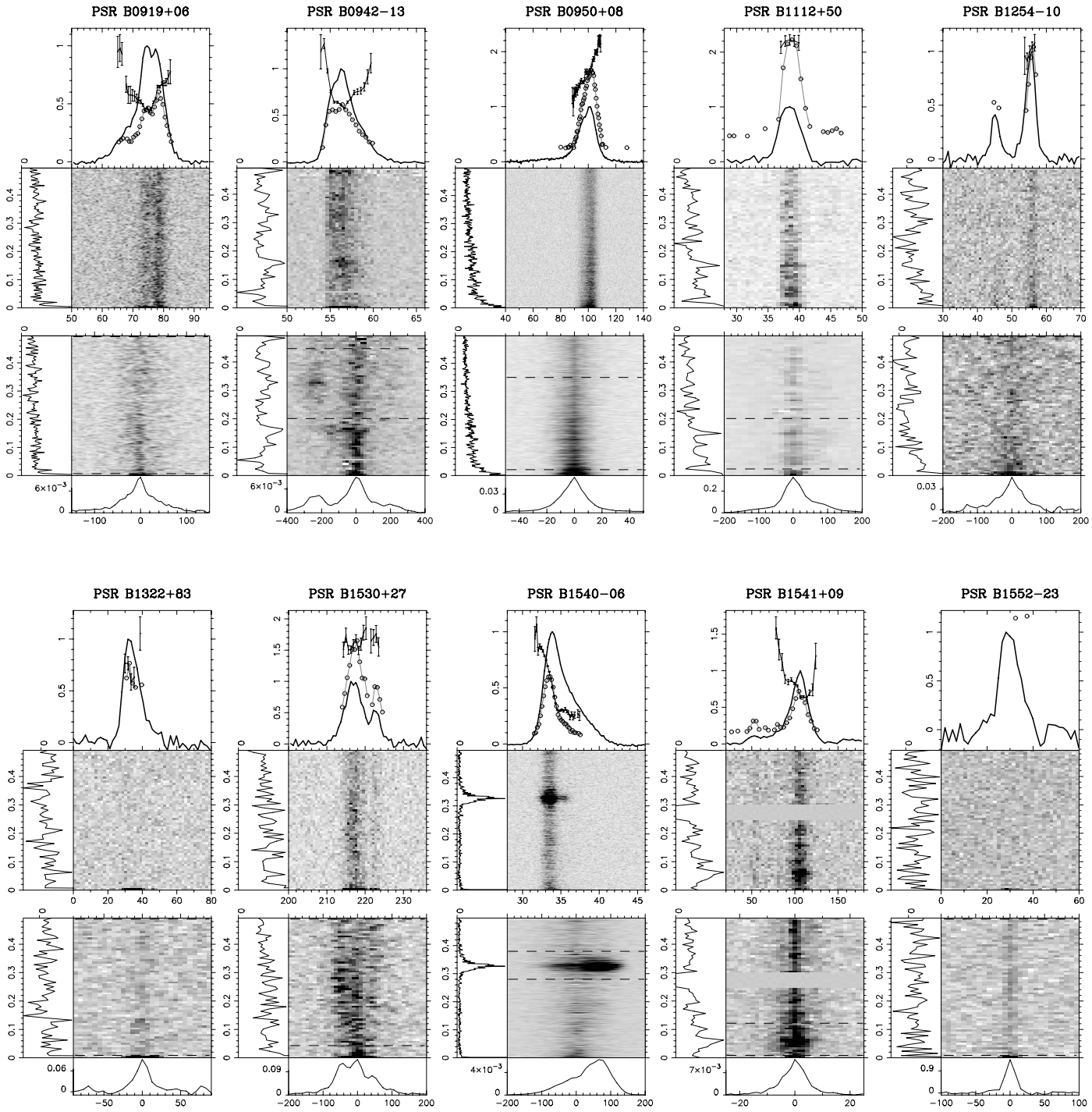

Fig. A.4. The integrated pulse profile (solid line) and the modulation index (solid points) are shown in the top plot, which is aligned with the LRFS. Below the LRFS is the 2DFS plotted. The integrated power of the spectra are shown the side- and bottom-panels of the spectra. See the main text and Fig. 1 for further details about the plots. The badly affected frequencies in the spectra are set to zero.

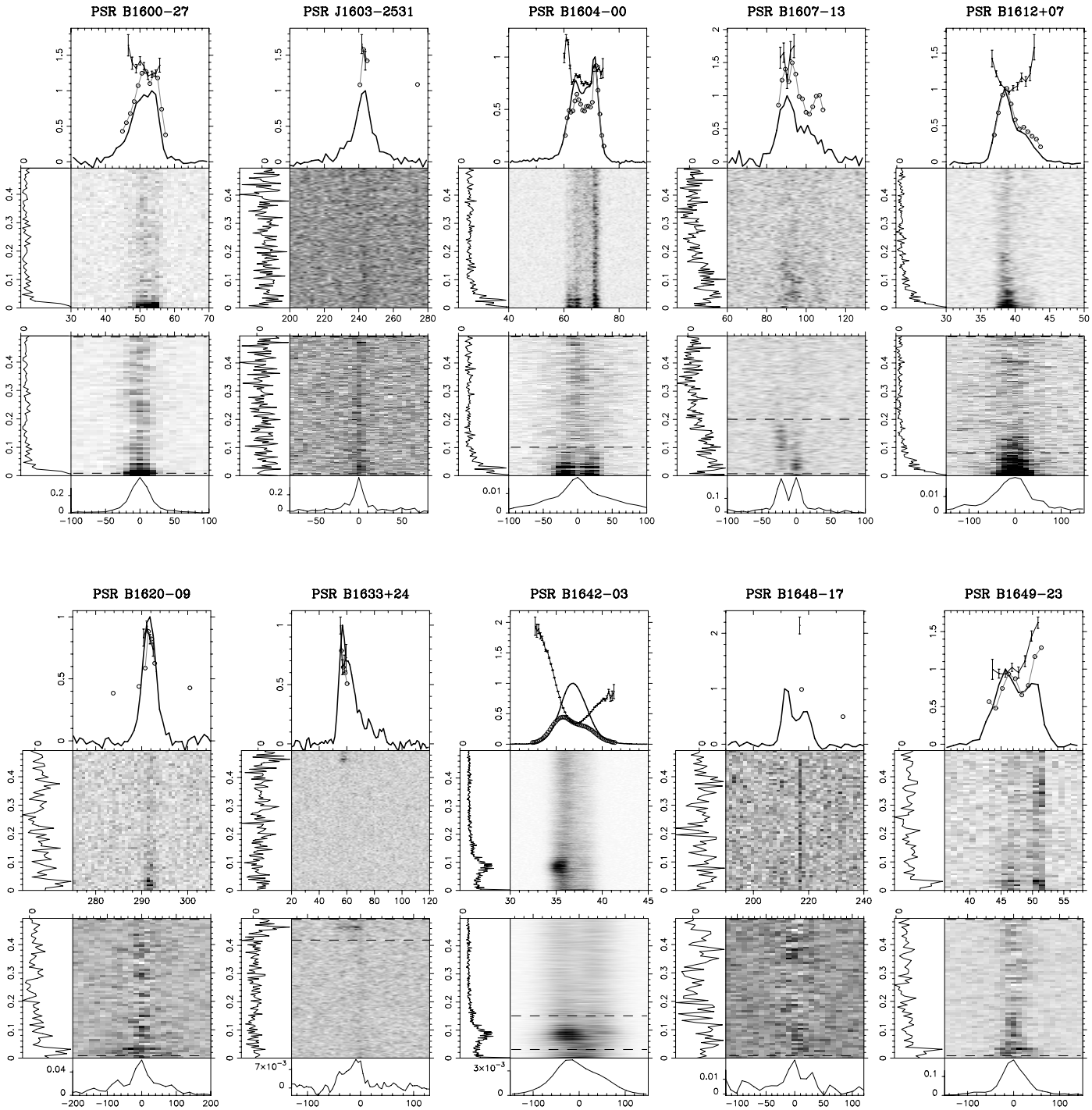

Fig. A.5. The integrated pulse profile (solid line) and the modulation index (solid points) are shown in the top plot, which is aligned with the LRFS. Below the LRFS is the 2DFS plotted. The integrated power of the spectra are shown the side- and bottom-panels of the spectra. See the main text and Fig. 1 for further details about the plots. The badly affected frequencies in the spectra are set to zero.

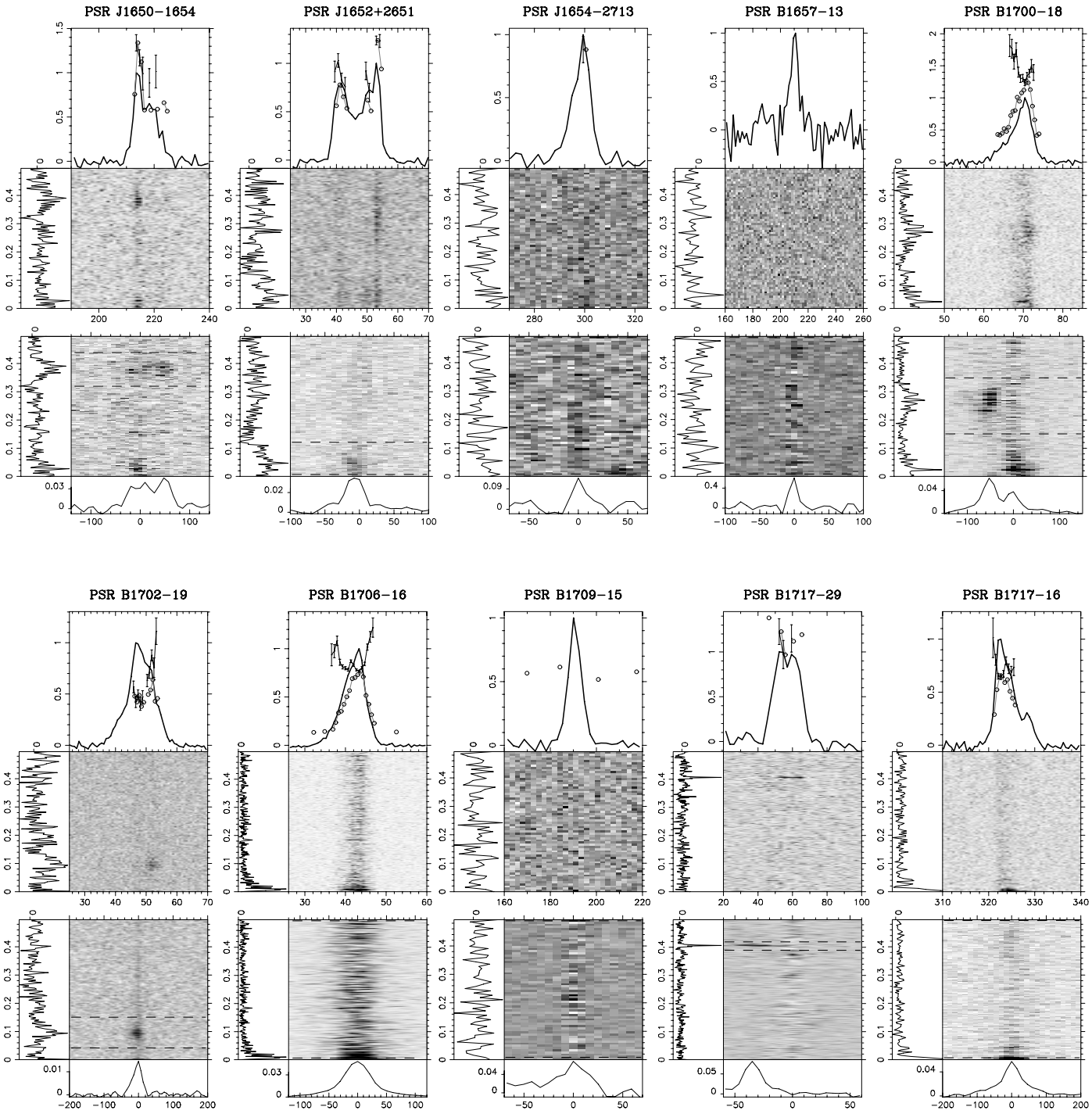

Fig. A.6. The integrated pulse profile (solid line) and the modulation index (solid points) are shown in the top plot, which is aligned with the LRFS. Below the LRFS is the 2DFS plotted. The integrated power of the spectra are shown the side- and bottom-panels of the spectra. See the main text and Fig. 1 for further details about the plots. The badly affected frequencies in the spectra are set to zero.

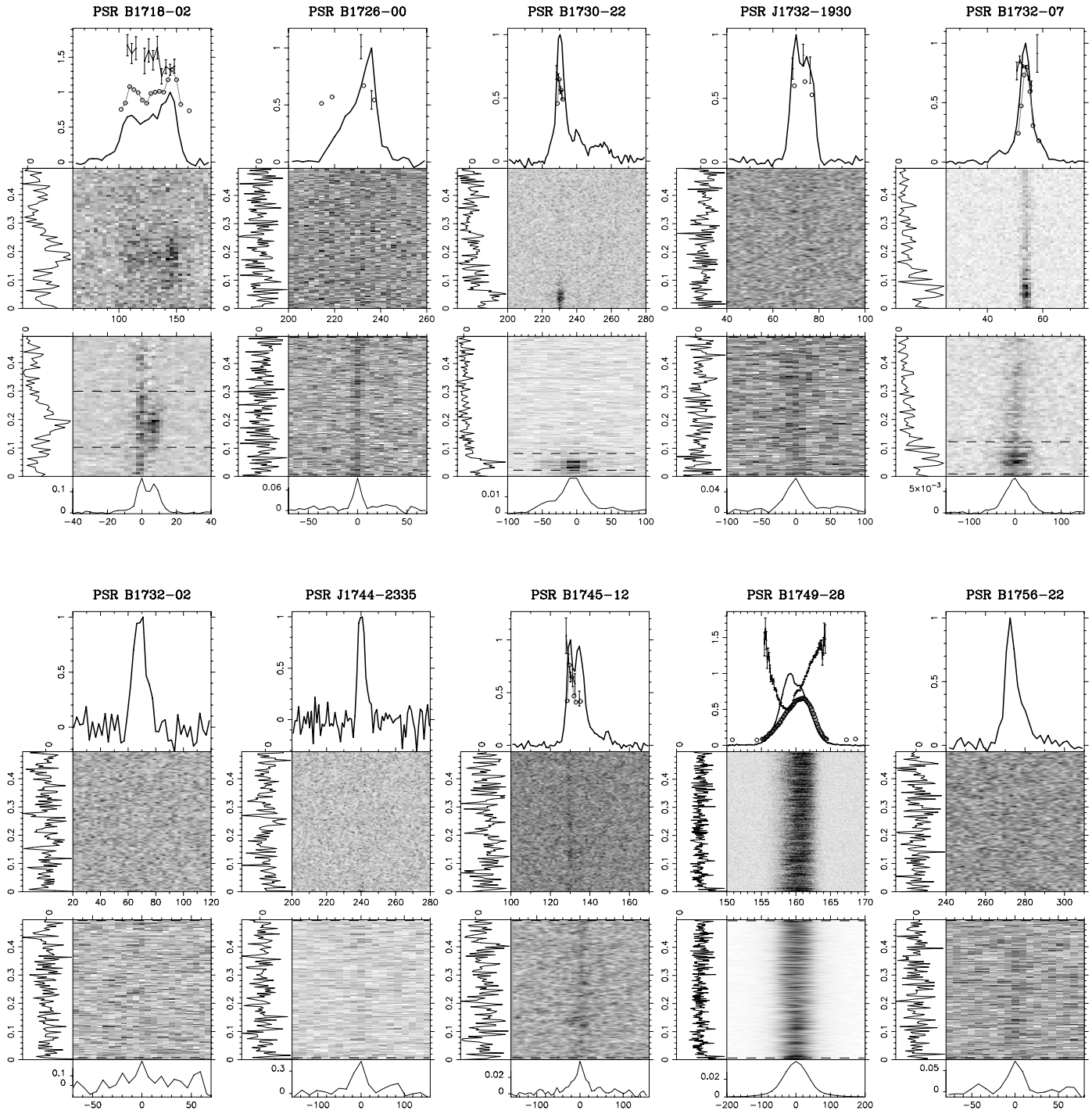

Fig. A.7. The integrated pulse profile (solid line) and the modulation index (solid points) are shown in the top plot, which is aligned with the LRFS. Below the LRFS is the 2DFS plotted. The integrated power of the spectra are shown the side- and bottom-panels of the spectra. See the main text and Fig. 1 for further details about the plots. The badly affected frequencies in the spectra are set to zero.

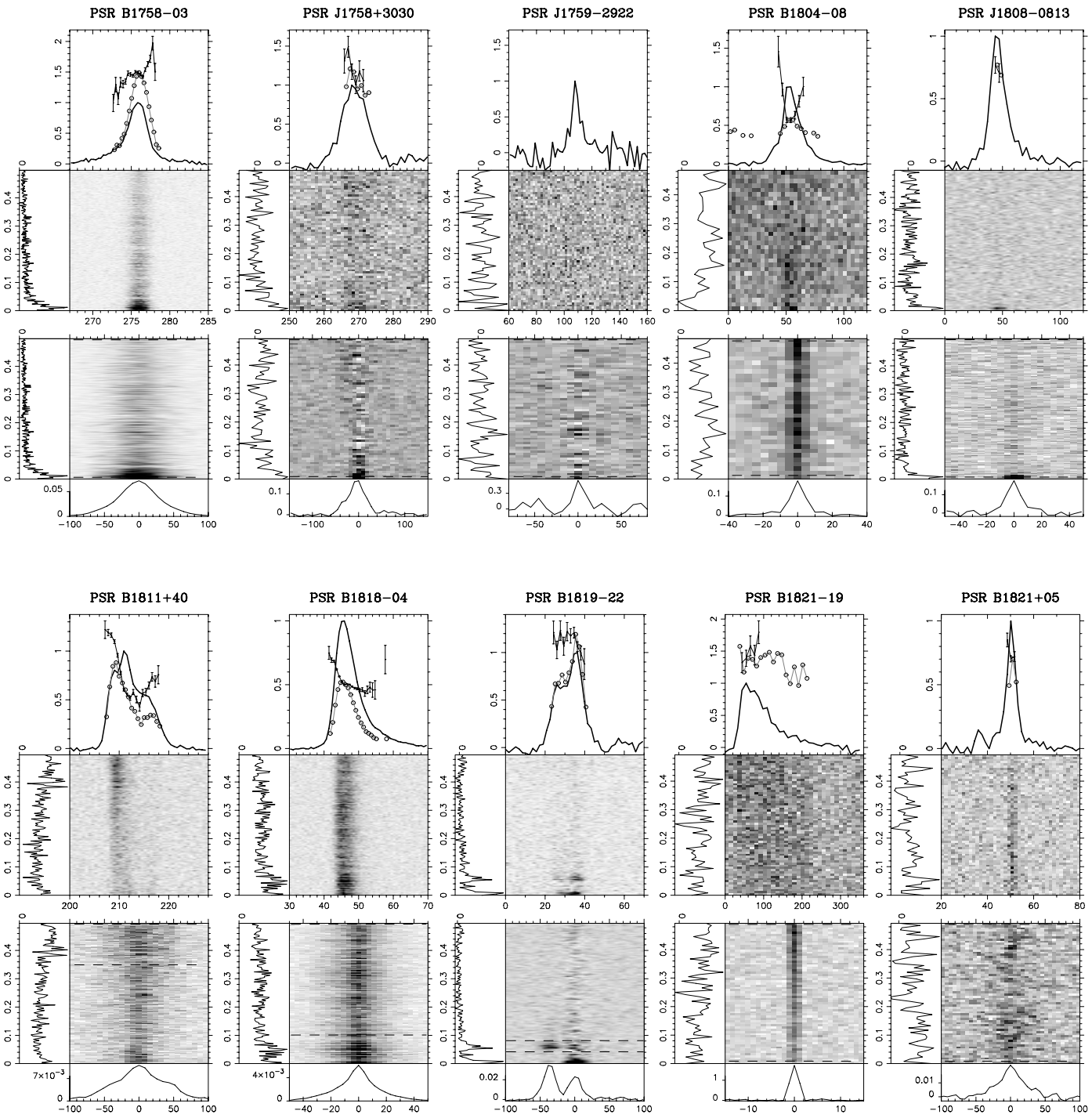

Fig. A.8. The integrated pulse profile (solid line) and the modulation index (solid points) are shown in the top plot, which is aligned with the LRFS. Below the LRFS is the 2DFS plotted. The integrated power of the spectra are shown the side- and bottom-panels of the spectra. See the main text and Fig. 1 for further details about the plots. The badly affected frequencies in the spectra are set to zero.

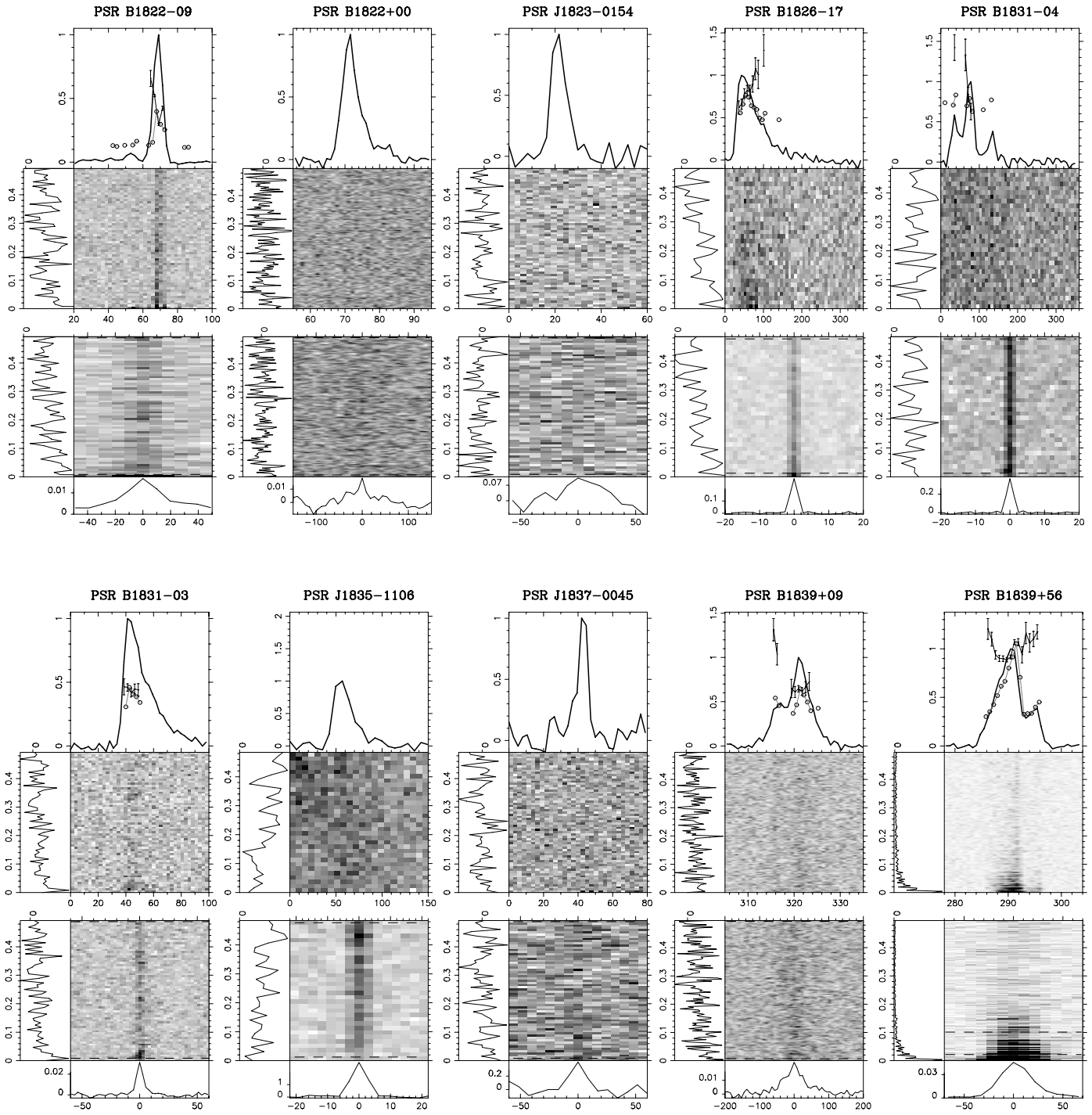

Fig. A.9. The integrated pulse profile (solid line) and the modulation index (solid points) are shown in the top plot, which is aligned with the LRFS. Below the LRFS is the 2DFS plotted. The integrated power of the spectra are shown the side- and bottom-panels of the spectra. See the main text and Fig. 1 for further details about the plots. The badly affected frequencies in the spectra are set to zero.

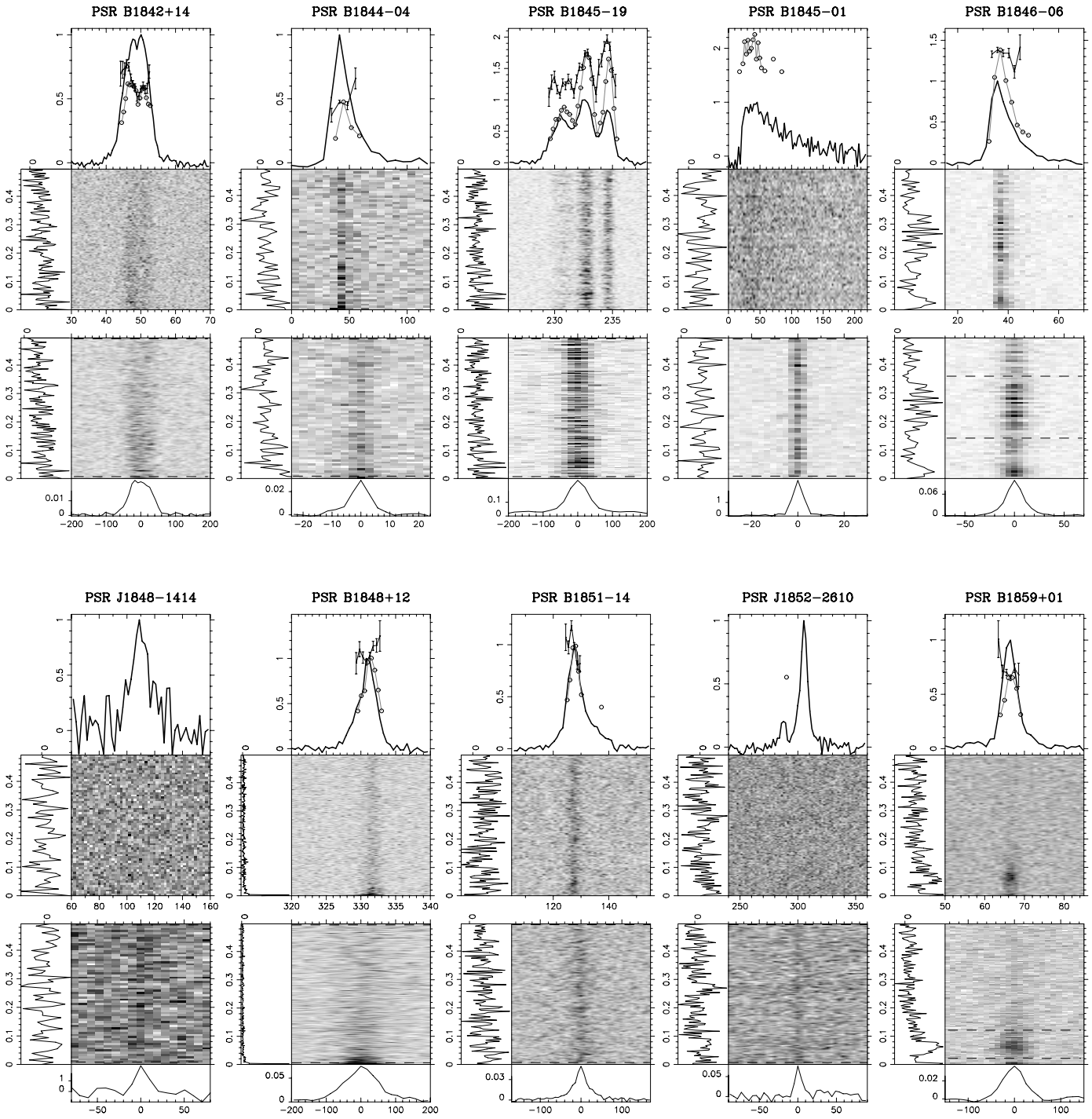

Fig. A.10. The integrated pulse profile (solid line) and the modulation index (solid points) are shown in the top plot, which is aligned with the LRFS. Below the LRFS is the 2DFS plotted. The integrated power of the spectra are shown the side- and bottom-panels of the spectra. See the main text and Fig. 1 for further details about the plots. The badly affected frequencies in the spectra are set to zero.

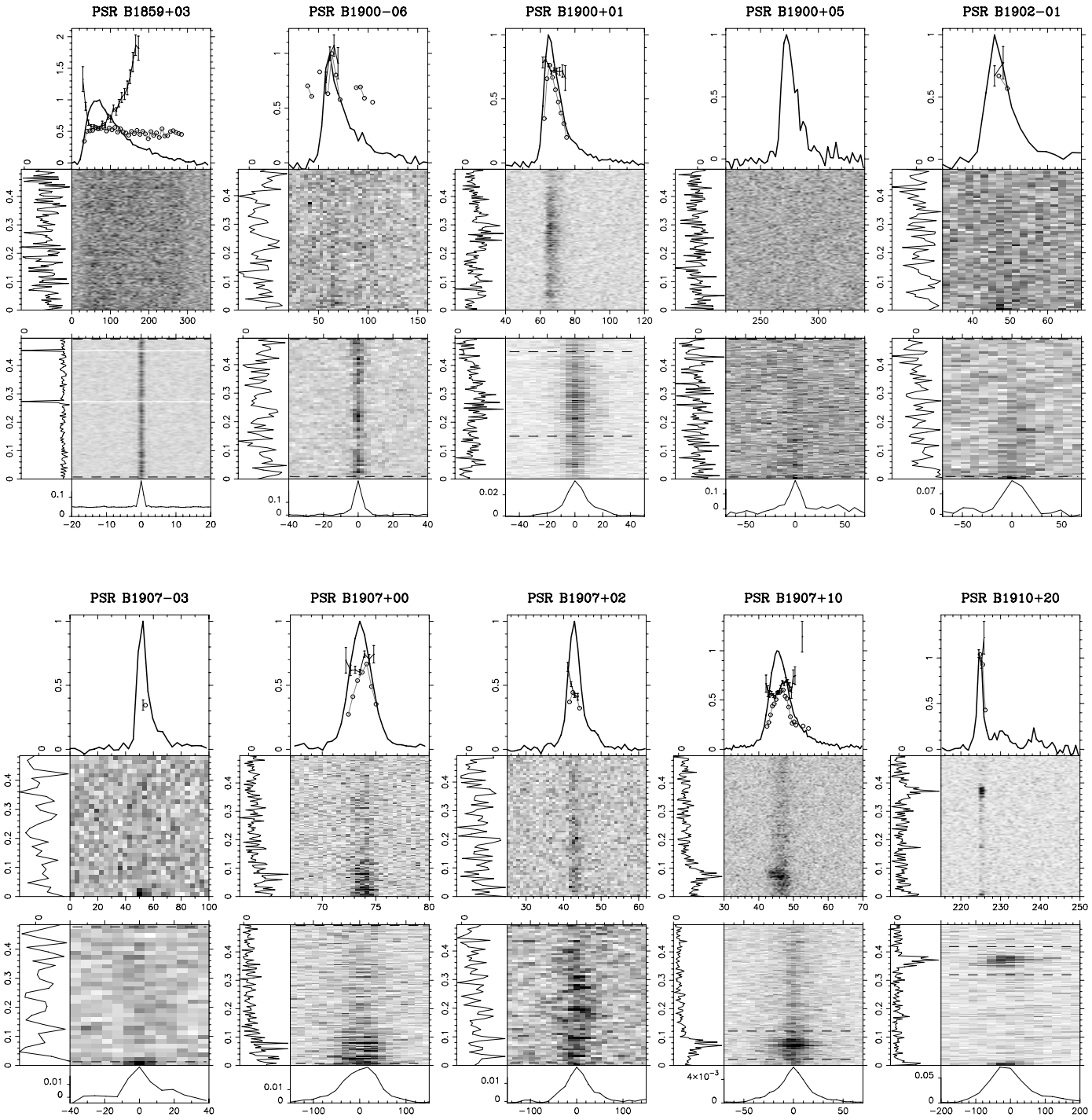

Fig. A.11. The integrated pulse profile (solid line) and the modulation index (solid points) are shown in the top plot, which is aligned with the LRFS. Below the LRFS is the 2DFS plotted. The integrated power of the spectra are shown the side- and bottom-panels of the spectra. See the main text and Fig. 1 for further details about the plots. The badly affected frequencies in the spectra are set to zero.

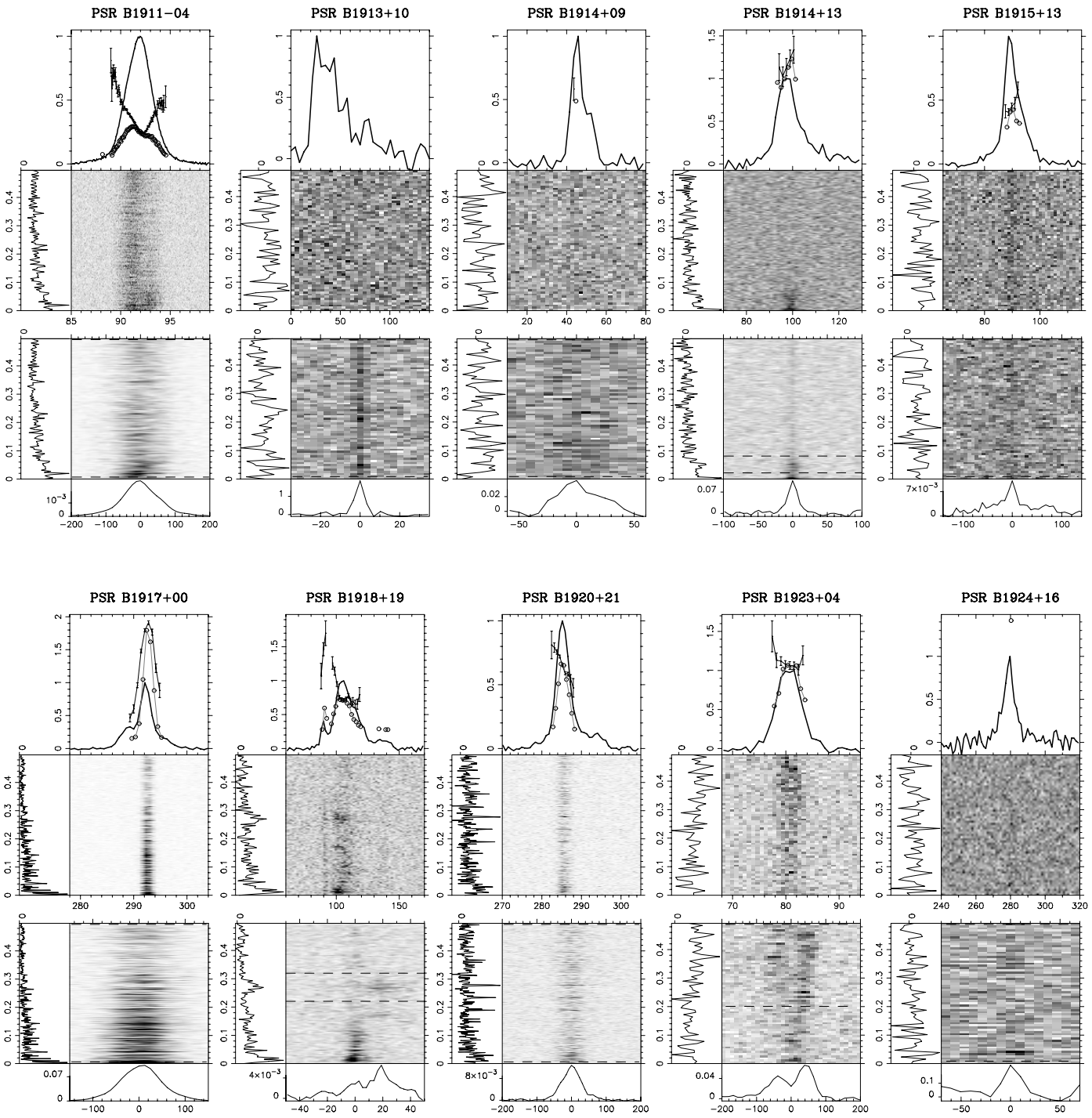

Fig. A.12. The integrated pulse profile (solid line) and the modulation index (solid points) are shown in the top plot, which is aligned with the LRFS. Below the LRFS is the 2DFS plotted. The integrated power of the spectra are shown the side- and bottom-panels of the spectra. See the main text and Fig. 1 for further details about the plots. The badly affected frequencies in the spectra are set to zero.

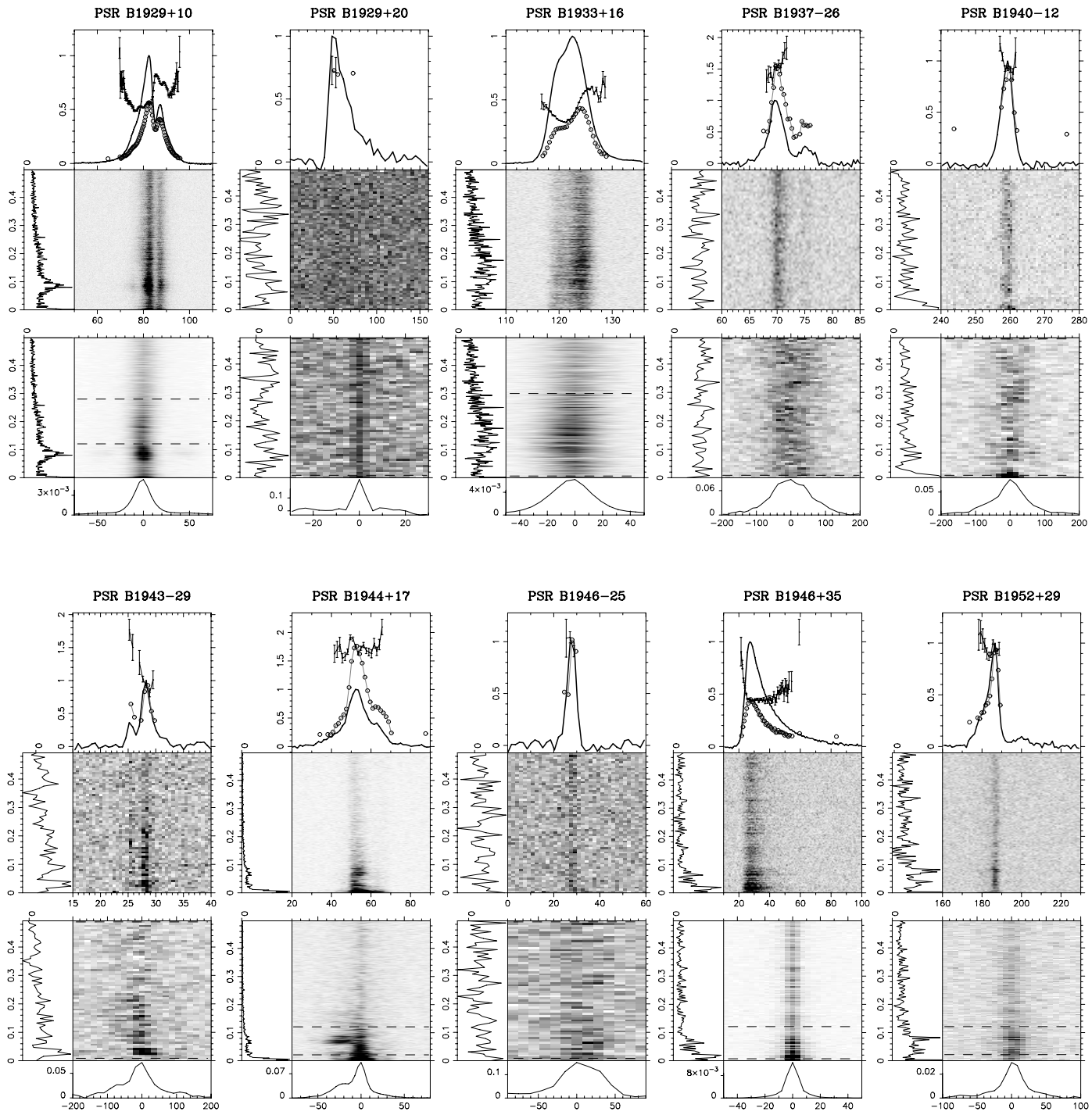

Fig. A.13. The integrated pulse profile (solid line) and the modulation index (solid points) are shown in the top plot, which is aligned with the LRFS. Below the LRFS is the 2DFS plotted. The integrated power of the spectra are shown the side- and bottom-panels of the spectra. See the main text and Fig. 1 for further details about the plots. The badly affected frequencies in the spectra are set to zero.

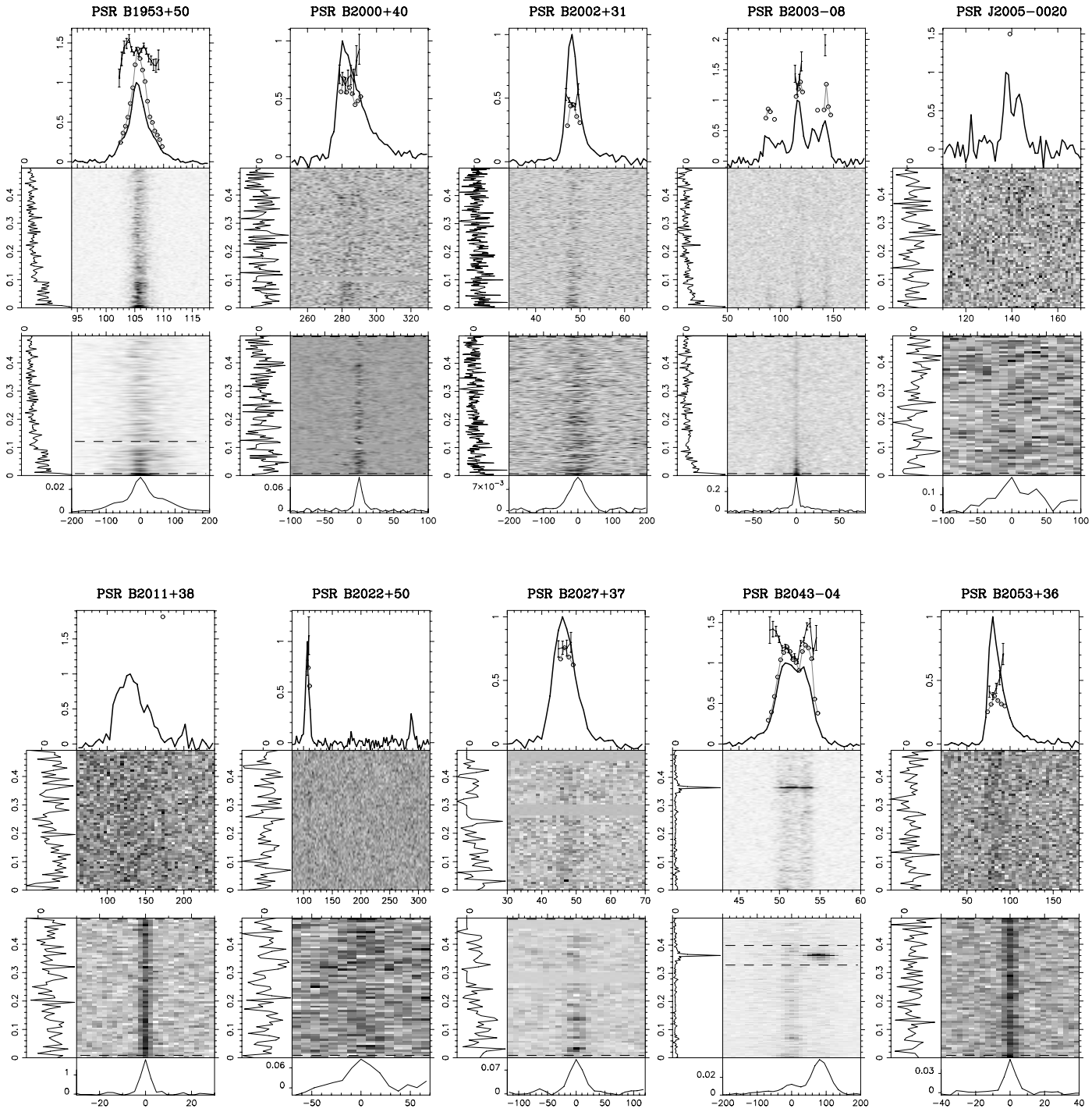

Fig. A.14. The integrated pulse profile (solid line) and the modulation index (solid points) are shown in the top plot, which is aligned with the LRFS. Below the LRFS is the 2DFS plotted. The integrated power of the spectra are shown the side- and bottom-panels of the spectra. See the main text and Fig. 1 for further details about the plots. The badly affected frequencies in the spectra are set to zero.

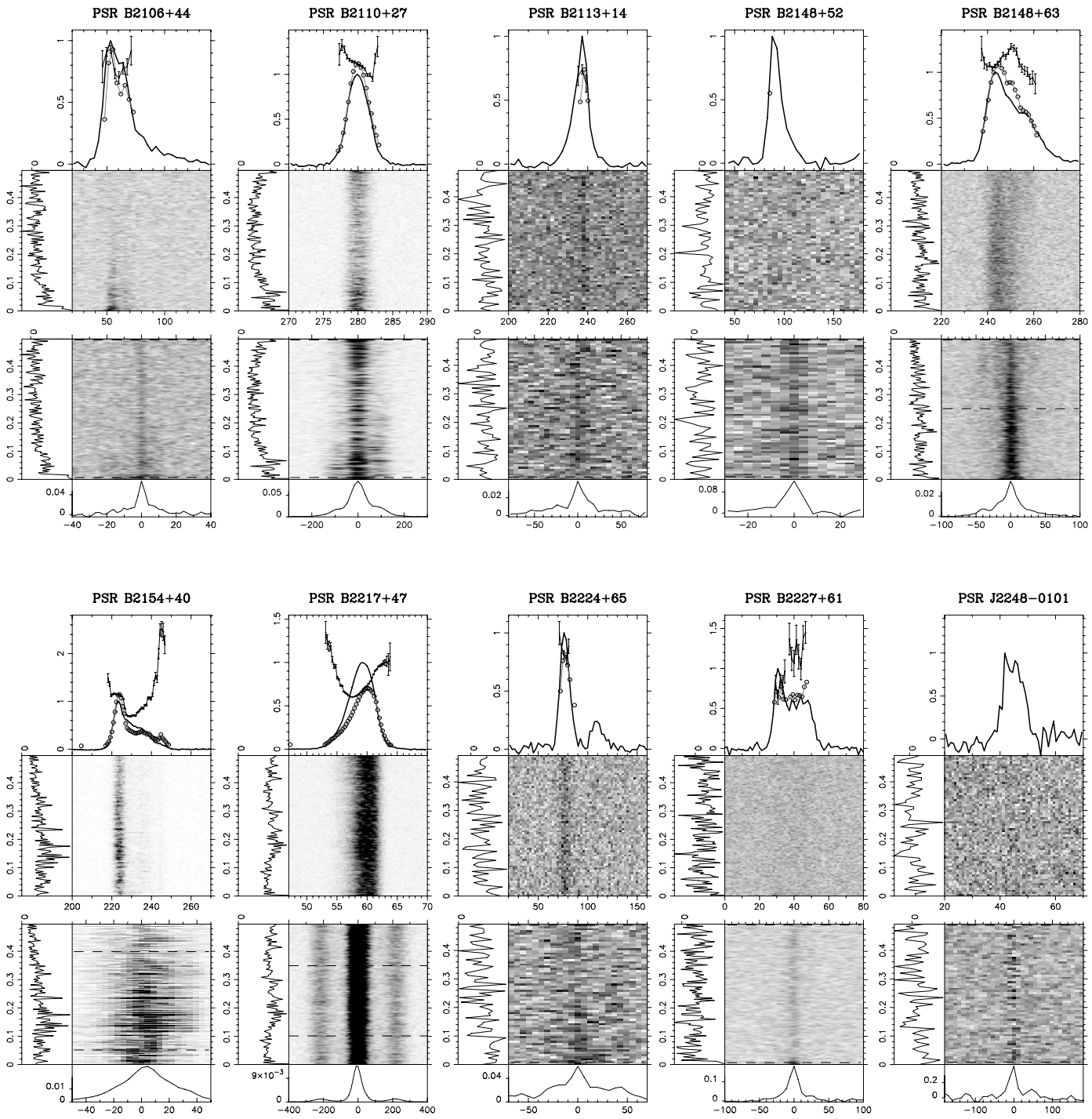

Fig. A.15. The integrated pulse profile (solid line) and the modulation index (solid points) are shown in the top plot, which is aligned with the LRFS. Below the LRFS is the 2DFS plotted. The integrated power of the spectra are shown the side- and bottom-panels of the spectra. See the main text and Fig. 1 for further details about the plots. The badly affected frequencies in the spectra are set to zero.

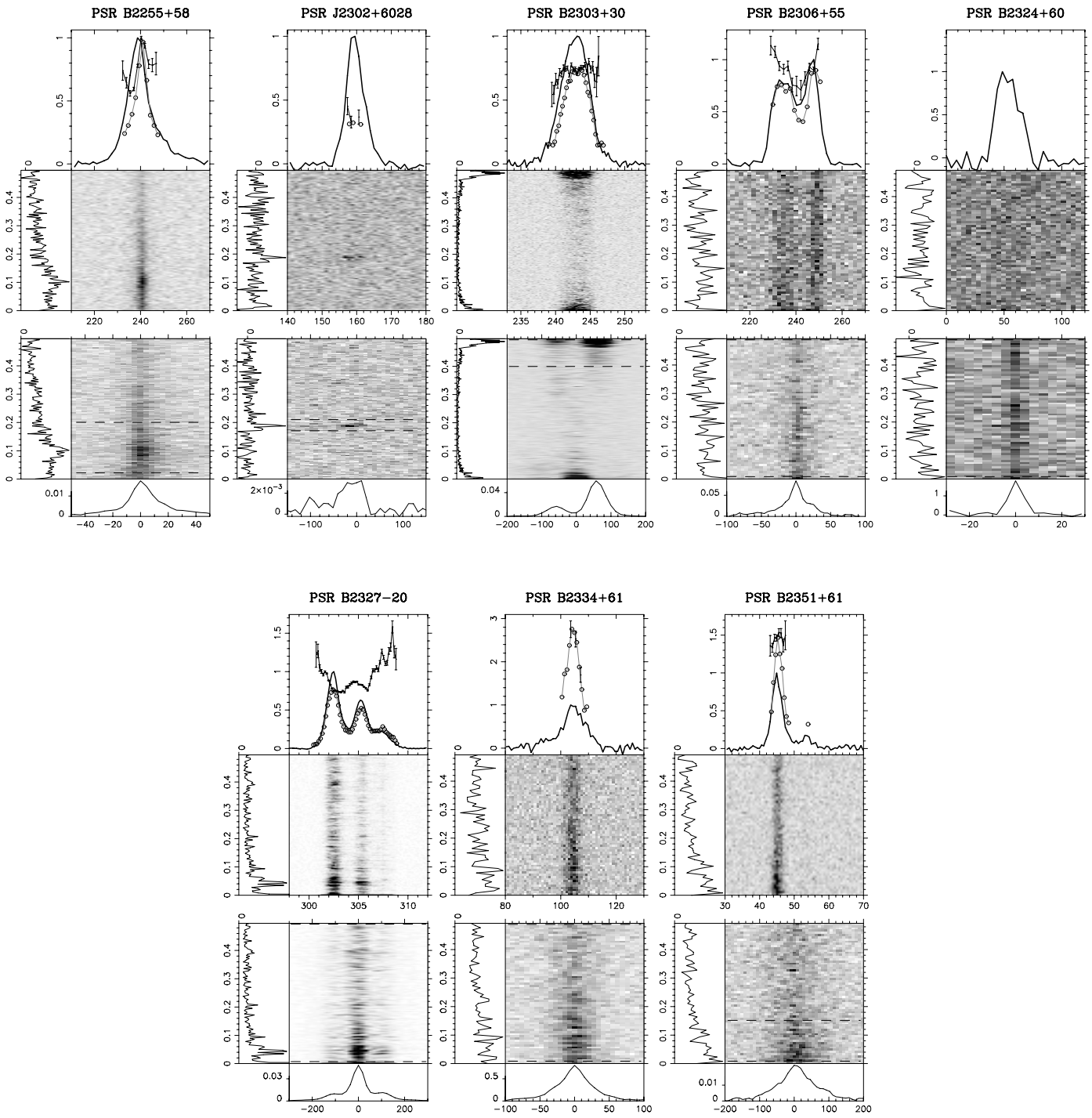

Fig. A.16. The integrated pulse profile (solid line) and the modulation index (solid points) are shown in the top plot, which is aligned with the LRFS. Below the LRFS is the 2DFS plotted. The integrated power of the spectra are shown the side- and bottom-panels of the spectra. See the main text and Fig. 1 for further details about the plots. The badly affected frequencies in the spectra are set to zero.

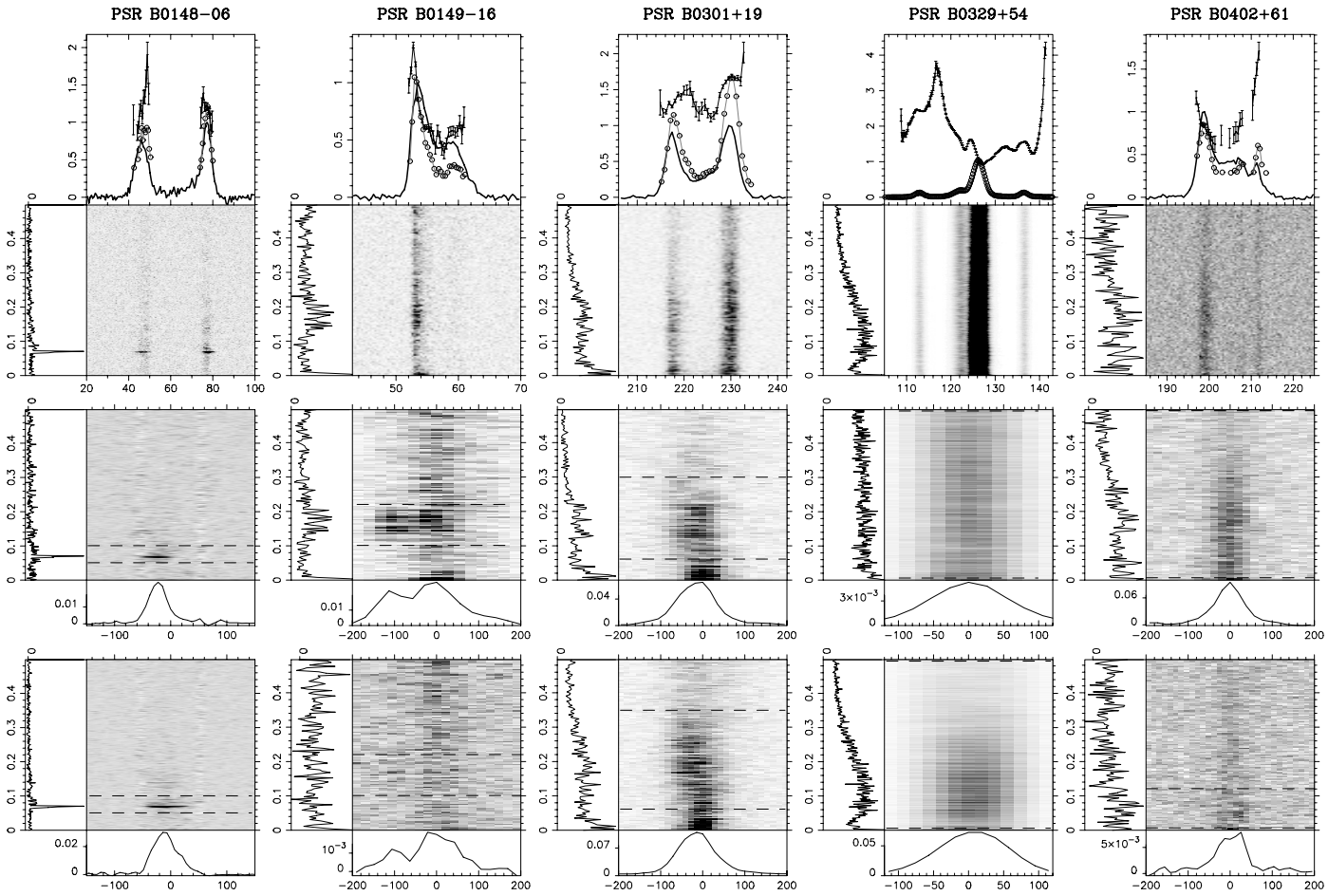

Fig. A.17. The integrated pulse profile (solid line) and the modulation index (solid points) are shown in the top plot, which is aligned with the LRFS. Below the LRFS are two 2DFSs plotted of different pulse longitude ranges. The integrated power of the spectra are shown the side- and bottom-panels of the spectra. See the main text and Fig. 1 for further details about the plots. The badly affected frequencies in the spectra are set to zero.

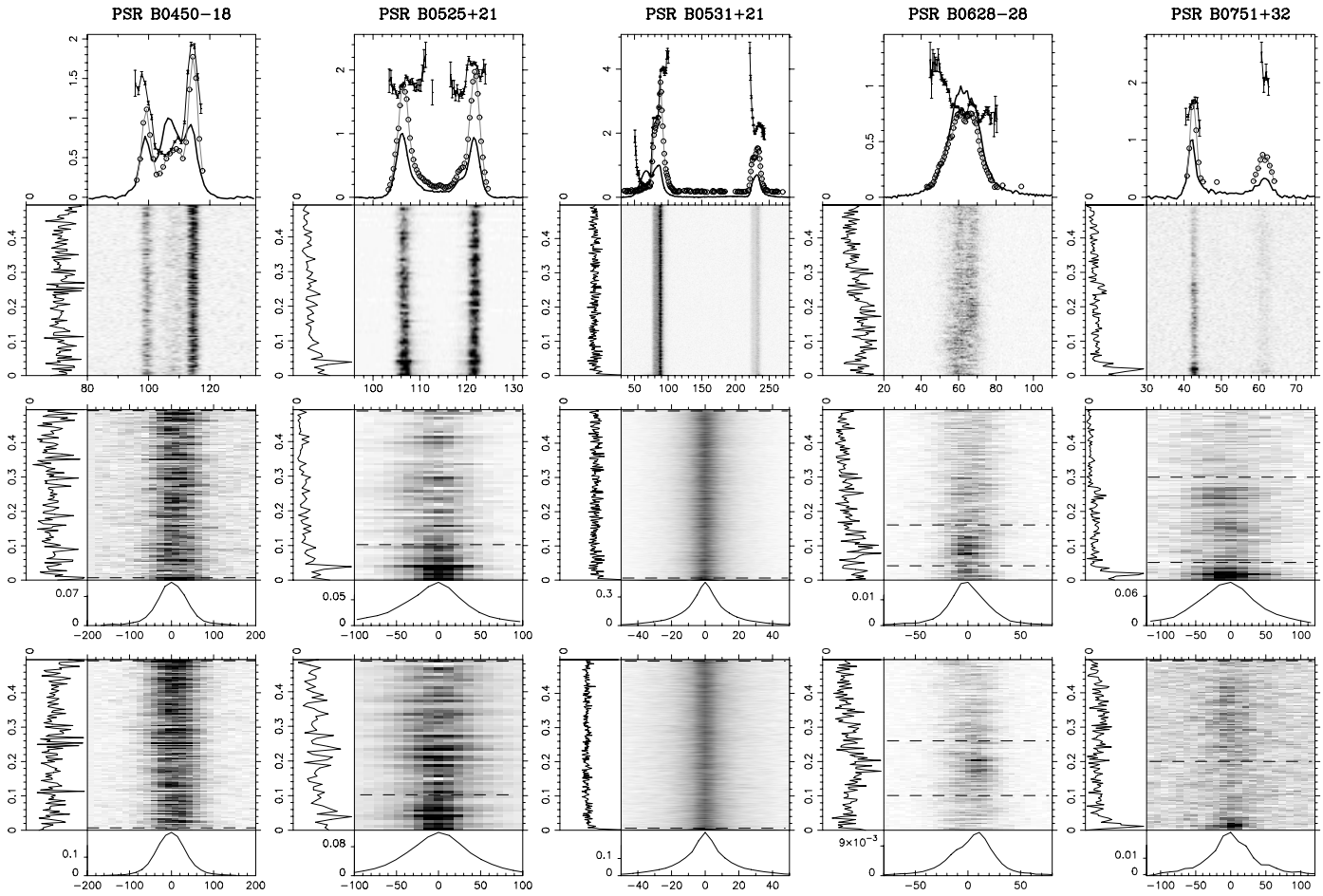

Fig. A.18. The integrated pulse profile (solid line) and the modulation index (solid points) are shown in the top plot, which is aligned with the LRFS. Below the LRFS are two 2DFSs plotted of different pulse longitude ranges. The integrated power of the spectra are shown the side- and bottom-panels of the spectra. See the main text and Fig. 1 for further details about the plots. The badly affected frequencies in the spectra are set to zero.

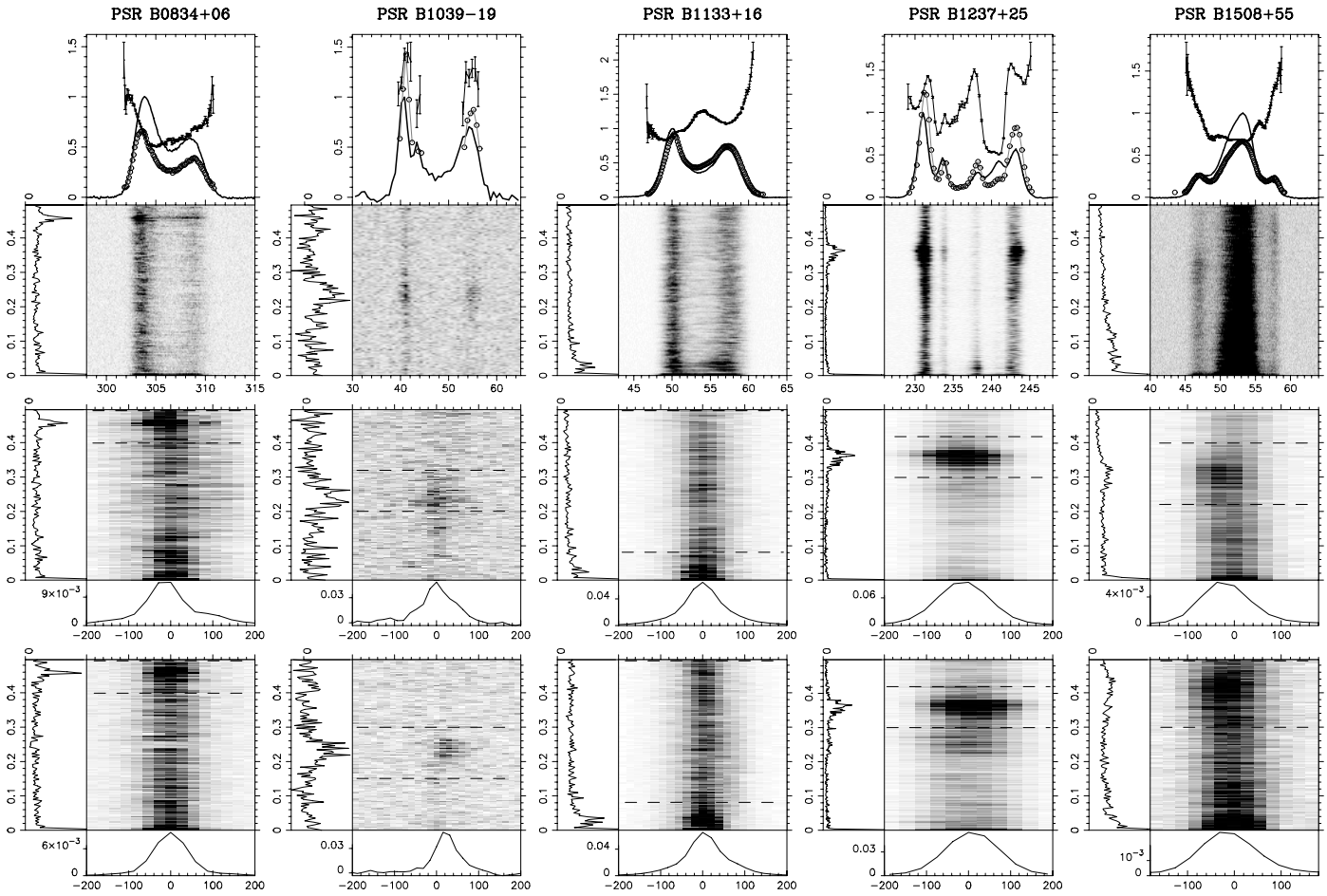

Fig. A.19. The integrated pulse profile (solid line) and the modulation index (solid points) are shown in the top plot, which is aligned with the LRFS. Below the LRFS are two 2DFSs plotted of different pulse longitude ranges. The integrated power of the spectra are shown the side- and bottom-panels of the spectra. See the main text and Fig. 1 for further details about the plots. The badly affected frequencies in the spectra are set to zero.

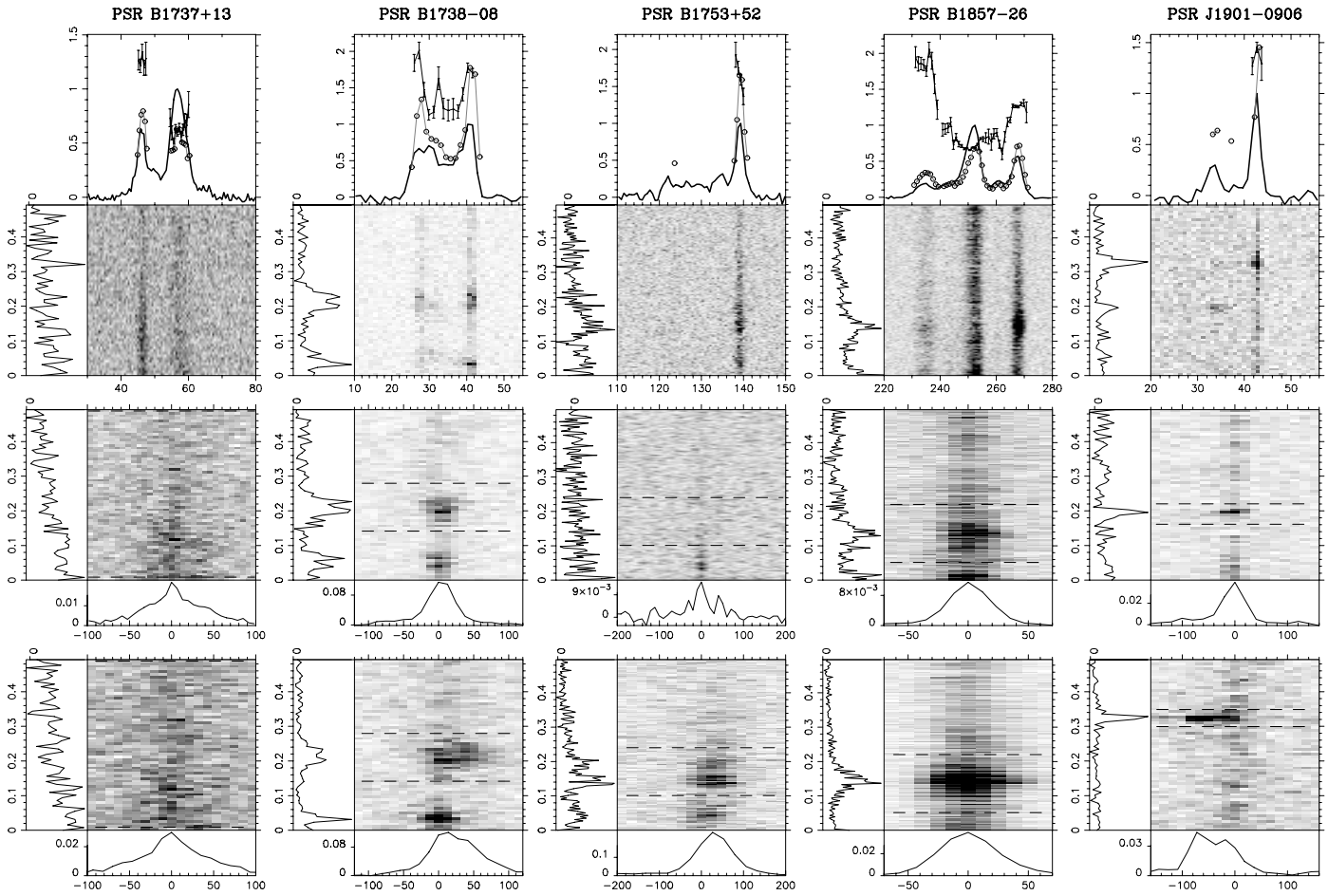

Fig. A.20. The integrated pulse profile (solid line) and the modulation index (solid points) are shown in the top plot, which is aligned with the LRFS. Below the LRFS are two 2DFSs plotted of different pulse longitude ranges. The integrated power of the spectra are shown the side- and bottom-panels of the spectra. See the main text and Fig. 1 for further details about the plots. The badly affected frequencies in the spectra are set to zero.

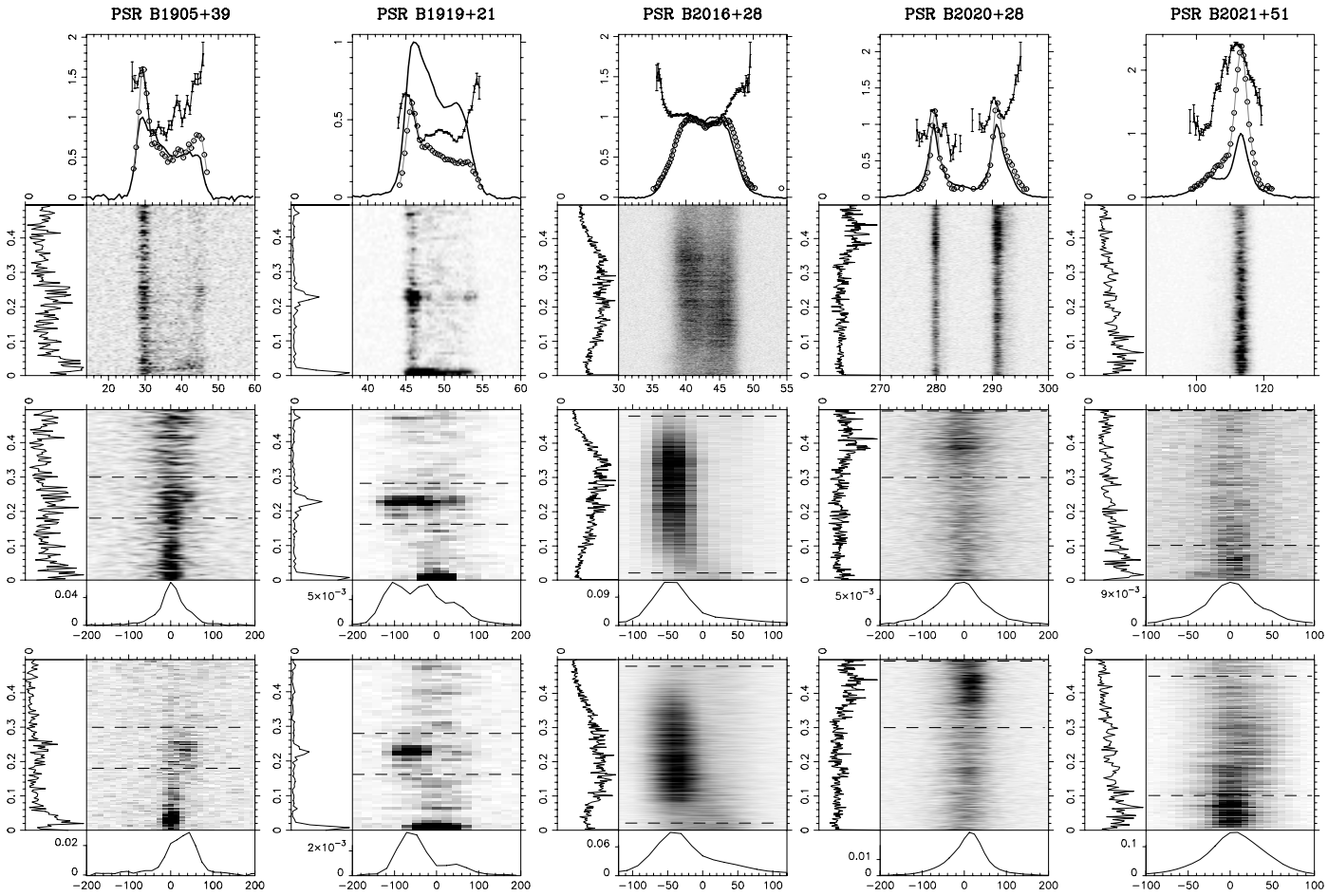

Fig. A.21. The integrated pulse profile (solid line) and the modulation index (solid points) are shown in the top plot, which is aligned with the LRFS. Below the LRFS are two 2DFSs plotted of different pulse longitude ranges. The integrated power of the spectra are shown the side- and bottom-panels of the spectra. See the main text and Fig. 1 for further details about the plots. The badly affected frequencies in the spectra are set to zero.

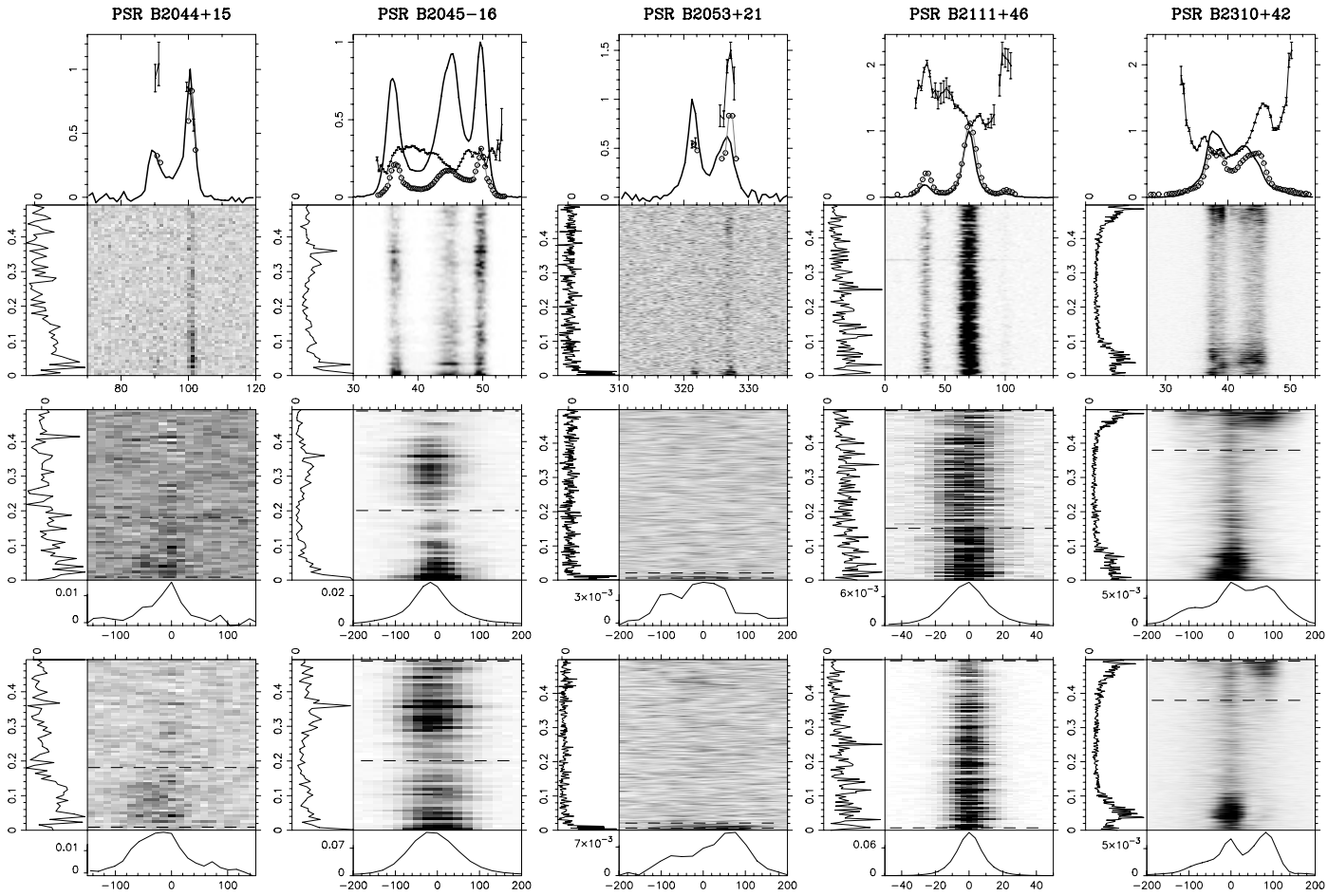

Fig. A.22. The integrated pulse profile (solid line) and the modulation index (solid points) are shown in the top plot, which is aligned with the LRFS. Below the LRFS are two 2DFSs plotted of different pulse longitude ranges. The integrated power of the spectra are shown the side- and bottom-panels of the spectra. See the main text and Fig. 1 for further details about the plots. The badly affected frequencies in the spectra are set to zero.

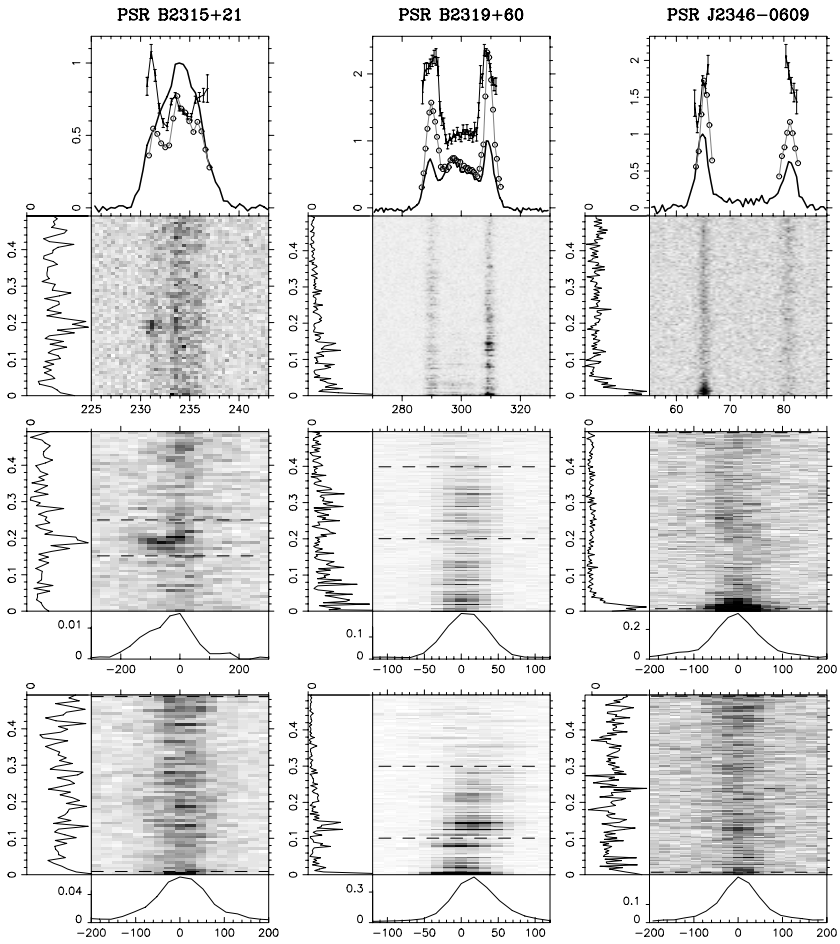

Fig. A.23. The integrated pulse profile (solid line) and the modulation index (solid points) are shown in the top plot, which is aligned with the LRFS. Below the LRFS are two 2DFSs plotted of different pulse longitude ranges. The integrated power of the spectra are shown the side- and bottom-panels of the spectra. See the main text and Fig. 1 for further details about the plots. The badly affected frequencies in the spectra are set to zero.